UNIVERSITY OF CALIFORNIA

Los Angeles

Stable and Clumped Isotope Analyses of Last Glacial Maximum Pluvial Lakes to Constrain Past Hydroclimate

A thesis submitted in partial satisfaction of

the requirements for the degree Master of Science

in Geochemistry

by

Lauren Mae Santi

2019

ABSTRACT OF THE THESIS

Stable and Clumped Isotope Analyses of Last Glacial Maximum

Pluvial Lakes to Constrain Past Hydroclimate

by

Lauren Mae Santi

Master of Science in Geochemistry

University of California, Los Angeles, 2019

Professor Aradhna K. Tripati, Chair

The Last Glacial Maximum (LGM; ~23,000-19,000 years ago) and subsequent deglaciation (~19,000-11,000 years ago) represents the last major global climatological transition. In the Western United States, the LGM and deglacial were both characterized by increased effective moisture and expansive lake systems, with most lake growth and maximum lake extents achieved during the deglacial period. In stark contrast, the modern Great Basin is characterized by aridity and low effective moisture. The factors contributing to these large-scale changes in hydroclimates are critical to resolve, given this region is poised to undergo future anthropogenic-forced climate changes with large uncertainties in model simulations for the 21st century. Furthermore, there are ambiguous constraints on the magnitude and even the sign of changes in key hydroclimate variables between the LGM and present-day in both proxy reconstructions and climate model analyses of the Western United States.

In this work, I present new stable and clumped isotope data from several ancient lakes, analyze this new data in concert with previously published data, and compare both new and existing results to climate model simulations. Radiocarbon dated samples from ancient lakes constrain lake elevation and the timing of lake level fluctuations. Using a hydrological modeling framework, clumped isotope data constrain several other hydroclimate variables including temperature, precipitation rate, and evaporation rate, which are all used to assess climate model simulations of the same hydrological variables.

In Chapter 1, I compile new and existing radiocarbon ages from post-LGM lake basins, and provide an analysis of changing effective moisture through time and space. In Chapter 2, I provide a detailed analysis of our data from one specific basin, Lake Surprise, and provide evidence of evaporation depression as a key driver of lake growth. Finally, in Chapter 3, I use clumped and stable isotope analysis of samples collected across the Great Basin (by UCLA students and others) to provide evidence for spatial and temporal variation in hydroclimate. Concomitant analysis of proxy data and climate model simulations provides a robust means to understand past climate change, and by extension, predict how current hydroclimates may respond to expected future climate forcings.

This thesis of Lauren Mae Santi is approved.

Robert Eagle Tripati

David K. Jacobs

Edwin Arthur Schauble

Aradhna K. Tripati, Committee Chair

University of California, Los Angeles

2019

TABLE OF CONTENTS

CHAPTER 2: CLUMPED ISOTOPE CONSTRAINTS ON INCREASED EFFECTIVE MOISTURE IN THE NORTHWEST GREAT BASIN, LAKE SURPRISE

LIST OF FIGURES

LIST OF TABLES

ACKNOWLEDGEMENTS

This work and all UCLA participants were supported by an NSF CAREER award (NSF EAR-1352212) to Aradhna Tripati. Lauren Santi and Alexandrea Arnold received support from the Center for Diverse Leadership in Science, and Alexandrea Arnold was also supported by a Cota-Robles Fellowship. Kate Maher provided funding for Lake Surprise sample collection by Daniel Ibarra, Sarah Lummis, and Chloe Whicker, supported by the National Science Foundation (NSF) grant EAR-0921134. Daniel E. Ibarra is supported by a Heising-Simons Foundation grant to C. Page Chamberlain.

We acknowledge the modeling groups, the Program for Climate Model Diagnosis and Intercomparison (PCMDI) and the WCRP's Working Group on Coupled Modelling (WGCM) for their roles in making available the WCRP CMI53 multi-model dataset. Support of this dataset is provided by the Office of Science, U.S. Department of Energy.

Chapter 1 of this thesis, titled “Lake Level Fluctuations in the Northern Great Basin for the Past 25,000 Years”, was previously submitted for the 2019 Desert Symposium in Zzyzx, CA. Bibliographic information for this publication is listed in References. In this chapter, Juan Lora provided guidance on climate model analysis and interpretation. John Mering and Charles Oviatt provided feedback on all drafts, especially on sections pertaining to Lake Bonneville. Daniel Ibarra and Alex Arnold provided extensive feedback and guidance throughout the writing process.

For Chapter 2 of this thesis, Chloe Whicker and Daniel Ibarra assisted in data collection. John Mering, Rico Lomarda, and Alex Arnold helped prepare and run samples on our mass spectrometers. Juan Lora and Daniel Ibarra provided help modeling and analyzing results. Daniel

Ibarra provided extensive feedback on drafts, and was instrumental in developing the isotopic model that forms a basis of this work.

For Chapter 3 of this thesis, Rico Lomarda and Alex Arnold helped prepare and run samples on the mass spectrometers. Alex Arnold was instrumental in planning and carrying out field work, which provided all the Lake Franklin samples and one Mud Lake carbonate used in this work. In this chapter, our analysis includes stable and clumped isotope data for sediments collected by our lab (from Lake Franklin, Mud Lake, Lake Surprise), novel analyses on previously published carbonates provided to our lab (Anne Egger-Lake Chewaucan; Victoria Petryshyn & Robert Dickerson-Mud Lake), and previously published clumped isotope results (Adam Hudson; Lake Chewaucan).

Finally, Aradhna Tripati served as a mentor and motivator throughout the writing and data analysis process. Thank you!

Lake Level Fluctuations in the Northern Great Basin for the Past 25,000 Years

Lauren Santi[1], Alexandrea Arnold[1], Daniel E. Ibarra[2],

Chloe Whicker[1], John Mering[1,3], Charles G. Oviatt[4], Aradhna Tripati[1]

[1] Department of Earth, Planetary, and Space Sciences, Department of Atmospheric and Oceanic Sciences, Institute of the Environment and Sustainability, Center for Diverse Leadership in Science, University of California, Los Angeles, California, USA

[2] Department of Geological Sciences, Stanford University, Stanford, California, USA

[3] School of Science, University of Waikato, Hamilton, New Zealand

[4]Department of Geology, Kansas State University, Manhattan, Kansas, 66506

ABSTRACT

During the Last Glacial Maximum (LGM; ~23,000 to 19,000 years ago) and through the last deglaciation, the Great Basin physiographic region in the western United States was marked by multiple extensive lake systems, as recorded by shoreline remnants and lake sediments. However, temporal constraints on the growth, desiccation, and timing of lake highstands remain poorly understood. Studies aimed at disentangling hydroclimate dynamics have offered multiple hypotheses to explain the growth of post-LGM lakes; however, a more robust understanding is currently impeded by a general paucity of spatially and temporally robust data. In this study, we present new data constraining the timing and extent of lake highstands at three post-LGM age pluvial lakes: Lake Newark, Lake Surprise, and Lake Franklin. This data is used in concert with previously published data for these basins and others from the Northern Great Basin including Lake Bonneville, Lake Chewaucan, and Lake Lahontan to compare the timings of lake growth and decay over a large spatial scale and constrain how regional hydroclimate evolved through the deglaciation.

INTRODUCTION

The American West is characterized by aridity and low precipitation, with many regions receiving less than 250 mm of rain per year. Furthermore, this region is projected to become even drier in the coming years, though climate models used for forecasting these changes disagree in the magnitude of future changes in regional precipitation (Seager et al., 2010; Scheff & Frierson, 2012). One approach to improve our understanding of different atmospheric processes that drive aridification in the West involves using paleoclimate data, in conjunction with data-model comparison, to study controls on past changes in the regional water balance.

In stark contrast to the arid present-day, during the Last Glacial Maximum (LGM; ~23 to 19 ka) and subsequent deglaciation (19 ka through ~11 ka, the onset of warming through the Younger Dryas and until the Holocene), the sedimentary and geomorphic record indicates that the region was marked by over 50 extensive lake systems (Hubbs & Miller, 1948; Mifflin & Wheat, 1979; Reheis, 1999; Reheis et al., 2014; Ibarra et al., 2018; McGee et al., 2018). The predominance of late Pleistocene lakes in this now-arid region indicates significant changes in the water cycle in response to changing climate forcing. Water balance calculations indicate that precipitation increases up to twice modern, as well as reduced evaporation rates, may be needed to explain the distribution of lakes at their greatest extent (e.g. Mifflin & Wheat 1979; Matsubara & Howard, 2009; Ibarra et al., 2014; Hudson et al., 2017; Ibarra et al., 2018; Quirk et al., 2018; Ibarra et al., 2019). These calculations also indicate that highstands (which largely occur after the LGM) cannot be singularly driven by low evaporation rates due to temperature depression associated with glacial periods. As such, there must be a significant contribution from precipitation driving these changes, particularly those leading to lake highstands (e.g., Ibarra et al., 2014).

While the most recent iteration of global climate models (PMIP3) has produced precipitation estimates for the LGM (21 ka), the next youngest ensemble of simulations is the mid Holocene (6 ka) (Braconnot et al., 2012). This large gap in time makes it difficult to tease apart temporal variations in atmospheric dynamics that may be contributing to lake growth. In fact, only one model has been used for transient simulations: Transient Climate Evolution 'TraCE', run through the National Center for Atmospheric Research Community Climate System Model Version 3 'CCSM3' (e.g. Liu et al., 2009; He, 2011). Comparison of PMIP3 precipitation simulations for the LGM show a general lack of agreement, indicating the atmospheric dynamics delivering precipitation to the region are not yet well understood (Fig. 1.1).

One set of constraints on the mechanism(s) driving changes in hydroclimate comes from studies that have dated carbonates and/or subaerial deposits (e.g., organic matter in soils) from paleoshorelines. These chronologies can be used to provide insights into potential mechanisms driving lake growth, including changes in precipitation. Recent work indicates non-synchronous lake highstands across the Great Basin, with some studies suggesting a latitudinal trend in the timing of maximum lake extent (Lyle et al., 2012; Munroe & Laabs, 2013a; Ibarra et al., 2014; Oster et al., 2015; Egger et al., 2018; McGee et al., 2018, Morrill et al., 2018). However, at present, the temporal and spatial evolution of lake highstands and stillstands is not chronologically constrained well enough to allow for meaningful insight into the atmospheric dynamics driving these changes, and therefore that is the focus of this initial work.

For this study, we collected tufa and gastropods shells from paleolake shorelines, including Lake Surprise, Lake Newark, and Lake Franklin (Fig. 1.2), and determined elevation-age histories using radiometric dating based on radiocarbon analysis. We use our radiocarbon ages and previously published work to constrain lake hydrographs and also estimate a pluvial

hydrologic index for each lake to further constrain past hydroclimate change in the northern Great Basin.

MATERIALS AND METHODS

Sample Collection

New samples consisted of both tufa and gastropod shells, which were collected from the shorelines of three closed basin paleolakes within the northern Great Basin in the western United States. These shorelines were identified through a combination of literature review (e.g. Reheis, 1999; Mifflin & Wheat, 1979; Hubbs & Miller, 1948; Ibarra et al., 2014), and Google Earth observations. At each site, care was made to ensure that all tufa and shells were *in situ*. In many cases, this necessitated digging pits ~1 meter into the ground using shovels and/or augers (following Munroe & Laabs, 2013). Post-excavation, the GPS coordinates of each sample were recorded, and the elevation of each sample was determined using the USGS Elevation Point Query Service, which reports ⅓ arc-second elevation data across the continental United States with an elevation resolution of ~3 meters. For a subset of lake basins (Lake Chewaucan and most of Lake Surprise), more precise LIDAR elevation datasets are available from previous publications (Ibarra et al., 2014; Egger et al., 2018).

Sample Preparation

Tufa and gastropod shells were first rinsed by hand in deionized water (DI) to remove loosely-held secondary material. If deemed necessary, they were sonicated in room temperature DI for up to 30 minutes to remove loosely held contaminants and particles on the sample surface. For shells with delicate internal chambers, a small pick or tweezers were used to carefully scrape away internal pieces of sand or secondary carbonate. For tufa collection, small handheld drills

were sometimes necessary to remove carbonate from a host rock. The resulting powder from this drilling process was ground using a mortar and pestle until the carbonate was a homogenous texture.

After creating a fine carbonate powder from each sample, a small amount of 3% H_2O_2 was added to each sample and left to react at room temperature for 1-4 hours. This process is commonly used to remove organic material (e.g. Mering, 2015; Tripati et al., 2010; Suarez & Passey, 2014). Post-reaction with H_2O_2, all samples were dried in an oven set below 50℃, and placed in a desiccator for storage prior to radiocarbon analysis (Tripati et al., 2010; Suarez and Passey, 2014; Defliese et al., 2015).

Radiocarbon Dating

Age control was provided by radiocarbon dating. In this study, radiocarbon dating was completed via Accelerator Mass Spectrometry (AMS) at UC Irvine. The uncertainty associated with the calibrated AMS ages was on the order of hundreds of years (Table 1.1). Note that several tufas were previously collected by Ibarra et al. (2014) and dated using only uranium-series methods (see note in Table 1.1). For all radiocarbon results (this study and others), we use *IntCal13* to convert conventional ^{14}C ages to calibrated ^{14}C ages, expressed as thousands of years before present, "ka" (Reimer et al., 2013). Reservoir corrections for *IntCal13* are made using the procedure outlined in Stuiver & Polach (1977), which uses independent age estimates to constrain correction magnitudes during each time interval. We plot the median calibrated probability and the 2σ uncertainty.

Hydrologic Index (HI)

The "pluvial hydrologic index" is a physical basin parameter that describes the ratio of lake surface area to tributary area. Historically, it has been used as a means to determine the partitioning of rainfall into runoff and evaporation and otherwise approximate past hydroclimate, assuming minimal change in drainage area and basin's hypsometric curvature (e.g., Mifflin & Wheat, 1979; Reheis, 1999; Ibarra et al., 2014; Ibarra et al., 2018). We calculate the HI of each basin as a function of sample elevation (z) using hypsometric curves for each lake basin from the HydroSHEDS/HydroBASINS datasets (Lehner et al., 2008; Lehner & Grill, 2013; Messager et al., 2016) using Equation 1, and summarize results in Table 1.2.

$$HI(z) = \frac{Lake\ Area(z)}{Lake\ Basin\ Area - Lake\ Area(z)} \qquad \text{Equation 1}$$

For the elevations added to the literature in this study, we use elevations pinned to a United States Geological Survey Digital 30 m Elevation Model. We note that the HI can be related to hydrologic cycle variables via steady-state mass balance equations (e.g., Mifflin & Wheat, 1979; Reheis, 1999; Ibarra et al., 2014) but for the purposes of this study do not carry out a formal hydroclimate scaling analysis.

Elevation Control

For each of the smaller lake basins analyzed (Chewaucan, Franklin, Newark, and Surprise), differential isostatic rebound is not taken into consideration for recorded GPS elevations. However, differential post-lacustrine isostatic rebound of up to 74 m is a known complicating factor at Lake Bonneville (e.g. Oviatt et al., 1992). For Lake Bonneville, most modern elevations plotted are translated to estimates of pre-rebound elevation using a linear

model described in Oviatt et al. (1992). We use isostatically adjusted lake areas calculated by Adams & Bills (2016). For Lake Lahontan, similar simple elevation correction models are not available, thus we do not correct for isostatic rebound, though we note that it may be as much as ~22 m (Adams et al., 1999).

RESULTS

We compile existing age control that defines hydrographs for a subset of northern Great Basin pluvial lakes with new data from Lakes Franklin, Newark, and Surprise (Fig. 1.3). We overlay simplified schematics of the implied paleo-lake histories for each basin that have been created based on existing data compilations and alternative schematics for Lakes Franklin, Newark, and Surprise, in light of new data from this study. In order to assess spatial gradients in moisture balance, we also plot HI against basin-center latitude and longitude (Fig. 1.4). We discuss the results in order of geographic position of basin, beginning with the southernmost basin.

Lake Newark

Pluvial Lake Newark (39.5°N, 115.7°W) was located in east-central Nevada. Kurth et al. (2011) provide eight radiocarbon ages of ancient shorelines and an estimated lake highstand 16.4 ± 0.3 ka, which is roughly coincident with that of nearby Lake Franklin (Redwine, 2003; Kurth et al., 2011). LGM lake levels were generally moderate, with a sharp transgression during the deglacial at ~16.7 ka followed by rapid decline to low levels. In this work, we provide two additional radiocarbon ages that increase the total range in paleolake elevations from previous studies and constrain moderate lake levels during the LGM and near desiccation by ~11 ka.

Lake Lahontan

Lake Lahontan (38.75–40.75°N, 117.5–120.5°W) was a spatially extensive lake system that, at its maximum extent, covered over 22,000 km^2 throughout northwestern Nevada, northeastern California, and southern Oregon (Russell, 1885). Lake Lahontan reached its highstand at 15.7 ± 0.3 ka (Adams & Wesnouwsky, 1998). This basin (and its associated subbasins) have been studied extensively, with radiocarbon dates from both lacustrine and subaerial carbonate materials (Adams, 1998; Benson et al., 2013; Benson et al., 1995; Hostetler & Benson, 1990; Petryshyn et al., 2016). Existing age control was compiled from Benson et al. (2013) and Adams et al. (2008) and schematic lake level curves after those references (as well as Reheis et al., 2014) are overlaid on Fig. 1.3c. During the LGM and early deglacial period, Lake Lahontan had a somewhat consistent shoreline at 1256 m (although there is a ~40 m spread in elevations at any given time). At ~17.8 ka, Lake Lahontan transgressed to a near highstand elevation of 1330 m, where it remained until ~14.1 ka. The 1338 m highstand at 15.7 ± 0.3 ka appears brief within the broader context of the higher elevation ages compiled by Benson et al. (2013) and Adams et al. (2008). Lahontan's regression is constrained to a fast decline in lake levels to 1206 m by 13.25 ka. Following this regression, the subbasins of Lahontan were isolated and are constrained primarily in the Pyramid and Winnemucca subbasins (see more detailed lake level curve of the deglaciation in Adams et al., 2008).

Lake Franklin

Lake Franklin (40.2°N, 115.3°W) was located in northeast Nevada, on the east side of the Ruby Mountains. With a pre-LGM shoreline elevation of 1823 m, lake transgression started slowly in the late LGM, accelerated at ~17.3 ka, and culminated in a lake highstand of 1850 m at

~17 ka. This highstand was followed by a regression to 1820 m by 14 ka (Munroe & Laabs 2013a; Munroe & Laabs 2013b). In this study, we report 12 new dates derived from gastropod shells to further refine the lake hydrograph. We modify an existing lake level curve from Munroe & Laabs (2013a) and overlay it on Fig. 1.3. Two high elevation samples, collected from a lagoonal marsh in Lillquist (1994), are not included in the lake level curve (but are plotted on the hydrograph), as these likely represent an overestimate of lake extent (see discussion in Munroe & Laabs, 2013a). While not significantly extending the temporal range of data, our dates lie well within previously published values on the lake hydrograph, and thus support the previously constructed lake level history by Munroe & Laabs (2013a).

Lake Bonneville

At its greatest extent, Lake Bonneville (38.5–43.5°N, 111.5–114.5°W) extended via multiple subbasins throughout central and northwest Utah, and into northeastern Nevada and southern Idaho. Lake Bonneville was comprised of the Bonneville Basin and the Sevier Subbasin, and contains the modern Great Salt Lake. This basin was spatially extensive (over 50,000 km^2), and has been studied in-depth in many publications since the original work by G.K. Gilbert (1890), including several recent studies constraining and compiling the lake hydrograph (e.g. Adams et al., 2008; Godsey et al., 2005; Godsey et al., 2011; McGee et al., 2012; Mering, 2015; Miller et al., 2013; Oviatt, 2015; Reheis et al., 2014). Existing radiocarbon ages come from both lacustrine and terrestrial proxies, and have been delineated as such in Fig. 1.3. The existing lake level curve indicates a gradual rise in lake levels prior to the LGM, with a potentially rapid transgression at ~19 ka. The maximum lake level attained at Lake Bonneville persisted between ~19-15 ka; however, as Lake Bonneville was not a closed basin during this

period of time, this lake level is not representative of a true hydraulic maximum (Oviatt, 2016). After this period, Lake Bonneville stabilized at several lower-elevation shorelines, which have been denoted on Fig. 1.3. We show a simplified lake level curve after Oviatt (2015) with ages from all the above-mentioned studies and compilations.

Lake Surprise

Lake Surprise (41.5°N, 120°W) was located on the border of northeast California and northwest Nevada. The geology and pluvial history of Lake Surprise was originally studied in Ibarra et al. (2014) and Egger et al. (2018). Our updated lake curve indicates a gradual increase in lake levels throughout the LGM and early deglacial period, culminating in a rapid rise occurring in less than 1 ka. Ibarra et al. (2014) first dated the post-LGM highstand at ~15.2 ka, and finds evidence of a maximum lake extent 176 meters above modern. In more recent work, Egger et al. (2018) added 12 radiocarbon dates to an existing repository of 21 dated samples, including a new higher elevation highstand age of ~16.0 ka. This rapid rise in lake levels is followed by a slow decline over the next ~5 ka. In this work, we sought to fill in ages from post-LGM but pre-highstand elevations, including new ages from the southernmost subbasin of Surprise Valley (Duck Flat). These ages compliment previously recorded ages at Lake Surprise by Ibarra et al. (2014) and Egger et al. (2018), but provide more detail by filling in missing gaps during the deglacial, including four tufa samples dated within ~2 ka of the highstand.

Lake Chewaucan

Lake Chewaucan (42.7°N, 120.5°W) was located in southern Oregon, and was comprised of four subbasins: Summer Lake, Upper Chewaucan Marsh, Lower Chewaucan Marsh, and

Albert Lake. Albert Lake and Summer Lake are modern lakes that become desiccated during mid to late summer each year, and at times completely dry up. In the past, these subbasins had variable connectivity, depending on the lake levels. Previously reconstructed lake levels (with most data deriving from Summer Lake) are compiled to produce a lake level curve for Lake Chewaucan (Hudson et al., 2017; Egger et al., 2018; Licciardi, 2001). Most recently, Egger et al. (2018) sought to reconstruct only the Summer Lake basin hydrograph due to the variable connectivity between the subbasins. There are two potential lake level trajectories for pre-LGM Lake Chewaucan, but both indicate a decrease in lake levels between 25-20 ka. Following an initial rise in lake levels, there is short desiccation at ~16 ka, prior to the highstand at 14-13 ka, where the lake reached 1356 m. Lake regression began ~13 ka, and continued throughout the remainder of the deglacial and into the early Holocene.

DISCUSSION

Timing of highstands and lake level fluctuations

Lake Newark

Although the data is sparse, there is evidence that paleolake levels increased sharply at Lake Newark at ~16.9 ka (Kurth et al., 2011). Two new radiocarbon dates from our study increase the temporal range of data, and indicate moderate lake levels prior to the LGM, as well as a continued decrease in lake extent during the late deglacial period.

Lake Lahontan

Data from Lake Lahontan encompasses both subaerial and lacustrine carbonates, with subaerial carbonates providing maximum lake extents, and most of these carbonates lying at

higher elevations than the lacustrine carbonates within a similar time frame, as expected. The hydrologic history of Lake Lahontan is one of the best-constrained, due to numerous studies contributing hundreds of lacustrine carbonate and subaerial measurements. The implied lake level history is overlaid on Fig. 1.3, and indicates a rapid rise from ~1260 m after the LGM at ~17.8 ka, to a highstand at ~1328 m, dated to 15.7 ka, before an eventual regression around 14.5 ka (Adams & Wesnousky, 1998; Benson et al., 1995; 2013; Benson, 2008; Adams et al., 2008).

Lake Franklin

New radiocarbon ages from Lake Franklin reported in this study support the timing of the maximum lake extent documented by Munroe & Laabs (2013a), who put together the first cohesive lake history using new radiocarbon data along with existing data from Lillquist (1994). The oldest radiocarbon date provides evidence that Lake Franklin may have once stood above 1850 m, indicating that an overall highstand for Lake Franklin was prior to the LGM, in contrast to neighboring pluvial lakes (Munroe & Laabs, 2013a). However, Munroe & Laabs (2013a) note that this sample (an assemblage of shells) may have been taken from the wrong stratigraphic unit, and for that reason, was not included in the hydrograph and is thus correspondingly marked with a question mark on Fig. 1.3.

During the early LGM (22.5-20 ka), Lake Franklin stood at an elevation of ~1823 m. Radiocarbon ages reflecting anomalously high lake elevations in this time period (~1850 m) are taken from lagoonal deposits (Lillquist, 1992), and likely reflect a near-shore environment above the main body of the lake. These are also set apart with question marks, and not used to construct the hydrograph itself (following Munroe & Laabs, 2013a).

Continuing to the late LGM, Lake Franklin rapidly grew to ~1830 m, where it remained relatively stable. There are two data points from this period that are outliers: one at 1840 m and one at 1823 m. These were excluded from the hydrograph because there is some uncertainty regarding their exact GPS location and stratigraphic context (see discussion in Munroe & Laabs, 2013a).

Between 16.8-17.3 ka, Lake Franklin rose from 1830 to its highstand elevation of 1850 m, a ~168% lake area increase. Munroe & Laabs (2013a) argue for a rapid and temporary regression during this time period, before returning again to 1850 m.

Following the pluvial maximum, the lake stabilized at 1843 m, and then 1840 m, with multiple radiocarbon ages from each beach ridge indicating that lake levels may have stabilized at both locations more than once. The new ages from this study fit well with the lake hydrograph trajectory described by Munroe & Laabs (2013a), with a rapid transgression to the post-LGM highstand, followed by shorelines that stabilized at 1843 m and 1840 m.

Lake Bonneville

Lake Bonneville is one of the most studied paleolakes in the Great Basin, with over 300 radiocarbon ages from lacustrine and subaerial carbonate and organic matter through the last deglacial (e.g. Benson et al., 2011; Kaufman & Broecker 1965; Broecker & Orr 1958; Godsey et al., 2011; Mering, 2015; Miller et al., 2013; Nishizawa et al., 2013; Oviatt, 2015; Reheis et al., 2014). Due to Bonneville's great spatial extent and depth, measurements of lake shorelines are approximately corrected for the effects of differential isostatic rebound that vary between different subbasins, with the greatest rebound in the center of the basin (Adams & Bills, 2016).

However, the reconstructed lake level history still shows a remarkably coherent story of lake level transgression and regression (Oviatt, 2016; Reheis et al., 2014).

Previously-defined lake level histories for Lake Bonneville have identified key events in the evolution of the lake. The initial rise of Lake Bonneville was quite rapid, potentially due to a diversion of the Upper Bear River, although there are other possible mechanisms, including a diversion from Cache Valley into the Great Salt Lake basin (Reheis et al., 2014). The lake reached its highstand at 18.6 ± 0.14 ka (McGee et al, 2012; Oviatt, 2015) where its maximum elevation was limited by intermittent overflow. This overflow limited its maximum pluvial extent, and is thus a key constraint for reconstructions of lake history. Putting a dramatic end to this highstand, Lake Bonneville catastrophically flooded to the nearby Snake River basin prior to ~18.2 ka (potentially much sooner, after rising to an overflow point near Red Rock Pass), and the shoreline stabilized at the new, "Provo Shoreline" level, where it remained for several thousand years (Godsey et al., 2005). The lake subsided rapidly from the Provo shoreline, and ceased to overflow, at about 15 ka (Godsey et al., 2011). With continued regression following the Provo Shoreline time, Lake Bonneville split into separate lakes, with Lake Gunnison persisting in the interior of the Sevier subbasin until ~10 ka, and the Gilbert-episode lake (a brief rise ~11.5 ka) encompassing the modern Great Salt Lake (but ~15 m higher) and extending to its west (Oviatt, 2014).

Samples at Lake Bonneville define a lake level "envelope", with subaerial samples indicating a maximum lake elevation, and lacustrine samples indicating a minimum lake elevation. Subaerial samples define a consistent maximum lake elevation between ~18-20 ka, but are intermixed with lacustrine carbonates during other time periods (e.g., 27-23 ka and 18.0-15.0 ka). This inconsistency could be explained by radiocarbon reservoirs within ancient Lake

Bonneville; however, many existing studies suggest that this effect is relatively small (Currey & Oviatt, 1985; Godsey, 2005; McGee et al., 2012). For example, McGee et al. (2012) show concordant radiocarbon and U-Th ages from Cathedral Cave in the main body of Lake Bonneville. Furthermore, Benson et al. (2011) show good correspondence between dates derived from a paleomagnetic secular variation model and radiocarbon ages from a sediment core taken from the western edge of the basin.

Nonetheless, some caution should be taken when interpreting radiocarbon ages when concurrent dating methods are not used. Additionally, concurrence between dating methods at a single location does not guarantee it can be extrapolated throughout the entire basin. For example, one area within ancient Lake Bonneville, Tabernacle Hill, is a site of current hot springs, high water tables, and tufa mounds dating to pre-Bonneville times, all of which indicate that groundwater could have provided a source of carbon for the Provo Lake. Ultimately, there is no indication of a major radiocarbon reservoir, but interpretation of radiocarbon ages should still consider this potential source of uncertainty.

Lake Surprise

Additional radiocarbon dates from pluvial Lake Surprise (this study) largely support the trend in lake levels indicated by previous work (Ibarra et al., 2014; Egger et al., 2018). New data from ~20 to 24 ka compare favorably with existing data, whilst filling in some temporal gaps at 20 ka. Similarly, new data collected just prior to the lake highstand at 15.2 ka is consistent with previous lake histories, which suggest a rapid increase in lake levels prior to the highstand (Ibarra et al., 2014; Ibarra et al., 2018). Several radiocarbon dates from this study show low lake levels until as late as almost 16 ka, indicating that Lake Surprise transgressed to its highstand

more rapidly than constrained by previous work, possibly suggesting a large and rapid precipitation forcing that is also observed at Lake Franklin and Lake Lahontan.

Lake Chewaucan

According to previous highstand estimates, Lake Chewaucan was the last studied lake to reach maximum levels during the deglacial, between 13-14 ka. As the most northwestern of the well-studied Great Basin lakes, the highstand is consistent with a northwest-trending change in moisture delivery.

Fig. 1.3 shows two potential trajectories for the Lake Chewaucan prior to 25 ka, one at very high lake levels and the other at low levels. There are several explanations for the possible trajectories. For one, the Summer subbasin sample locality (from which these older samples were collected) contains the most active faults of the region, so samples could potentially be displaced from their original elevations (see discussion in Egger et al., 2018; Liccardi, 2001). Second, as tufa defines a minimum (but not absolute) shoreline, there is a chance that both sets of elevations could be correct, but the samples <1340 m formed deeper underwater. However, we view this explanation as unlikely; as tufa formation requires sunlight, its formation is limited to the photic zone near the lake surface (Egger et al., 2018; Felton et al., 2006, Nelson et al., 2005). Prior to the ultimate highstand elevation, there is the possibility of a slight lake desiccation around 17 ka. This is similar to observations made at Lake Surprise (see below; Egger et al., 2018), but not to the same magnitude.

Summary of Lake Level Histories

Overall, we observe non-synchronicity in the timing of lake highstands, progressing from the southeast to the northwest during the deglacial period. In many cases, lake transgressions to their highstand levels (from moderate stillstand levels) happened in a relatively short period of time between 17 and 14 ka, while regressions tended to occur over a much longer period. New data from this study provides higher temporal resolution for hydrographs, and in some cases, extends the timeline of hydrographs.

Spatial Variability in Hydrologic Indices

The hydrologic index (HI) is a useful indicator for past water balance because it normalizes changes in lake elevation to basin area, such that proportional changes can be directly compared between basins of vastly different sizes. Assuming minimal changes in groundwater storage or inputs, the HI can be directly related to the mass balance of the watershed (see example applications in Mifflin & Wheat, 1979; Reheis, 1999; Ibarra et al., 2014). Additionally, when plotting HI versus latitude or longitude, trends may indicate latitudinal or longitudinal gradients in catchment-scale moisture balance. All sites except Lake Bonneville show an increase in HI following the LGM. Lake Bonneville, because it was an overflowing lake after the LGM (Oviatt, 2016), did not record meaningful HI for the deglacial.

The latitudinal gradient in HI shows a significant increase in maximum deglacial HI with latitude, with the highest HI of 0.530 attained by Lake Chewaucan (Fig. 1.4; Table 1.2). The longitudinal trend in HI shows a dipole, with lower values between 115°W and 120°W (roughly coincident with the eastern and western borders of Nevada). Lakes in the west and east have contributing watersheds that include the high-altitude Sierra Nevada and Uinta Mountains, which

may account for part of this pattern. Here we primarily focus on a longitudinal spread (111°W to 121°W) of lakes with minimal latitudinal variation (38°N to 43°N), and further work is needed in the southern Great Basin to more robustly constrain latitudinal trends.

Overall, the lower-latitude sites with a longitude between 115°W and 120°W experience the smallest change in HI during the deglacial. This is likely not biased due to low sampling resolution, as the lake basins from the two smallest HI's (corresponding to Lakes Franklin and Lahontan), have a significant amount of data, and demonstrate well-defined shorelines and hydrographs. The fine scale trends in moisture gradients inferred from HI values could be consistent with vapor transport by atmospheric rivers (Lora et al., 2016), or other transport mechanisms (e.g., Morrill et al., 2018; McGee et al., 2018), though further work on the numerous pluvial lakes in the Great Basin will be needed for this hypothesis to be tested.

CONCLUSIONS

Constraining the timing of lake highstands has important implications for understanding the terrestrial and atmospheric processes that transport moisture and impart changes on the basin-scale hydrological cycle. Post-LGM lake highstands at Great Basin pluvial lakes have previously shown non-synchronicity, with lake highstands progressing from the southeast to the northwest during the deglacial period (McGee et al., 2018). This study added 22 additional carbonate ages to the existing repository of data, and synthesized this new data with existing data from the literature. Overall, new data largely supports previously noted temporal trends in lake highstands, with the most recent highstands occurring in the northwestern lake basins.

New data from this study provide additional insight into previously compiled lake hydrographs. For example, radiocarbon ages from Lake Surprise provide more precise

constraints on the timing of the lake highstand, and support a fast transgression at ~16 ka, suggesting a large precipitation forcing similar to Lake Lahontan and Lake Franklin. Additionally, new ages from Lake Newark expand the temporal range of data, and provide a better idea of pre-LGM lake levels. Finally, new data from Lake Franklin and Lake Surprise fill in temporal gaps in existing data, and largely support previously constructed lake hydrographs.

Our analysis of pluvial hydrologic index (HI) with latitude and longitude reveals systematic spatial trends that will provide targets for future climate modeling efforts (e.g. Ivanovich et al., 2016). The highest post-LGM HI values are found at high latitudes, and either west of 120°W, or east of 115°W. Given further work, this spatial variability in HI could be used to robustly infer temporal and spatial changes in atmospheric moisture sources, and will provide targets for future transient simulations of the deglaciation.

FIGURES

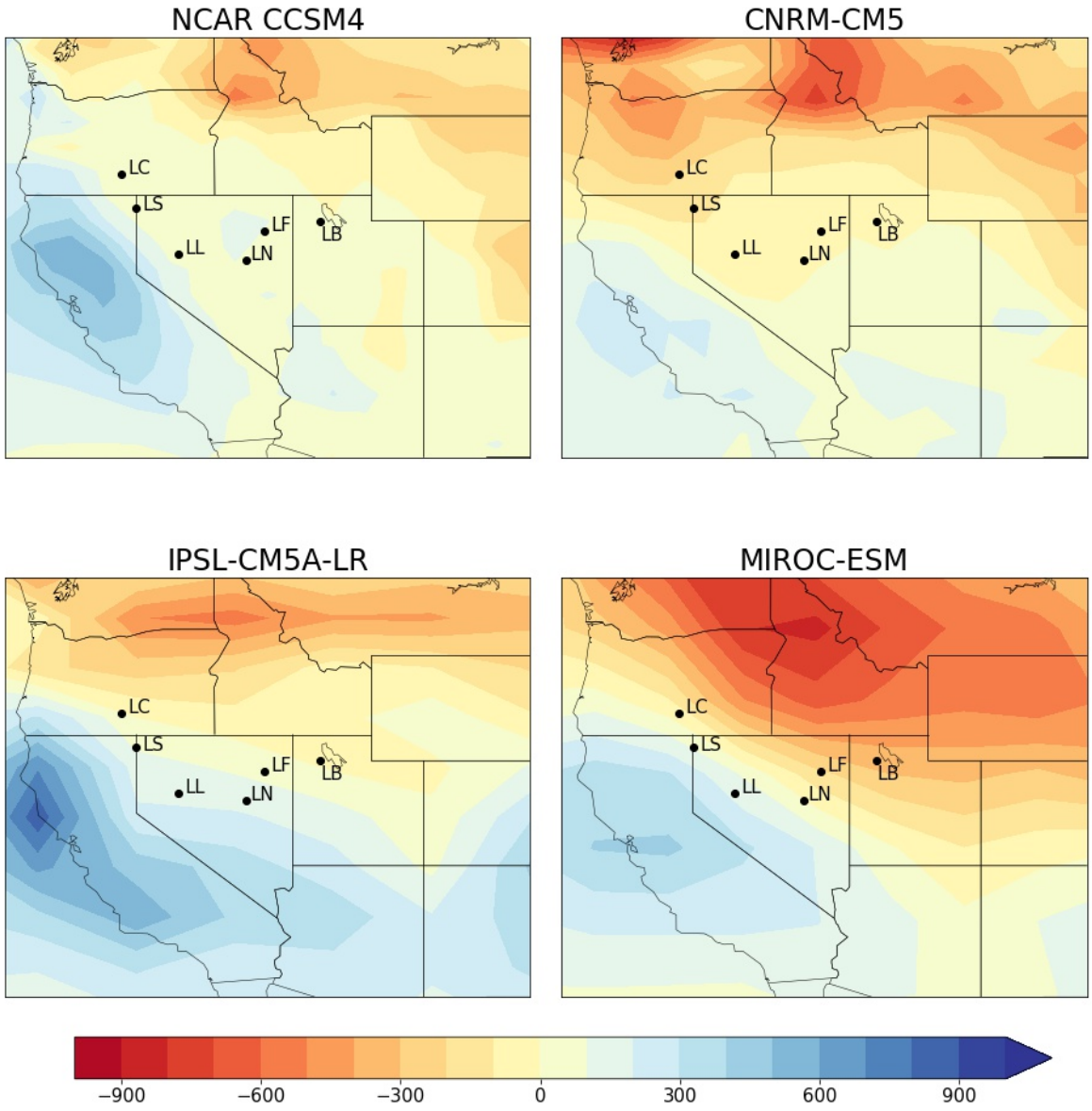

Figure 1.1: PMIP3-derived precipitation anomaly maps of the western United States from individual simulations. The annual precipitation anomaly is calculated as LGM minus preindustrial simulation, in mm/year. The LGM simulation is set to 21 ka, while the preindustrial simulation represents "0 ka". No bias correction was applied and all maps were made using the original resolution of the climate model output. The centroids of watershed polygons discussed in this study are plotted for reference. Model output is from the World Climate Research Programme's Coupled Model Intercomparison Project phase 5 (CMIP5) database. Labels = Lake Surprise (LS), Lake Newark (NL) and Lake Franklin (LF). Other lakes include: Lake Bonneville (LB), Lake Lahontan (LL), and Lake Chewaucan (LC).

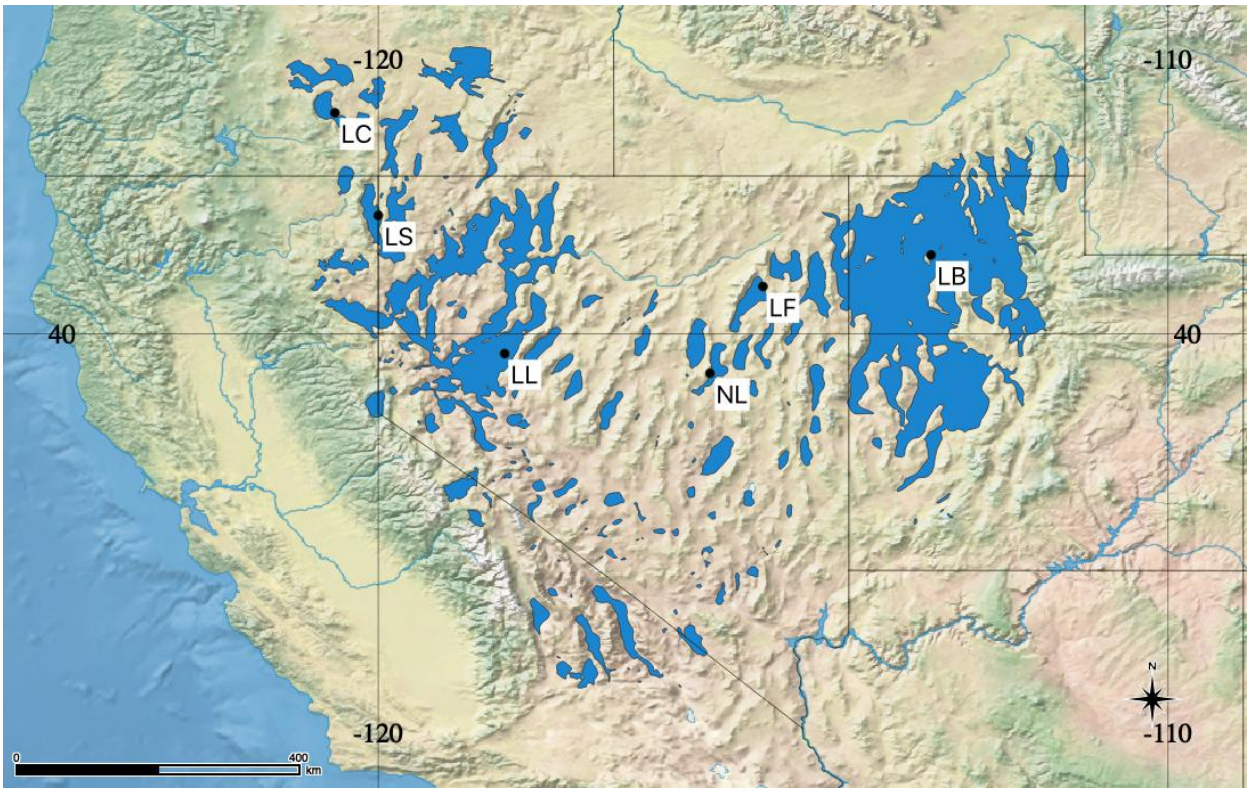

Figure 1.2: Pluvial lakes included in this study or plotted in Figure 3. New ages are from: Lake Surprise (LS), Lake Newark (NL) and Lake Franklin (LF). Other lakes include: Lake Bonneville (LB), Lake Lahontan (LL), and Lake Chewaucan (LC). Blue area is maximum pluvial lake extent during the LGM and deglacial, digitized from Mifflin & Wheat (1979) estimates (Map made using *Natural Earth* physical vector data).

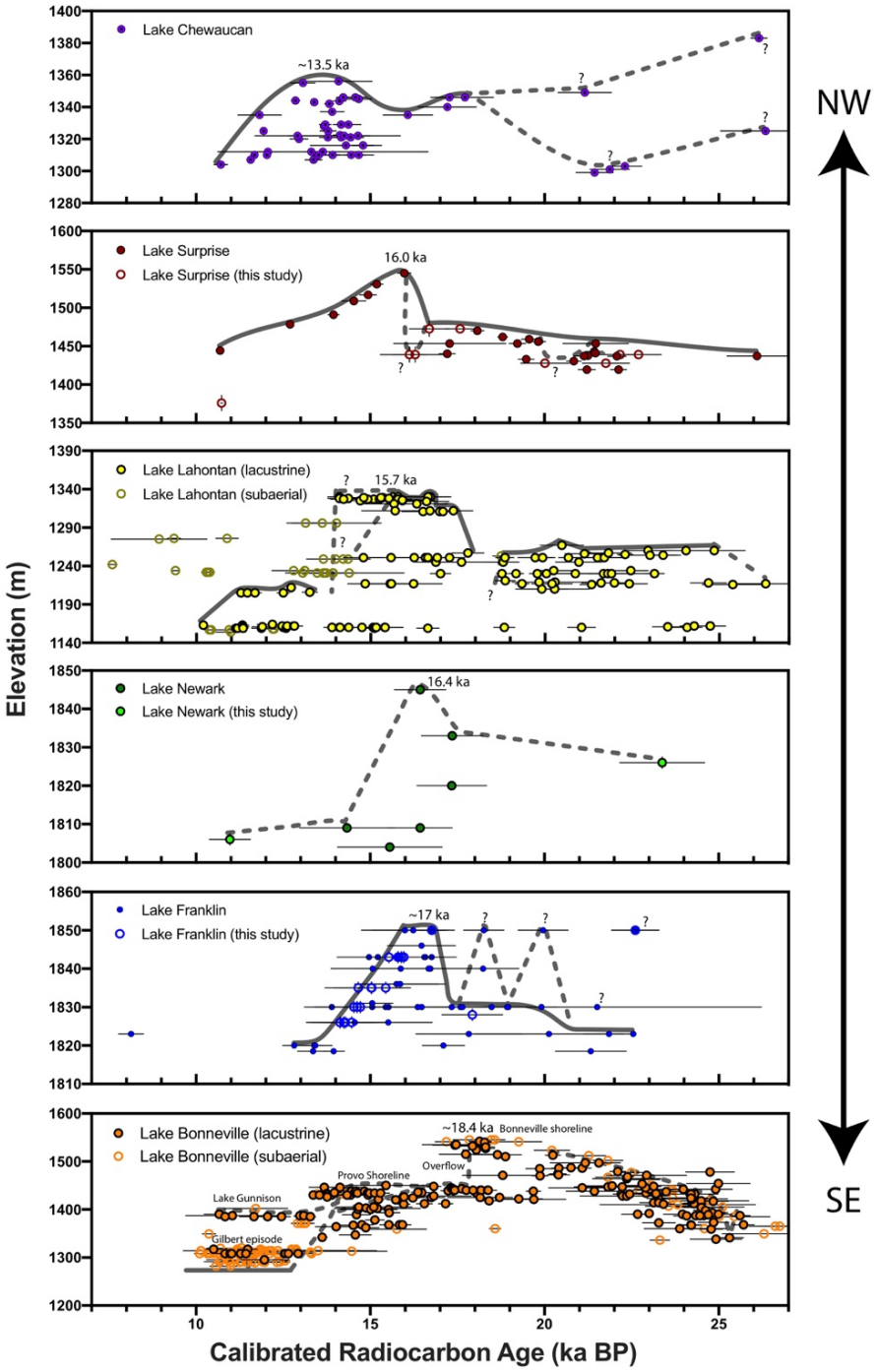

Figure 1.3: Radiocarbon based lake hydrographs for northern Great Basin pluvial lakes. Basins are plotted from geographic northwest to southeast. Lake Bonneville and Lake Lahontan data define lake elevation envelopes (see Oviatt, 2015; Benson et al., 2013; Adams et al., 2008), with terrestrial materials delineating a maximum lake extent, and lacustrine materials indicating a minimum lake extent. Projected lake level histories are overlaid on each basin. Some of these lake level histories have been altered from previous publications based on new data from this study. Errors in calibrated radiocarbon ages represent 2σ uncertainties and elevation errors are the same as originally reported for previous data, and are ±1.5 m for this study. Chewaucan data after Egger et al., (2018) and Liccardi (2001), Lake Lahontan data after Benson et al., (2013) and Adams et al., (2008), Lake Franklin data after Munroe & Laabs (2013), Lake Surprise data after Ibarra et al. (2014) and Egger et al. (2018), and Lake Bonneville data after Oviatt et al. (2015) and Mering (2015).

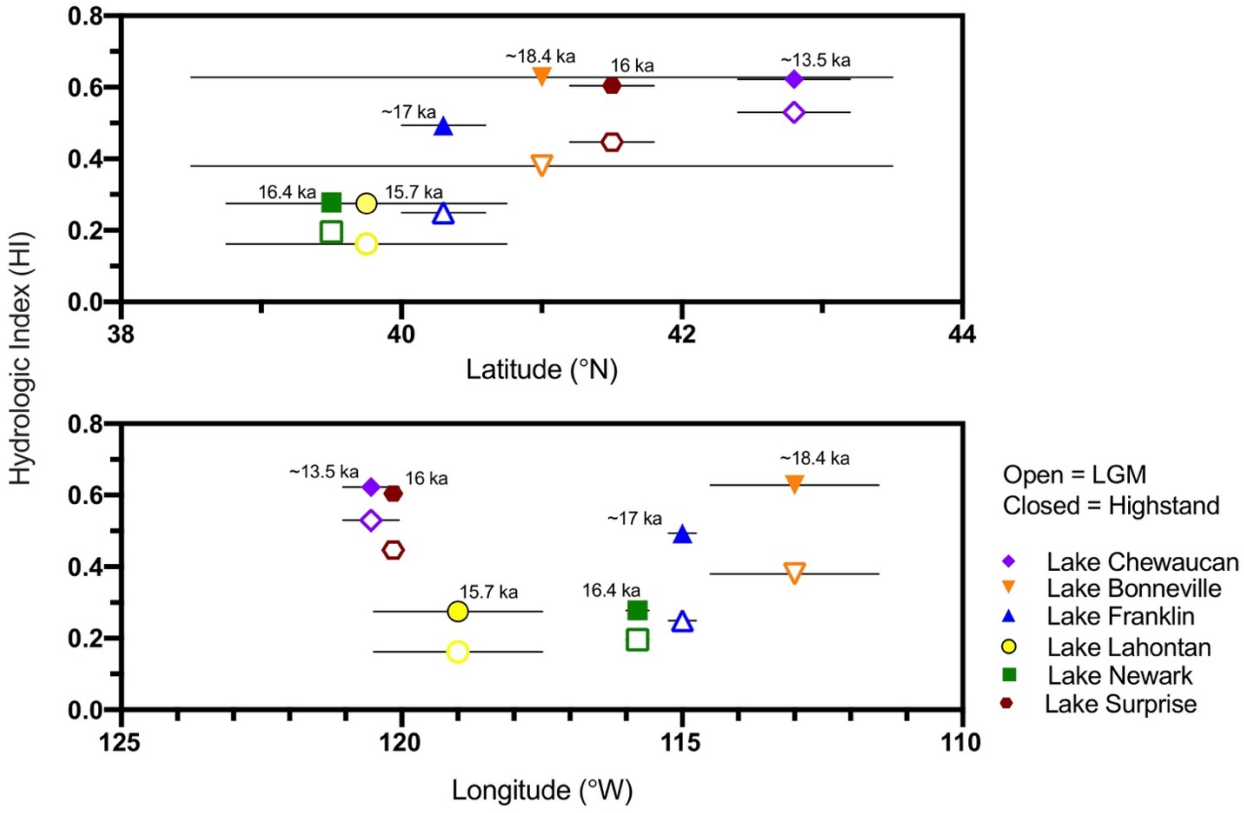

Figure 1.4: Hydrologic Indices (HI) plotted as a function of basin-center latitude (a) and longitude (b), with horizontal bars indicating the maximum geographic span of the lake. Filled shapes indicate the maximum HI during the LGM (19-23 ka), while clear shapes indicate the maximum HI during the LGM and the deglacial intervals. For each reported HI, the corresponding timing of each highstand is indicated. HI values are reported in Table 1.2. For Lake Bonneville, the deglacial HI is the maximum HI prior to spillover.

TABLES

Table 1.1: New Radiocarbon Ages for Northern Great Basin Pluvial Lakes

Lake Basin	Sample Name	Sample Type	GPS Location	^{14}C Age (ka)	^{14}C Age SD	IntCal13 Age (ka)	2σ min	2σ max	Elevation (m)	HI
Franklin	FranklinRW1_60_1A	Gastropod shell	40,6472N; -115.1388W	12.260	0.110	14.233	13.821	14.765	1826	0.21
Franklin	FranklinRW1_60_2A	Gastropod shell	40.1832N; -115.3760W	12.370	0.120	14.466	14.044	15.020	1826	0.21
Franklin	FranklinRW1_60_2B	Gastropod shell	40.1832N; -115.3760W	12.200	0.130	14.127	13.752	14.715	1826	0.21
Franklin	FranklinRW2_90_1A	Gastropod shell	40.2813N; -115.3760W	12.520	0.190	14.713	14.041	15.339	1838	0.36
Franklin	FranklinRW2_90_1B	Gastropod shell	40.2813N; -115.3760W	12.400	0.160	14.530	13.999	15.133	1838	0.36
Franklin	FranklinRW3_78_1A	Gastropod shell	40.2809N; -115.3601W	12.480	0.120	14.654	14.163	15.122	1841	0.39
Franklin	FranklinRW3_78_1B	Gastropod shell	40.2809N; -115.3601W	12.910	0.120	15.437	15.093	15.818	1841	0.39
Franklin	FranklinRW3_78_1C	Gastropod shell	40.2809N; -115.3601W	12.670	0.120	15.027	14.377	15.454	1841	0.39
Franklin	FranklinFRB_170_1	Tufa	40.6472N; -115.1388W	14.730	0.180	17.925	17.492	18.362	1848	0.48
Franklin	FranklinHS1_86_1A	Gastropod shell	40.2477N; -115.1388W	13.230	0.140	15.891	15.408	16.277	1843	0.49
Franklin	FranklinHS186_1B	Gastropod shell	40.2477N; -115.1388W	12.980	0.160	15.529	15.088	16.029	1843	0.49
Franklin	FranklinHS1_86_1C	Gastropod shell	40.2477N; -115.1388W	13.280	0.140	15.960	15.493	16.361	1843	0.49
Newark	NewarkLmt3_185_1	Tufa	39.4776N; -115.7882W	19.420	0.250	23.383	22.777	24.001	1826	0.20
Newark	NewarkLmt4_50_1	Tufa	39.4547N; -115.7790W	9.650	0.120	10.973	10.658	11.253	1806	0.14
Surprise	SVDI12-T4A*	Tufa	41.4299N; -119.9752W	18.780	0.270	22.697	22.039	23.354	1439	0.33
Surprise	SVDI12-T4B*	Tufa	41.4299N; -119.9752W	18.350	0.270	22.181	21.532	22.807	1439	0.33
Surprise	SVDI12-T7*	Tufa	41.4280N; -119.9725W	14.460	0.170	17.613	17.141	18.008	1472.5	0.42
Surprise	SVDI12-T3A*	Tufa	41.4299N; -119.9752W	18.030	0.280	21.823	21.083	22.443	1427.8	0.31
Surprise	SVDI12-T3B*	Tufa	41.4299N; -119.9752W	16.590	0.290	20.016	19.279	20.713	1427.8	0.31
Surprise	SVCW17-PT1	Tufa	40.9771N; -119.8755W	13.520	0.340	16.303	15.289	17.288	1475	0.44
Surprise	SVCW17-PT2	Tufa	40.9770N; -119.8755W	13.390	0.160	16.109	15.642	16.609	1475	0.44
Surprise	SVCW17-PT3	Tufa	40.9764N; -119.8747W	13.790	0.190	16.684	16.126	17.258	1477	0.45

*Originally collected and dated by uranium-series only in Ibarra et a. (2014). Three of the five samples are concordant (at 2σ) with uranium-series ages from the same hand-sample reported by Ibarra et al. (2014) (see their Table 5: SVDI12-T7 = 16.67 ± 6.57; SVDI12-T4 = 19.80 ± 2.00; SVDI12-T3 = 18.33 ± 1.82).

Table 1.2: Calculated hydrologic indices for each basin

Pluvial Lake	LGM Maximum Hydrologic Index (19-23 ka BP)	Deglacial Highstand Hydrologic Index (11-19 ka BP)
Chewaucan	0.530	0.622
Surprise	0.447	0.604
Lahontan	0.162	0.275
Newark	0.196	0.278
Franklin	0.249	0.494
Bonneville	0.380	0.628[a]

[a] Bonneville shoreline prior to spillover at ~18 ka

REFERENCES

Adams, K.D., and Bills, B.G. (2016), Chapter 8. Isostatic rebound and palinspastic restoration of the Bonneville and Provo shorelines in the Bonneville basin, UT, NV, and ID, in Oviatt, C.G., Shroder Jr., J.F., editors, Lake Bonneville: A Scientific Update: Developments in Earth Surface Processes, 20, 145–164.

Adams, K. D., Goebel, T., Graf, K., Smith, G. M., Camp, A. J., Briggs, R. W., & Rhode, D. (2008). Late Pleistocene and early Holocene lake-level fluctuations in the Lahontan Basin, Nevada: Implications for the distribution of archaeological sites. *Geoarchaeology*, *23*(5), 608-643.

Adams, K. D., & Wesnousky, S. G. (1998). Shoreline processes and the age of the Lake Lahontan highstand in the Jessup embayment, Nevada. *Geological Society of America Bulletin*, *110*(10), 1318-1332.

Adams, K. D., Wesnousky, S. G., & Bills, B. G. (1999). Isostatic rebound, active faulting, and potential geomorphic effects in the Lake Lahontan basin, Nevada and California. *Geological Society of America Bulletin*, *111*(12), 1739-1756.

Benson, L.V., Kashgarian, M., & Rubin, M. (1995). Carbonate deposition, Pyramid Lake subbasin, Nevada: 2. Lake levels and polar jet stream positions reconstructed from radiocarbon ages and elevations of carbonates (tufas) deposited in the Lahontan basin. *Palaeogeography, Palaeoclimatology, Palaeoecology*, *117*(1-2), 1-30.

Benson, L. V., Lund, S. P., Smoot, J. P., Rhode, D. E., Spencer, R. J., Verosub, K. L., Louderback, L. A., Johnson, C. A., Rye, R.O., & Negrini, R. M. (2011). The rise and fall of Lake Bonneville between 45 and 10.5 ka. *Quaternary International*, *235*(1-2), 57-69.

Benson, L. V., Smoot, J. P., Lund, S. P., Mensing, S. A., Foit Jr, F. F., & Rye, R. O. (2013). Insights from a synthesis of old and new climate-proxy data from the Pyramid and Winnemucca lake basins for the period 48 to 11.5 cal ka. *Quaternary International*, *310*, 62-82.

Braconnot, P., Harrison, S. P., Kageyama, M., Bartlein, P. J., Masson-Delmotte, V., Abe-Ouchi, A., Otto-Bleisner, B., & Zhao, Y. (2012). Evaluation of climate models using palaeoclimatic data. *Nature Climate Change*, *2*(6), 417.

Broecker, W. S., McGee, D., Adams, K. D., Cheng, H., Edwards, R. L., Oviatt, C. G., & Quade, J. (2009). A Great Basin-wide dry episode during the first half of the Mystery Interval? *Quaternary Science Reviews*, *28*(25-26), 2557-2563.

Broecker, W. S., & Orr, P. C. (1958). Radiocarbon chronology of Lake Lahontan and Lake Bonneville. *Geological Society of America Bulletin*, *69*(8), 1009-1032.

Defliese, W. F., Hren, M. T., & Lohmann, K. C. (2015). Compositional and temperature effects of phosphoric acid fractionation on Δ47 analysis and implications for discrepant calibrations. *Chemical Geology*, *396*, 51-60.

Egger A.E., Ibarra, D.E., Widden, R, Langridge R.M., Marion, M, & Hall, J. (2018). Influence of Pluvial Lake Cycles on Earthquake Recurrence on the Northwestern Basin and Range, USA. *Geological Society of America* Special Paper 536, 1-28.

Felton, A., Jewell, P. W., Chan, M., & Currey, D. (2006). Controls of tufa development in pleistocene lake Bonneville, Utah. *The Journal of geology*, 114(3), 377-389.

Gilbert, G. K. (1890). *Lake Bonneville* (Vol. 1). US Government Printing Office, 1-438.

Godsey, H. S., Currey, D. R., & Chan, M. A. (2005). New evidence for an extended occupation of the Provo shoreline and implications for regional climate change, Pleistocene Lake Bonneville, Utah, USA. *Quaternary Research*, *63*(2), 212-223.

Godsey, H. S., Oviatt, C. G., Miller, D. M., & Chan, M. A. (2011). Stratigraphy and chronology of offshore to nearshore deposits associated with the Provo shoreline, Pleistocene Lake Bonneville, Utah. *Palaeogeography, Palaeoclimatology, Palaeoecology*, *310*(3-4), 442-450.

He, F. (2011). Simulating transient climate evolution of the last deglaciation with CCSM 3. *Doctoral dissertation, University of Wisconsin, Madison,*72(10), 1-171.

Hostetler, S., & Benson, L. V. (1990). Paleoclimatic implications of the high stand of Lake Lahontan derived from models of evaporation and lake level. *Climate dynamics*, *4*(3), 207-217.

Hubbs, C.L., and Miller, R.R. (1948). The zoological evidence: Correlation between fish distribution and hydro- graphic history in the desert basins of western United States, in The Great Basin with emphasis on glacial and postglacial times: *Bulletin of the University of Utah*, 38(20), 17–166.

Ibarra, D. E., Egger, A. E., Weaver, K. L., Harris, C. R., & Maher, K. (2014). Rise and fall of late Pleistocene pluvial lakes in response to reduced evaporation and precipitation: Evidence from Lake Surprise, California. *Geological Society of America Bulletin*, *126*(11-12), 1387-1415.

Ibarra, D. E., Oster, J. L., Winnick, M. J., Caves Rugenstein, J. K., Byrne, M. P., & Chamberlain, C. P. (2018). Warm and cold wet states in the western United States during the Pliocene–Pleistocene. *Geology*, *46*(4), 355-358.

Ibarra, D. E., Oster, J. L., Winnick, M.J., Rugenstein, J. K. C., Byrne, M. P., & Chamberlain, C. P. (2018). Lake Area Constraints on Past Hydroclimate in the Western United States:

Application to Pleistocene Lake Bonneville. *Lake Bonneville Geology Conference Proceedings*, 1-8.

Ivanovic, R., Gregoire, L., Kageyama, M., Roche, D., Valdes, P., Burke, A., Drummond, R., Peltier, W & Tarasov, L. (2016). Transient climate simulations of the deglaciation 21-9 thousand years before present (version 1)-PMIP4 Core experiment design and boundary conditions. *Geoscientific Model Development*, 9(7), 2563-2587.

Jones, M. D., Roberts, C. N., & Leng, M. J. (2007). Quantifying climatic change through the last glacial–interglacial transition based on lake isotope palaeohydrology from central Turkey. *Quaternary Research*, *67*(3), 463-473.

Kaufman, A., & Broecker, W. (1965). Comparison of Th230 and C14 ages for carbonate materials from Lakes Lahontan and Bonneville. *Journal of geophysical Research*, *70*(16), 4039-4054.

Kurth, G., Phillips, F. M., Reheis, M. C., Redwine, J. L., & Paces, J. B. (2011). Cosmogenic nuclide and uranium-series dating of old, high shorelines in the western Great Basin, USA. *Geological Society of America Bulletin*, *123*(3-4), 744-768.

Lehner, B., & Grill, G. (2013). Global river hydrography and network routing: baseline data and new approaches to study the world's large river systems. *Hydrological Processes*, *27*(15), 2171-2186.

Lehner, B., Verdin, K., and Jarvis, A. (2008). New Global Hydrography Derived From Spaceborne Elevation Data. *Eos, Transactions American Geophysical Union*, 89(10), 93–94.

Licciardi, J. M. (2001). Chronology of latest Pleistocene lake-level fluctuations in the pluvial Lake Chewaucan basin, Oregon, USA. *Journal of Quaternary Science: Published for the Quaternary Research Association*, *16*(6), 545-553.

Lillquist, K. D. (1994). Late Quaternary Lake Franklin: lacustrine chronology, coastal geomorphology, and hydrostatic deflection in Ruby Valley and northern Butte Valley, Nevada. *Doctoral dissertation, University of Utah, Salt Lake City, Utah*, 2618-2618.

Liu, Z., Otto-Bliesner, B. L., He, F., Brady, E. C., Tomas, R., Clark, P. U., Carlson, A. E., Lynch-Stieglitz, J., Curry, W, & Erickson, D. (2009). Transient simulation of last deglaciation with a new mechanism for Bølling-Allerød warming. *Science*, *325*(5938), 310-314.

Lora, J. M., Mitchell, J. L., & Tripati, A. E. (2016). Abrupt reorganization of North Pacific and western North American climate during the last deglaciation. *Geophysical Research Letters*, *43*(22), 11-796.

Lyle, M., Heusser, L., Ravelo, C., Yamamoto, M., Barron, J., Diffenbaugh, N. S., Herbert, T., & Andreasen, D. (2012). Out of the tropics: the Pacific, Great Basin Lakes, and Late Pleistocene water cycle in the western United States. *Science*, *337*(6102), 1629-1633.

Matsubara, Y., & Howard, A. D. (2009). A spatially explicit model of runoff, evaporation, and lake extent: Application to modern and late Pleistocene lakes in the Great Basin region, western United States. *Water Resources Research*, *45*(6), 1-18.

McGee, D., Moreno-Chamarro, E., Marshall, J., & Galbraith, E. D. (2018). Western US lake expansions during Heinrich stadials linked to Pacific Hadley circulation. *Science advances*, *4*(11), 1-10.

McGee, D., Quade, J., Edwards, R. L., Broecker, W. S., Cheng, H., Reiners, P. W., & Evenson, N. (2012). Lacustrine cave carbonates: Novel archives of paleohydrologic change in the Bonneville Basin (Utah, USA). *Earth and Planetary Science Letters*, *351*, 182-194.

Mering, J. A. (2015). New constraints on water temperature at Lake Bonneville from carbonate clumped isotopes. *Doctoral dissertation, UCLA*. 1-178.

Messager, M.L., Lehner, B., Grill, G., Nedeva, I., and Schmitt, O. (2016). Estimating the volume and age of water stored in global lakes using a geo-statistical approach. *Nature Communications*, 7:13603, 1-11.

Mifflin, M.D., and Wheat, M.M. (1979). Pluvial Lakes and Estimated Pluvial Climates of Nevada. *Nevada Bureau of Mines and Geology Bulletin,* 94, 1-57.

Miller, D. M., Oviatt, C. G., & Mcgeehin, J. P. (2013). Stratigraphy and chronology of Provo shoreline deposits and lake-level implications, Late Pleistocene Lake Bonneville, eastern Great Basin, USA. *Boreas*, *42*(2), 342-361.

Morrill, Carrie, Daniel P. Lowry, and Andrew Hoell. (2018). Thermodynamic and dynamic causes of pluvial conditions during the last glacial maximum in Western North America. *Geophysical Research Letters,* 45(1), 335-345.

Munroe, J. S., & Laabs, B. J. (2013a). Latest Pleistocene history of pluvial Lake Franklin, northeastern Nevada, USA. *GSA Bulletin*, *125*(3-4), 322-342.

Munroe, J. S., & Laabs, B. J. (2013b). Temporal correspondence between pluvial lake highstands in the southwestern US and Heinrich Event 1. *Journal of Quaternary Science*, *28*(1), 49-58.

Nelson, S. T., Wood, M. J., Mayo, A. L., Tingey, D. G., & Eggett D. (2005). Shoreline tufa and tufaglomerate from Pleistocene Lake Bonneville, Utah, USA: stable isotopic and mineralogical records of lake conditions, processes, and climate. *Journal of Quaternary Science*, 20(1), 3-19.

Nishizawa, S., Currey, D. R., Brunelle, A., & Sack, D. (2013). Bonneville basin shoreline records of large lake intervals during Marine Isotope Stage 3 and the Last Glacial Maximum. *Palaeogeography, palaeoclimatology, palaeoecology*, *386*, 374-391.

Oster, J. L., Ibarra, D. E., Winnick, M. J., & Maher, K. (2015). Steering of westerly storms over western North America at the Last Glacial Maximum. *Nature Geoscience*, *8*(3), 201.

Oviatt, C. G., Currey, D. R., & Sack, D. (1992). Radiocarbon chronology of Lake Bonneville, eastern Great Basin, USA. *Palaeogeography, Palaeoclimatology, Palaeoecology*, *99*(3-4), 225-241.

Oviatt, C. G., & Jewell, P. W. (2016). The Bonneville shoreline: reconsidering Gilbert's interpretation. *In Developments in Earth Surface Processes,* 20, 88-104.

Oviatt, C. G. (2015). Chronology of Lake Bonneville, 30,000 to 10,000 yr BP. *Quaternary Science Reviews*, *110*, 166-171.

Oviatt, C. G. (2014). *The Gilbert Episode in the Great Salt Lake Basin, Utah*. Miscellaneous Publication 14-3, Utah Geological Survey.

Petryshyn, V. A., Rivera, M. J., Agić, H., Frantz, C. M., Corsetti, F. A., & Tripati, A. E. (2016). Stromatolites in Walker Lake (Nevada, Great Basin, USA) record climate and lake level changes~ 35,000 years ago. *Palaeogeography, palaeoclimatology, palaeoecology*, *451*, 140-151.

Quirk, B.J., Moore, J. R., Laabs, B.J., Caffee, M. W., & Plummer, M. A. (2018). Termination II, Last Glacial Maximum, and Lateglacial chronologies and paleoclimate from Big Cottonwood Canyon, Wasatch Mountains, Utah. *Bulletin*, 130(11-12), 1889-1902.

Redwine, J. L. (2003). The Quaternary pluvial history and paleoclimate implications of Newark Valley, east-central Nevada, derived from mapping and interpretation of surficial units and geomorphic features. *Doctoral dissertation, Humboldt State University*, 1-385.

Reheis, M. (1999). Highest pluvial-lake shorelines and Pleistocene climate of the western Great Basin. *Quaternary Research*, *52*(2), 196-205.

Reimer, P. J., Bard, E., Bayliss, A., Beck, J. W., Blackwell, P.G., Ramsey, C. B., Buck, C. E., Cheng, H., Edwards, R. L., Friedrich, M., & Grootes. P.M. (2013). IntCal13 and Marine13 radiocarbon age calibration curves 0-50,000 years cal BP. *Radiocarbon*, 55(4), 1869-1887.

Russell, I. C. (1885). *Geological history of Lake Lahontan: a Quaternary lake of northwestern Nevada* (Vol. 11). US Government Printing Office, 6.

Scheff, J., & Frierson, D. M. (2012). Robust future precipitation declines in CMIP5 largely reflect the poleward expansion of model subtropical dry zones. *Geophysical Research Letters*, *39*(18), 6p.

Seager, R., & Vecchi, G. A. (2010). Greenhouse warming and the 21st century hydroclimate of southwestern North America. *Proceedings of the National Academy of Sciences*, 107(50), 21277-21282.

Stuiver, M., & Polach, H. A. (1977). Discussion reporting of 14 C data. *Radiocarbon*, *19*(3), 355-363.

Suarez, M. B., & Passey, B. H. (2014). Assessment of the clumped isotope composition of fossil bone carbonate as a recorder of subsurface temperatures. *Geochimica et Cosmochimica Acta*, *140*, 142-159.

Tripati, A. K., Eagle, R. A., Thiagarajan, N., Gagnon, A. C., Bauch, H., Halloran, P. R., & Eiler, J. M. (2010). 13C–18O isotope signatures and 'clumped isotope thermometry in foraminifera and coccoliths. *Geochimica et cosmochimica acta*, *74*(20), 5697-5717.

Clumped isotope Constraints on Increased Effective Moisture in the Northwest Great Basin, Lake Surprise

Lauren Santi[1], Alexandrea Arnold[1], Daniel E. Ibarra[2],

Chloe Whicker[1], John Mering[1,3], Rico Lomarda[1], Juan M. Lora[1,4], Aradhna Tripati[1]

[1] Department of Earth, Planetary, and Space Sciences, Department of Atmospheric and Oceanic Sciences, Institute of the Environment and Sustainability, Center for Diverse Leadership in Science, University of California, Los Angeles, California, USA

[2] Department of Geological Sciences, Stanford University, Stanford, California, USA

[3] School of Science, University of Waikato, Hamilton, New Zealand

[4] Department of Geology and Geophysics, Yale University, New Haven, Connecticut, USA

ABSTRACT

The transition in the American Southwest from lakes in the late Pleistocene to modern aridity implies large changes in the regional water cycle, but whether changes in hydrology were driven by increased precipitation rates due to changes in atmospheric dynamics, decreased evaporation rates resulting from temperature depression and lowered solar insolation, or some combination of the two, remains uncertain. Here we report thermodynamically-derived estimates of changes in temperature, precipitation, and lake evaporation rates, as well as the isotopic composition of precipitation, using clumped isotope data from an ancient lake in the northwestern Great Basin. We use our thermodynamic estimates to evaluate the prediction skill of ten climate models in regional predictions for these variables. Our reconstructions indicate the disappearance of Lake Surprise coincided with decreasing evaporation rates. Since the LGM, precipitation rates have also increased, possibly due to a shift in storm tracks and/or a change in the average landfall location of atmospheric rivers.

INTRODUCTION

The American West is characterized by its aridity and low precipitation, with many regions receiving less than 250 mm of rain per year. Furthermore, this region is projected to become even drier with ongoing anthropogenic warming (Maloney et al., 2013). During the Last Glacial Maximum (LGM; ~23,000-19,000 years ago) and subsequent deglaciation (~19,000-11,000 years ago), the sedimentary record and landscape geomorphology indicate that the region was much wetter and marked by extensive lake systems in most inward-draining basins (Mifflin & Wheat, 1979; Reheis, 1999). Paleo-shoreline observations indicate that where these lakes once existed, dry salt flats now instead mark the landscape (Supplementary Fig. 2.S1). This dramatic change in hydroclimate has motivated substantial work on the response of regional climate to glacial-deglaciation transitions. This geological transition is also of interest because it can shed light on the accuracy of climate models used for simulating temperature, precipitation, and evaporation changes in the past and future.

There are multiple hypotheses on the timing and importance of various mechanisms driving changes in regional hydroclimate in the Southwest. In the present day, the northeastern Great Basin has the highest seasonal precipitation in the winter months. Hence, one group of hypotheses have centered around the response of the mid-latitude jet stream and storm track to changing climate forcing (e.g. Hostetler & Benson, 1990; Kirby et al., 2013; Munroe & Laabs, 2013); a related hypothesis highlights changes in atmospheric rivers and concomitant changes in atmospheric moisture convergence (Lora et al., 2017; Lora, 2018). Field and modeling studies hypothesize that both the strength and position of the jet stream could be important: it is thought that the Laurentide ice sheet deflected the jet stream south during the LGM, shifting the storm track and resulting in a tendency for lake highstands to occur along a SE-NW trend, modulated

by ice sheet regression during the deglacial (e.g. Lyle et al., 2012; Oster et al., 2015; McGee et al., 2018).

Previous compilations of lake hydrographs for a range of pluvial lakes do, in fact, suggest that deglacial lake highstands did not occur simultaneously; instead, changes in regional hydrology may have occurred earlier in the southeast, progressing to the northwest through time (e.g. Lyle et al., 2012; Ibarra et al., 2014; Hudson et al., 2017; McGee et al. 2018; Santi et al., 2019). A closer look indicates that this interpretation may be an oversimplification of the process; Wong et al. (2016) suggest that the intensity of the storm track (in terms of low level eddy kinetic energy) was controlled by meltwater fluxes from the ice sheet, which altered the meridional temperature gradient and circulation in the eastern Pacific; Lora et al. (2016) also find that a strengthened jet stream during the early deglaciation resulted in higher precipitation along most of the west coast. Other studies suggest alternative moisture sources were important during the LGM, like increased summer precipitation (Lyle et al., 2012), and changes in evaporation rates (Kirby et al., 2013; Ibarra et al., 2014).

There is also proxy-derived evidence of evaporation depression occurring in Lakes Bonneville and Lahontan (e.g. Mifflin & Wheat, 1979; Kaufman, 2003; Mering, 2015), and in the Great Basin as a whole (Smith & Street-Perrot, 1983). Climate models indicate LGM increases in both summer and winter effective precipitation, P-E, in the region, but driven both by decreased evaporation and increased precipitation, as controlled by various components of the moisture budget (Lora, 2018). Although there are a number of circulation changes that have been suggested to explain the observed changes in hydroclimate, it has been difficult to robustly test them because of a lack of data constraining evaporation rates and precipitation rates.

From a mass balance perspective, lake growth or reduction is achieved primarily via changes in precipitation, evaporation, or a combination of the two (Mifflin & Wheat, 1979; Matsubara & Howard, 2009; Broecker, 2010). Various proxy evidence from the LGM and deglacial period (e.g. packrat middens, halite inclusions, tree lines, and pollen) indicate cold and wet conditions (Galloway, 1970; Lowenstein et al., 1998; Matsubara & Howard, 2009; Thomson et al., 1999). While studies have attempted to quantify past evaporation and precipitation rates, invoking either reduced or elevated precipitation rates compared to modern, and reduced evaporation rates compared to modern values (Matsubara & Howard, 2009; Ibarra et al., 2014), there is significant uncertainty associated with these measurements, largely due to a lack of accurate constraints on temperature or on water $\delta^{18}O$. Therefore, values for reconstructed precipitation rates range from 80-260% of modern and evaporation rates span 12-90% of modern values, with temperature depressions anywhere from 3-15 ℃ (e.g. Matsubara & Howard, 2009; Ibarra et al., 2014).

In this work, we use clumped isotopes, a thermodynamically-based tool for estimating carbonate precipitation temperatures (Ghosh et al., 2006; Schauble et al., 2006; Eiler, 2007; Bernasconi et al., 2018), in order to constrain past temperature and water isotope changes during the LGM and deglaciation for Lake Surprise, located in the northwest Great Basin. This small lake is in a hydrologic transition zone between the Great Basin and the Pacific Northwest. Our sediment geochemistry-derived data are combined with different sets of assumptions within a hydrological modelling framework to estimate precipitation and basin-wide evaporation rates, producing estimates that are thermodynamically-based. We use these results in concert with information on lake level fluctuations to test hypotheses about the timing and magnitude of hydroclimate changes, and to evaluate climate model skill. We compare clumped-isotope derived

results to published pollen-derived estimates of past hydroclimate (Bartlein et al., 2011; Lora et al., 2017).

BACKGROUND

Geologic and Climatic Setting of Surprise Valley, California

Lake Surprise was located in the northwest Great Basin, along the borders of Nevada and California, contained within the modern Surprise Valley (Supplementary Fig. 2.S1). At its greatest extent, Lake Surprise covered 1366 km^2, or ~36% of its respective watershed (e.g. Russell, 1927; Reheis, 1999; Personius et al., 2009; Ibarra et al., 2014; Egger et al., 2018). In contrast to these former hydrological conditions, potential evaporation now vastly exceeds precipitation; basin-wide average precipitation and pan evaporation rates are 566±165 mm/yr and 905±80 mm/yr, respectively (Ibarra et al., 2014). As a result, modern Surprise Valley has the same arid climate that characterizes much of the Great Basin; however, due to its proximity to the Pacific northwest, it receives more precipitation than the southern Great Basin (Guirguis & Avissar, 2008).

Previous Work on past Hydroclimate in Surprise Valley, California

Published studies of Lake Surprise tracked the evolution of the lake shoreline through time, finding an abrupt increase in effective precipitation leading to the lake highstand at 16 ka, followed by a much slower decline in lake levels (Ibarra et al., 2014; Egger et al., 2018; Santi et al., 2019). Ibarra et al. (2014) used the timing of lake level fluctuations and carbonate oxygen isotope measurements to constrain a mass balance model for precipitation rates, but did not have constraints on temperature or water $\delta^{18}O$. Regional pollen studies also provide nearby constraints

on past precipitation rates; pollen data from a locality 4° north of pluvial Lake Surprise supports a local decrease in precipitation rates since the LGM, the magnitude of which is greater than the average decrease across the Great Basin (Bartlein et al., 2011).

Carbonate Clumped Isotope Thermometry

Carbonate clumped isotope thermometry is a geochemical method to constrain past temperatures that can be applied to sediments (e.g. Ghosh et al., 2006; Eiler, 2007; Tripati et al., 2010; Bernasconi et al., 2018). It is based on the measurement of the overabundance of "clumped" or doubly-substituted bonds in carbonate groups of minerals (^{13}C-^{18}O-^{16}O) above their stochastic distributions, which is temperature dependent (Ghosh et al., 2006; Schauble et al., 2006). Gas source mass spectrometry of CO_2 produced through the digestion of carbonate in orthophosphoric acid is used to determine the abundance of the doubly-substituted isotopologue with a mass of 47 amu (^{13}C-^{18}O-^{16}O), and the overabundance of this isotopologue in a sample (relative to a stochastic value) is denoted by Δ_{47}, defined as:

$$\Delta_{47}\,(‰) = [(R^{47}/(R^{47}_{stochastic}) - 1) - (R^{46}/(R^{46}_{stochastic}) - 1) - (R^{45}/(R^{45}_{stochastic}) - 1)] \times 1000$$

Equation 1

The utility of clumped isotope analysis lies in the thermodynamic preference for clumped bonds to occur at certain temperatures; clumping decreases with increased temperature, and this trend scales with $1/T^2$ (T in Kelvin). The isotope exchange reaction that forms clumped bonds:

$$Ca^{12}C^{18}O^{16}O_2 + {}^{13}Ca^{16}O_3 \rightarrow Ca^{13}C^{18}O^{16}O_2 + Ca^{12}C^{16}O_3$$

Equation 2

takes place at equilibrium within a single phase, with lower temperatures favoring a greater abundance of ^{13}C-^{18}O "clumped" bonds (Schauble et al., 2006). Hence, the temperature of carbonate formation can be determined from the Δ_{47} parameter, without knowledge of the isotopic composition of the fluid in which a given sample formed.

In the years since the publication of the first clumped isotope measurements of CO_2 (Eiler & Schauble, 2014) and carbonate minerals (Ghosh et al., 2006), the field of carbonate clumped isotope geochemistry has evolved. Calibrations have been published that incorporate data from numerous studies relating empirical predictions (Ghosh et al., 2006), measurement of laboratory synthesized carbonate (Kelson et al., 2017; Bernasconi et al., 2018), and studies in modern well-constrained carbonate forming environments (Tripati et al., 2010). The community has explored interlaboratory offsets (Dennis et al., 2011) and identified best practices, including sample pre-cleaning for some types of samples (Tripati et al., 2010) and identifying that most calibration discrepancies are due to differences in standardization protocols and data handling (Dennis et al., 2011; Bernasconi et al., 2018). For this work, we use the calibration of Bernasconi et al. (2018) because it uses the same carbonate standard-based reference frame as our data.

METHODOLOGY

Samples

We measured the stable and clumped isotope composition of 1 modern sample and 35 older carbonate (tufa) samples from Surprise Valley. These samples were described and ages determined using radiocarbon and/or uranium-series measurements in prior publications, and are also described in Supplement Table 2.S1 (Ibarra et al., 2014; Egger et al., 2018; Santi et al.,

2019). We use gas source mass spectrometry for clumped isotope (Δ_{47}) analysis, which simultaneously provides carbonate $\delta^{13}C$ and $\delta^{18}O$.

Age estimates

For all radiocarbon results, we use *IntCal13* to convert conventional ^{14}C ages to calibrated ^{14}C ages, expressed as thousands of years before present, "ka" (Supplemental Table 2.S1). We plot the median calibrated probability and the 2σ uncertainty.

Clumped Isotope Constrained Model for Precipitation and Evaporation

To model the hydroclimate drivers of Lake Surprise, we combine the clumped isotope-constrained precipitation and evaporation (P and E) modeling approach used by Mering (2015) on Lake Bonneville, with the isotope mass balance model of Ibarra et al. (2014) used for Surprise Valley, which was modified from Jones et al. (2007). Similar isotope-based mass balance approaches have been applied to both modern transient and Pleistocene steady-state calculations for other mid-latitude lake systems in the western United States and Europe (*cf.* Jones et al., 2007; Ibarra et al., 2014), but fundamentally have lacked a thermodynamic constraint on temperature or robust estimate of water $\delta^{18}O$. We also include calculations from two additional empirically-derived equations for P and E in the Supplement (Matsubara & Howard, 2009). We note that the latter empirical equations depend only on temperature, and are thus not as robust as the precipitation and evaporation results reported in the main text.

We calculate evaporation rates using a modified Penman equation for lake evaporation (Linacre, 1993), as done in previous Great Basin paleoclimate analyses (e.g. Ibarra et al., 2014; Mering, 2015). This equation uses mean annual air temperatures (MAATs) derived from

clumped isotopes and a warm-season (April - October; AMJJASO) water to air transfer function (Hren & Sheldon, 2012) (See Supplement).

For precipitation estimates, we first determine the runoff coefficient, K_{run}, using a Budyko relationship, as proposed by Broecker (2010), to constrain covariation between precipitation and K_{run}. We model evaporating vapor $\delta^{18}O$ based on the Craig & Gordon (1965) evaporation model (as simplified by Gat, 1996). To evaluate uncertainty, we carry out a Monte Carlo procedure (n=2,500 calculations per sample). We include sensitivity analyses for our inputs of wind speed ("u"), $\delta^{18}O$ of precipitation ("$\delta^{18}O$"), Budyko landscape parameter ("ω"), and relative humidity ("RH"). For the sensitivity analysis, we set each "constant" parameter to its mean value, and vary a single input parameter within a reasonable range of values, as implied by the 1σ uncertainty of the input variable.

Reconstructed lake evaporation rates are converted to weighted evaporation rates for more direct comparison to evapotranspiration ("ET") output from steady-state models. We assign weights to lake evaporation rates based on the size of the lake area, and to ET over land (ET as estimated in our precipitation model), based on the size of the tributary area. The Supplement describes the modeling equations used and their adaptation for Lake Surprise.

RESULTS

Shoreline Geochronology and Carbonate $\delta^{18}O$ and $\delta^{13}C$ Ratios

A synthesis of Lake Surprise elevations (Fig. 2.1a) shows a rapid rise in lake levels occurring in less than 500 years, culminating in a highstand at 16 ka (Santi et al., 2019). This rapid rise in lake levels is seen in several other late Pleistocene pluvial lakes, including Lake Franklin and Lake Lahontan (e.g. Benson et al., 2013; Munroe & Laabs, 2013; Santi et al.,

2019), and at Lake Surprise, is followed by a slow decline over the next ~5 ka. There is significant variation in carbonate and water $\delta^{18}O$, occurring on a ~1000 year timescale, with quasi-periodic behavior during the LGM (Figs. 2.1b & 2.2b, respectively). There are local minima in carbonate and water $\delta^{18}O$, coincident with the lake highstand, with increasing values following the lake highstand at 16 ka. At the same time, there is little evidence for temporal variability in carbonate $\delta^{13}C$ (Fig. 2.1c). The strong positive covariance between carbonate $\delta^{13}C$ and carbonate $\delta^{18}O$ observed in these data for Lake Surprise (Fig. 2.1d) is consistent with closed basin behavior and evaporative enrichment, indicating the lake system is appropriate for steady-state isotopic analysis (e.g. Talbot 1990; Ibarra et al., 2014; Horton et al., 2016).

Clumped Isotope Constraints on Past Hydroclimates

Analysis of modern microbialites and tufas, and other types of lacustrine carbonates indicate this proxy can be robustly used to reconstruct temperature, with growth temperatures typically indicating formation in the summer or spring through fall (Petryshyn et al., 2015; Horton et al., 2016; Bernasconi et al., 2018). Our modern carbonate sample implies a present-day water temperature of 17.6± 2℃, while our LGM samples indicate an average past water temperature of 10.2± 1℃. Using a water to air transfer function (Hren & Sheldon, 2012; see Supplement), our calculated modern water temperature translates to a modern MAAT of 10.3± 2℃, while our LGM samples correspond to an average MAAT of 0.3± 1℃. Our modern MAAT is similar to annually-averaged modern temperature at nearby Cedarville, CA (9.2± 1℃), suggesting that our calibration and transfer functions are able to accurately constrain MAAT. The offset between modern MAAT from Cedarville, CA and our LGM MAAT indicates 8.9± 1.4℃ of air warming since the LGM.

To a first order, reconstructed water temperatures appear relatively constant throughout the LGM, but show a slight decrease during the early to mid-deglacial, and a local minimum at ~16 ka, roughly coincident with the lake highstand (Fig. 2.2a). With the exception of one LGM-aged sample, all data indicates that water temperatures were lower than modern, as estimated using our modern sample.

In Figs. 2.2c-2.2d, we show reconstructed precipitation and weighted evaporation rates. Reconstructed precipitation rates are close to their modern values during the LGM, and stabilize during the deglacial period, to slightly below their modern value of 566 $\pm$165 mm/yr. Weighted evaporation rates decrease throughout the LGM and stabilize during the deglacial period, and are below the modern pan evaporation rate at Lake Surprise as well as the modern lake evaporation rates at several extant Great Basin lakes (e.g. The Great Salt Lake, Salton Sea, Mono Lake; Meyers, 1962).

Pollen Derived Estimates of Precipitation

Compilations of proxy data provide an invaluable means to quantify past climate, as each proxy is likely sensitive to different components of the water balance. For example, pollen data is thought to be sensitive to changes in available energy during growing seasons, while lake level fluctuations likely reflect changes in effective moisture, or P-E (Liu et al., 2018). Pollen data have already been used to provide robust quantitative paleoclimate estimates at both regional and global scales (Bartlein et al., 2011; Izumi & Bartlein, 2016), and have been compared and evaluated against other proxy estimates and results from steady state model simulations (e.g. Matsubara & Howard, 2009; Lora et al., 2017; Liu et al., 2018).

For our analysis, we compare precipitation anomalies derived from clumped isotope analysis to pollen and plant macrofossil precipitation anomalies from Bartlein et al. (2011), who include multiple estimates within the Great Basin. These estimates indicate precipitation anomalies (LGM minus modern) ranging from -1235 to 721 mm/yr, with a mean of -138 $\pm$ 545 mm/yr. Hence, while pollen anomalies show a wide degree of variability, they also indicate an overall decrease in regional precipitation rates during the LGM, in spite of the continued existence and growth of lakes.

Evaluation of Climate Model Simulations of Hydroclimate Change

We compare our results to simulations carried out by nine models that participated in the Paleoclimate Modelling Intercomparison Project, phase 3 (PMIP3). PMIP3 produced equilibrium simulations for the LGM (21 ka) and the mid Holocene (6 ka). A caveat is that with only two reference points bracketing the LGM and deglacial period, it is difficult to make detailed assessments of earth climate responses to glacial-deglacial conditions, and to evaluate changes to water balance at local (i.e. lake basin) or regional scales (i.e. Western North America). Previous work comparing PMIP precipitation simulations for the LGM indicate a general lack of agreement between models (Oster et al., 2015; Lora et al., 2017; Lora, 2018), and thus the comparison of model results to proxy data offers an opportunity to evaluate model skill (e.g. Hargreaves et al., 2013; Lora et al., 2017; Lora, 2018).

As a method of visually assessing individual climate model skill, we compare MAAT anomalies from clumped isotope analysis to MAAT temperature anomalies from steady-state PMIP3 climate model simulations for the LGM and pre-industrial era (Fig. 2.3). From clumped isotope analysis, we estimate an 8.9$\pm$ 1.4℃ anomaly from LGM-averaged MAAT (0.3℃) and

modern MAAT at Cedarville, CA (9.2℃). In Figs. 2.4-2.5, we similarly compare average precipitation and weighted evaporation anomalies for all Lake Surprise samples (23-19 ka), to anomalies from PMIP3 simulations, with LGM-averaged precipitation and evaporation anomalies of -76±185 mm/yr and -368± 100 mm/yr, respectively.

Following Hargreaves et al. (2013), we quantitatively evaluate climate model skill using an equation that weighs the ability of individual climate models to simulate the Earth's changing climate, as implied by clumped isotope results for MAAT, precipitation rate, and weighted evaporation rate (Fig. 2.6; Equation S12). Negative and zero values indicate that the models have little or no skill in reproducing Earth's climatic response, while numbers approaching the maximum value of one indicate a high degree of model skill. We calculate model skill for steady-state PMIP3 models and one transient climate model: Transient Climate Evolution (TraCE) using the Community Climate System Model Version 3 (CCSM3) (e.g., Lora, 2016). On average, PMIP3 and TraCE demonstrate consistently moderate skill (~0.3-0.5) in reproducing past temperature and evaporation rates, with more variable skill in reproducing past precipitation rates: six models show slight skill in reproducing precipitation rates, while four have negative skill. Temperature, evaporation, and precipitation model skill averages are 0.44, 0.27, and -0.25, respectively.

Potential Sensitivity of Results to Modeling Assumptions

Our isotope mass balance model relies on several assumptions regarding input parameters. We assume that RH, $\delta^{18}O$ of precipitation, u, and ω (which describes the partitioning of rainfall into runoff) at the LGM were identical to modern values. We include a model sensitivity analysis to show the effect of varying each of these four parameters within reasonable

ranges. Otherwise, the remaining input variables are set to their mean modern values (RH= 0.58, u =1.9 m/s, $\delta^{18}O$ of precipitation = -14.57‰, ω = 2.6). We show this sensitivity two ways: 1) We first average all sample $\delta^{18}O$, $\delta^{13}C$, elevation, and water temperature input values and create a new "average sample" on which to apply our analysis, and 2) we perform the sensitivity analysis on each individual sample (n = 35), and plot the median y-values.

DISCUSSION

Shoreline Geochronology and Carbonate $\delta^{18}O$ and $\delta^{13}C$ Ratios

The lake hydrograph for Lake Surprise (Fig. 2.1a) indicates there was a rapid increase in lake levels at 16 ka, suggesting a large and rapid change in effective precipitation that is also observed in neighboring pluvial lakes (Ibarra et al., 2014; Santi et al., 2019). While there are many possible causes for this abrupt change in effective moisture, we hypothesize that it may be indicative of a rapid acceleration of ice sheet regression, which is thought to have begun ~15 ka (Lora et al., 2016). This alteration in ice sheet extent would likely be associated with a shift in the storm track or a change in the average landfall location of atmospheric rivers, both of which could increase effective moisture.

In contrast to its rapid rise, the lake regression is much more prolonged, which is a notable point of contrast to other late-Pleistocene lakes, including Lake Franklin, Lake Chewaucan, and Lake Lahontan (e.g. Santi et al., 2019). We suggest that this gradual decrease in lake levels could be due to the significant depth of Lake Surprise at its maximum extent (~180 m, versus ~90 m for nearby Lake Chewaucan; Egger et al., 2018), its high hydrologic index compared to more southerly lakes Franklin, Lahontan, and Bonneville (Santi et al., 2019), or the

relative lack of western-boundary orographic barriers, compared to other lake basins (e.g. the southern Cascades to the west of Lake Chewaucan) (Egger et al., 2018).

Clumped Isotope Constraints on Past Hydroclimates

We estimate 7.4±2.2℃ of water warming and 8.9±1.4℃ of air warming since the LGM at Lake Surprise. As a point of comparison, nearby Lake Chewaucan tufas have been used to reconstruct mean annual lake temperature for the modern (13 ± 2℃) and LGM (6.2 ± 2℃) (Hudson et al., 2017); indicating 6.8±2.8℃ of lake water warming, and 10.0±2.8℃ of air warming since the LGM (Hren & Sheldon, 2012). Our temperature anomaly of 8.9±1.4℃ is thus consistent with reconstructions from nearby Lake Chewaucan, and also with Great Basin temperature depressions estimated from pollen (10-11℃; Galloway, 1970), hydrologic mass balance modeling (10℃; Smith & Street-Perrot, 1983), and packrat midden plant assemblages (8℃; Thompson et al., 1999).

Our reconstructed shift in water $\delta^{18}O$ of ~4‰ (Fig. 2.2b) could be due to changes in the dominant lake moisture source; for example, the $\delta^{18}O$ of water associated with the North Pacific storm track is isotopically depleted relative to the $\delta^{18}O$ of water associated with atmospheric rivers (e.g. Welker et al., 2012). We also note that summer precipitation is isotopically enriched relative to winter precipitation, so this pattern could reflect a shift in the seasonality of precipitation (Welker et al., 2012). A ~4‰ change in water $\delta^{18}O$ could alternatively be explained by decreasing temperature, with a change of -0.24‰ to -0.48‰ per ℃ expected for water cooling from a starting temperature of 20℃ (Dansgaard, 1964). We view a 4‰ change in water $\delta^{18}O$ as viable, as the isotopic composition of lakes is known to change on the order of 10-15‰

on geologic time scales, due to variation in both precipitation source and temperature (e.g. Edwards & McAndrews, 1989; Wolfe et al., 2007).

To a first order, weighted evaporation rates at Lake Surprise decrease throughout the LGM and deglaciation, stabilizing below the modern pan evaporation rate of 905 mm/yr by ~20 ka (Fig. 2.2d). While these weighted evaporation rates may not be directly comparable to pan evaporation rates, we interpret the sign of evaporation change as evidence of evaporation depression as a main cause of lake growth in the region. Further, we note that our deglacial evaporation rates at Lake Surprise are below modern lake evaporation rates at the Great Salt Lake (1070 mm/yr), the Salton Sea (2032 mm/yr), and Mono Lake (915 mm/yr; Meyers, 1962).

There are several potential sources of uncertainty in any equation used to estimate evaporation rates. Empirical equations for evaporation are typically reliant on three main categories of controlling parameters: water supply, energy for evaporation, and water vapor transport. The first of these, water supply, can limit evaporation rates in water-scarce or arid regions, or in locations where the evaporating surfaces are frozen over. If Lake Surprise was frozen for significant portions of each year, actual evaporation rates would have been lower than our results suggest. However, since our calculated evaporation rates are already lower than modern pan evaporation rates, and decrease throughout the LGM and deglacial periods, our conclusions would not be significantly altered if we are overestimating lake evaporation.

Our formulation for lake evaporation instead incorporates measurements constraining the latter two parameters: energy for evaporation, and water vapor transport. Inputs of temperature, latitude, and elevation all impact the amount of incoming energy for evaporation. As latitude and elevation have not changed significantly through time, Δ_{47} derived temperature is how net radiation (and thus, available energy) is altered in this equation.

Water vapor transport is also included in many models for evaporation, as it provides a mechanism to remove saturated air from above the evaporating surface. Many evaporation models incorporate measurements of wind speed, relative humidity, or vapor pressure deficit into evaporation estimates. Our lake evaporation model incorporates estimates of surface wind speed, as this is commonly measured at weather stations across the United States. As past wind speed is not a straightforward variable to constrain, we use modern wind speed instead, but include this parameter in our sensitivity analysis in the Supplement (Fig. 2.S2-2.S3).

In Fig. 2.2c, we show estimates of past precipitation rates using our isotope mass balance model. We find precipitation rates to be initially elevated relative to modern; however, by the time of the lake highstand at 16 ka, calculated precipitation falls to below modern values. This finding is significant, as it implies that lake growth (and increased effective moisture) was achieved despite a below-modern precipitation rate. Lowered precipitation rates during the deglacial period are consistent with our lowered lake evaporation rates, as steady-state requires a long-term balance between inputs and outputs. While the rapid lake growth at 16 ka suggested by our data (106 m in ~500 years) does require a significant short-term surplus of precipitation over evaporation, the fast timescale over which lake transgression occurred (Fig. 2.1a) coupled with the comparatively course sampling resolution of our data, could explain why this positive P-E anomaly is not reflected in Fig. 2.1.

Comparison with Pollen and other Proxy Data

Existing Great Basin proxy estimates are summarized in Matsubara & Howard, 2009 (their Table 1). Our thermodynamically-derived LGM-average precipitation rates (490 mm/yr; 80% of modern) are in line with most Great Basin estimates calculated using different types of

proxies, while also helping to more accurately constrain the sign of changes which was previously unclear. Prior reconstructions indicate moderate levels of precipitation during the LGM, relative to modern, with some supporting less precipitation (e.g. 80% of modern, Galloway et al., 1970), the same (100% of modern, Hostetler et al.,1994), or more precipitation (120% of modern, Lemons et al.,1996; 130% of modern, Ibarra et al., 2014).

Fig. 2.4 shows a direct comparison of our proxy-derived precipitation anomalies to those derived from pollen across the Great Basin. Pollen precipitation anomalies indicate both wetter and drier LGM conditions (Bartlein et al., 2011). We calculate a small precipitation anomaly at Lake Surprise, indicating slightly less precipitation during the LGM. Our estimate is similar to a pollen estimate at a similar longitude, but at 45°N.

Our estimates of LGM and deglacial weighted evaporation rates are much lower than modern lake evaporation rates in the Great Salt Lake (1070 mm/yr), the Salton Sea (2032 mm/yr), and Mono Lake (915 mm/yr; Meyer, 1962), as well as the modern pan evaporation rate at Lake Surprise (905 mm/yr). Similar to precipitation rates, our data indicate decreasing weighted evaporation rates throughout the LGM and deglacial periods (Fig. 2.2d). This trend of LGM evaporation change is consistent with mass balance models (-10%; Mifflin & Wheat, 1979), thermal evaporation models (-42%, Hostetler & Benson, 1990), and tree lines/pollen (-50%, Galloway et al., 1970), providing evidence of evaporation depression as a cause of deglacial lake growth.

Evaluation of Climate Model Simulations of Hydroclimate Change

PMIP3

Fig. 2.3 shows the surface temperature anomaly between the LGM and preindustrial era, as reproduced by PMIP3 and clumped isotope data. We find reasonable model-data agreement (±2℃) for all PMIP3 models, with all models and proxy data suggesting LGM temperature depression.

In Fig. 2.4, we plot the precipitation anomalies reproduced by both PMIP3 and proxy data. Using our LGM samples from Lake Surprise, we find robust evidence for a negative precipitation anomaly. This finding is significant, as most PMIP3 climate models show a transition from wetter-than-modern to drier-than-modern climates along a line that is projected through northern CA. The exact latitude of this transition zone varies between models; CNRM-CM5 shows this transition along the CA/NV border at Lake Tahoe, while NCAR CCSM4 shows this transition occurring along the border at the approximate location of Lake Surprise. With respect to our LGM precipitation average (~80% of modern), we infer that Lake Surprise may have been located near this transition zone. We find good model-data agreement (±100 mm/yr) for 6/9 PMIP3 models, with model-data discrepancies >100 mm/yr for NCAR-CCSM4, IPSL-CM5A-LR, and MIROC-ESM. Regardless, most PMIP3 anomalies are within analytical error calculated for our Lake Surprise precipitation anomaly ($\pm$ 185 mm/yr).

In Fig. 2.5, we plot the average weighted evaporation anomaly, as reproduced by PMIP3 and proxy data. We find the best model-data agreement (±100 mm/yr) for MIROC-ESM and MRI-CGCM3, though all models agree on the sign of the evaporation anomaly (negative). Overall, MRI-CGCM3 shows the best qualitative agreement with proxy reconstructions of T, P,

and E using clumped isotopes, indicating moderate to low precipitation rates, and lowered evaporation rates during the deglacial period and the transgression of Lake Surprise.

Model Skill

We report model skill for temperature, precipitation rate, and weighted evaporation, for both steady-state (PMIP3) and transient (TraCE) climate models (Fig. 2.6). With regard to temperature, we calculate positive model skill for all models, with a 10-member average of 0.42. We calculate positive model skill for precipitation in 6/10 models; these six models have an average model skill of 0.08. However, the 10-member ensemble mean for precipitation has an average model skill of -0.25, due to poor model skill calculated for NCAR CCSM4, FGOALS, IPSL-CM5A-LR, and MIROC-ESM.

A similar assessment of climate model skill in the Great Basin was performed by Lora (2018), who compiled proxy estimates from sediment yields (Lemons et al.,1996), pollen and plant macrofossils (Bartlein et al., 2011), tufa (Ibarra et al., 2014), and uranium isotopes (Maher et al., 2014). Similar to Lora (2018), our top performing models with respect to precipitation include COSMOS, CNRM-CM5, MRI-CGCM3, while underperforming models include MIROC-ESM and NCAR CCSM4. Unlike Lora (2018), GISS-E2-R (p150) demonstrates positive model skill in this study, while FGOALS indicates negative model skill. However, as Lake Surprise lies along a sharp precipitation gradient in both of these PMIP3 model simulations (Fig. 2.4), we note that our calculation of model skill is limited by the spatial resolution of model output, and is sensitive to the exact model coordinates chosen as the centroid of Lake Surprise.

As PMIP3 provides estimates of evapotranspiration (ET), we assess model skill in terms of weighted evaporation derived from lake evaporation, rather than lake evaporation itself (See

Supplement). When compared to weighted evaporation rates from proxy data, we show consistent positive model skill for all PMIP3 evapotranspiration simulations. Overall, all PMIP3 models and our data suggest significant evaporation depression during the LGM. The highest-performing models—NCAR CCSM4, GISS-E2-R (p150), and MPI-ESM-P—and our data predict ~200-300 mm/yr of evaporation depression during the LGM.

Potential Sensitivity of Results to Modeling Assumptions

Evaporation (Fig. 2.S2 in Supplement)

As relative humidity is increased from 45 to 65%, projected lake evaporation decreases, due to a smaller moisture gradient between the lake surface and overlying air. One assumption we make in our usage of the Linacre (1993) equation for evaporation is a constant difference between air and dew point temperatures, which itself is influenced by relative humidity. However, we note that elevated humidity would cause dew point temperature to fall closer to air temperature, resulting in lower calculated evaporation rates. Hence, even if LGM relative humidity were higher than modern values, our main conclusion (lowered evaporation rates) would remain the same.

As we increase input wind speed from 0 m/s to 6 m/s, our projected lake evaporation rate increases. This evaporation increase occurs for similar reasons as the change resulting from relative humidity; strong winds can drive evaporation by removing saturated air and increasing the vapor pressure deficit between the air and evaporating surface. Although modest increases in LGM wind speed have been modeled over water (e.g. Lora et al., 2016), these changes have not been found over land near Lake Surprise, at least not on a fine enough spatial scale. Calculations of evaporation rate are insensitive to input values for water $\delta^{18}O$ or ω.

Precipitation (Fig. 2.S3 in Supplement)

Similar to evaporation rates, precipitation rates are negatively correlated with relative humidity and positively correlated to wind speed. This is not necessarily an intuitive meteorological outcome, but is due to the inclusion of lake evaporation in the numerator of our calculation of precipitation rate (Equation S7). We find that water $\delta^{18}O$ and modeled precipitation are positively correlated with precipitation rate. The total range of input water $\delta^{18}O$ comes from modern tap water, wells, springs, and rivers. As water $\delta^{18}O$ is dependent on relative humidity, atmospheric water source, and other factors, there may be some temporal variability in water $\delta^{18}O$, which is why it is included in this analysis. Our model is reasonably sensitive to changes in input water $\delta^{18}O$, over a 4‰ range, our resulting precipitation rates roughly double. One benefit of clumped isotope analysis is it allows for independent constraints on water $\delta^{18}O$ (Fig. 2.2b). We show that lake $\delta^{18}O$ varies by $\lesssim$4‰ for the duration of our analysis.

Finally, precipitation and ω are positively correlated. The total range of ω for this sensitivity analysis is chosen based on the range of interpolated values in Greve et al. (2015) for western North America ($2 \lesssim \omega \lesssim 3$). Our mean input value ($\omega = 2.6$) is reasonable for the modern western US as a whole, although this parameter is sensitive to changes in vegetation and aridity, both of which have changed over the last ~20 ka (e.g. Madsen et al., 2001; Greve et al., 2015). Overall, post-LGM precipitation rates are not significantly elevated relative to modern values, unless we assume wind speeds were ~50% greater during the LGM and deglacial period, relative to modern, for which there is no evidence to support.

CONCLUSIONS

Constraining the timing of lake highstands has important implications for understanding the terrestrial and atmospheric processes that transport moisture and impart changes on the basin-scale hydrological cycle. We use previously compiled lake level histories to summarize major events in the growth and decay of late-Pleistocene Lake Surprise. We see evidence of a fast lake transgression at ~16 ka, suggesting a large effective precipitation forcing. While the abruptness of this lake transgression is similar to nearby Lakes Lahontan and Chewaucan, the regression of Lake Surprise occurs more gradually than in these lake basins. We suggest this slow regression may be due to lake geometry, with both lake depth and hydrologic index playing a role, or due to the smaller orographic barriers to the west of Lake Surprise, compared to other lakes, like Lake Chewaucan.

Stable isotope data does suggest a temporal trend in $\delta^{18}O$ of precipitation leading towards a minimum, coincident with the lake highstand at 16 ka; however, we note that this trend could be explained by both changing water sources or changing water temperatures. Studies typically suggest that the isotopic composition of water undergoing cooling (isobaric or moist adiabatic) at a starting point of 20℃, changes at a rate of 0.24‰ or 0.48‰ per ℃, respectively (Dansgaard, 1964). With these numbers in mind, we note that a portion, or even all, of the 4‰ decrease in the $\delta^{18}O$ of precipitation between the LGM and lake highstand could be explained by our estimated ~10℃ decrease in average water temperature in the same period of time, without necessitating variations in moisture source.

In addition to lake shoreline data, estimates of past temperature from clumped isotope analysis on lake sediments offer further insight into past hydroclimate. From a modern carbonate, we calculate a surface water temperature of 17.6± 2℃, and an average surface water

temperature of 10.2± 1℃ from our LGM age samples. Using modern air temperature at Cedarville, CA, we estimate 8.9± 1.4℃ of air warming since the LGM; using modern and LGM carbonate samples, we estimate 7.4± 2.2℃ of water warming since the LGM. From Δ_{47} derived temperatures, we estimate past evaporation rates and precipitation rates using a range of empirically-based equations. We find that lake growth was aided by decreasing evaporation rates, along with moderate precipitation rates (~ 80% of modern).

We perform qualitative and quantitative assessments of model skill at the location of Lake Surprise. By showing clumped isotope derived anomalies of temperature, precipitation, and evaporation on PMIP3 anomaly plots, we are able to visually assess which models are best able to reproduce the hydroclimate anomalies implied by our data. For a more quantitative comparison, we calculate model skill with respect to each variable of interest.

When applied to temperature and evaporation reconstructions, every model demonstrates similar positive skill scores. However, only 6/10 models demonstrate skill with regard to precipitation rates. Overall, the best performing models are CNRM-CM5, COSMOS-ASO, MPI-ESM-P and MRI-CGCM3, while the poorest performing models are NCAR CCSM4, FGOALS, MIROC-ESM and GISS-E2-R (150). Our four top-performing models all demonstrated positive skill in a similar study by Lora (2018) in the Great Basin, while two of our poorest-performing models, NCAR CCSM4 and MIROC-ESM, are amongst the worst performers in his study. In the future, a similar quantitative analysis compiling estimates from different paleolakes throughout the Great Basin may be used as a tool to further constrain which climate models are most in line with proxy reconstruction on a wider spatial scale.

We include a sensitivity analysis as a means of assessing the inherent variability in our model precipitation and evaporation reconstructions due to choices of input parameters: wind

speed, relative humidity, $\delta^{18}O$ of precipitation and the Budyko landscape parameter. While our results are sensitive to these input variables, we see robust evidence of decreased precipitation rates during the LGM and deglacial period, barring large changes in surface wind speed. Importantly, we note that increased moisture availability is due mostly to decreased lake evaporation rates rather than increased precipitation rates, because calculated precipitation rates are, overwhelmingly, less than or equal to modern values.

Ultimately, this work sheds light on factors that supported ancient large-scale lakes in the Western US, and why they disappeared, representing a proof-of-concept for a method that is broadly applicable to paleoclimate reconstructions and model evaluation using sediments from small closed basin lakes. Similar clumped isotope reconstructions for multiple sites in the Western US, in concert with isotope-enabled simulations, may allow for further constraints on hydroclimates and the refinement of water vapor sources.

FIGURES

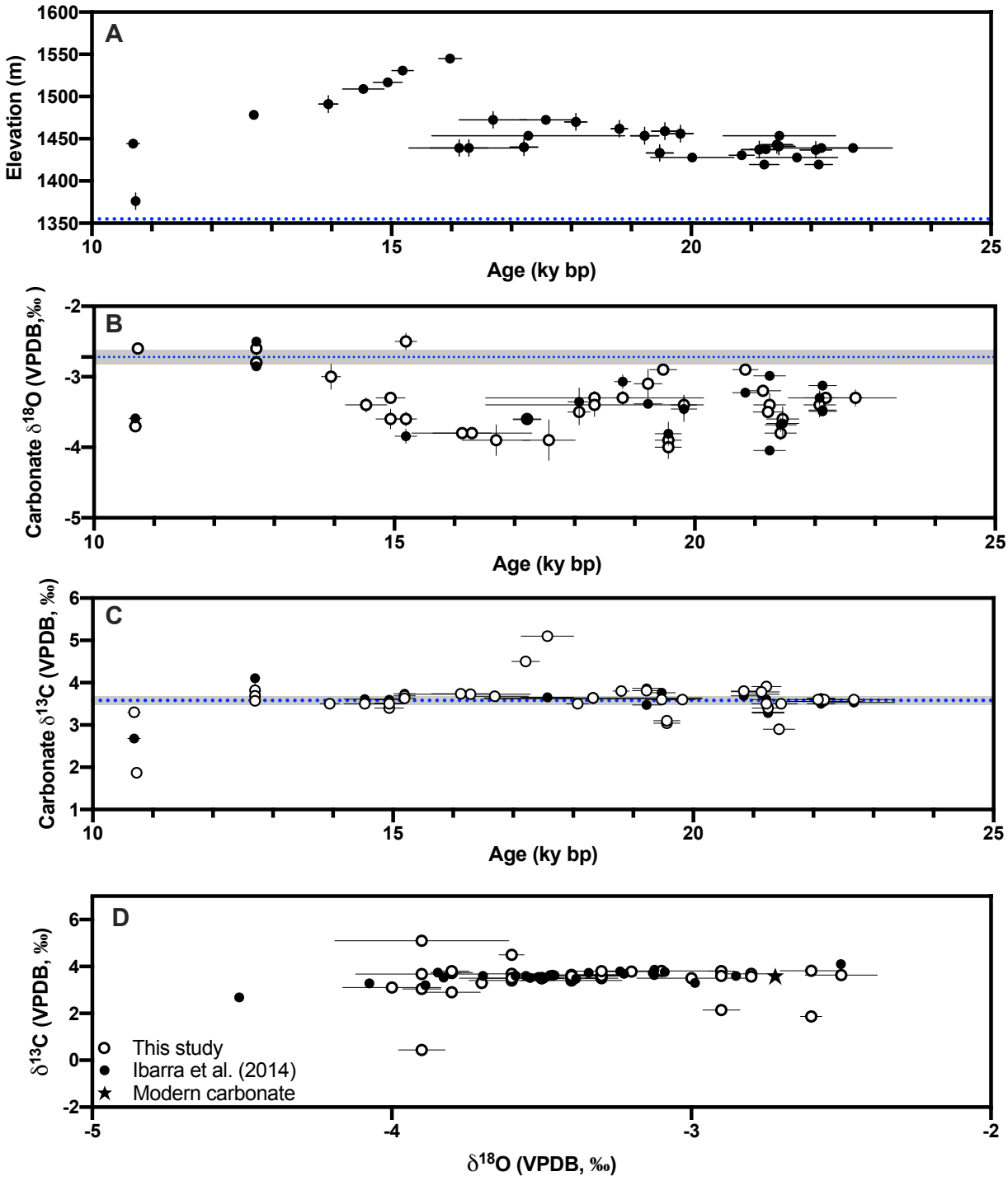

Figure 2.1: Lake hydrograph and stable isotope measurements. Modern values are plotted in blue and the shaded area indicates uncertainty associated with modern values (when applicable).

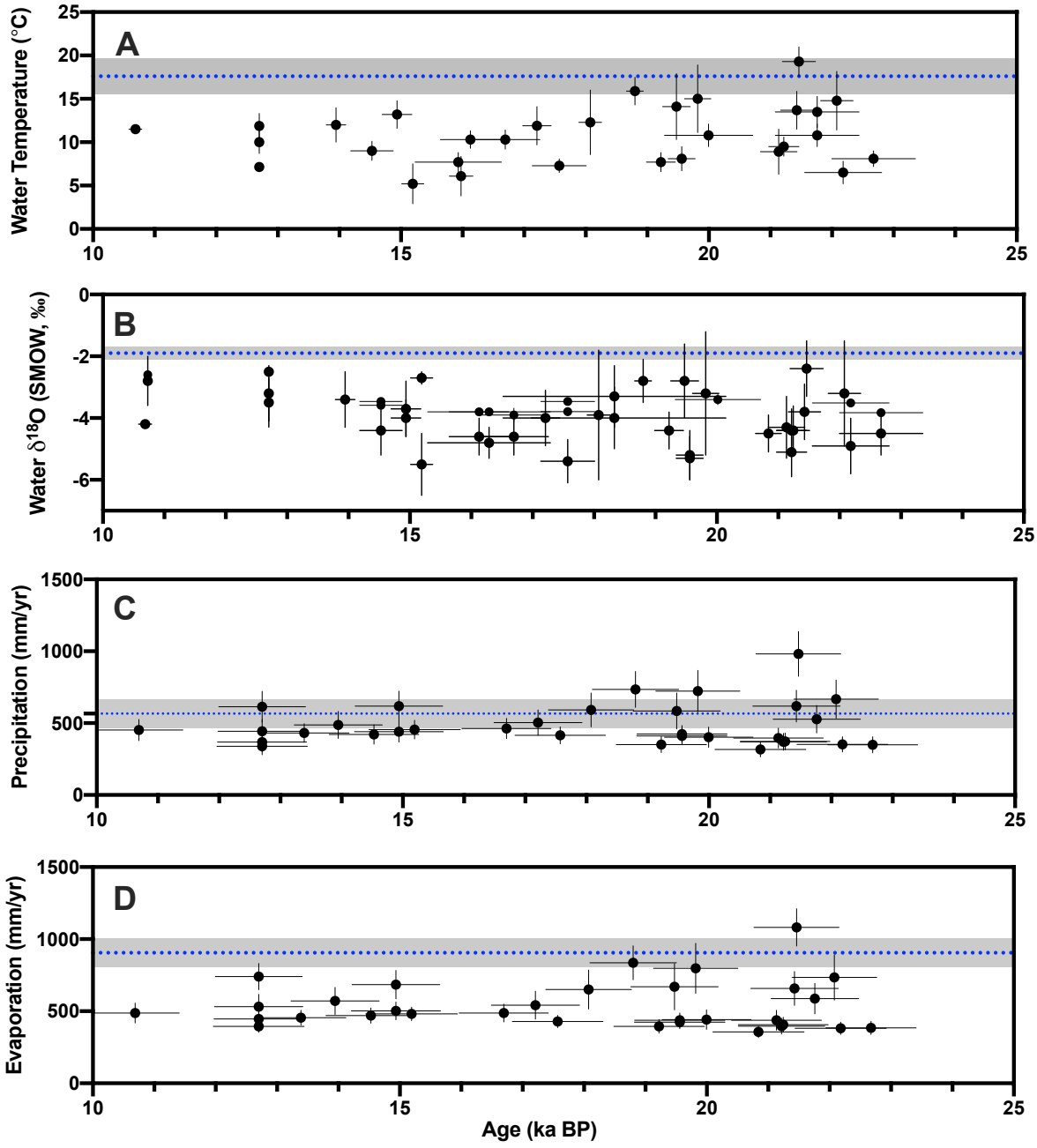

Figure 2.2: Reconstructed water temperature (a), water $\delta^{18}O$ (b), precipitation rates (c), and evaporation rates (d). Modern values are plotted in blue and the shaded area indicates uncertainty associated with modern values.

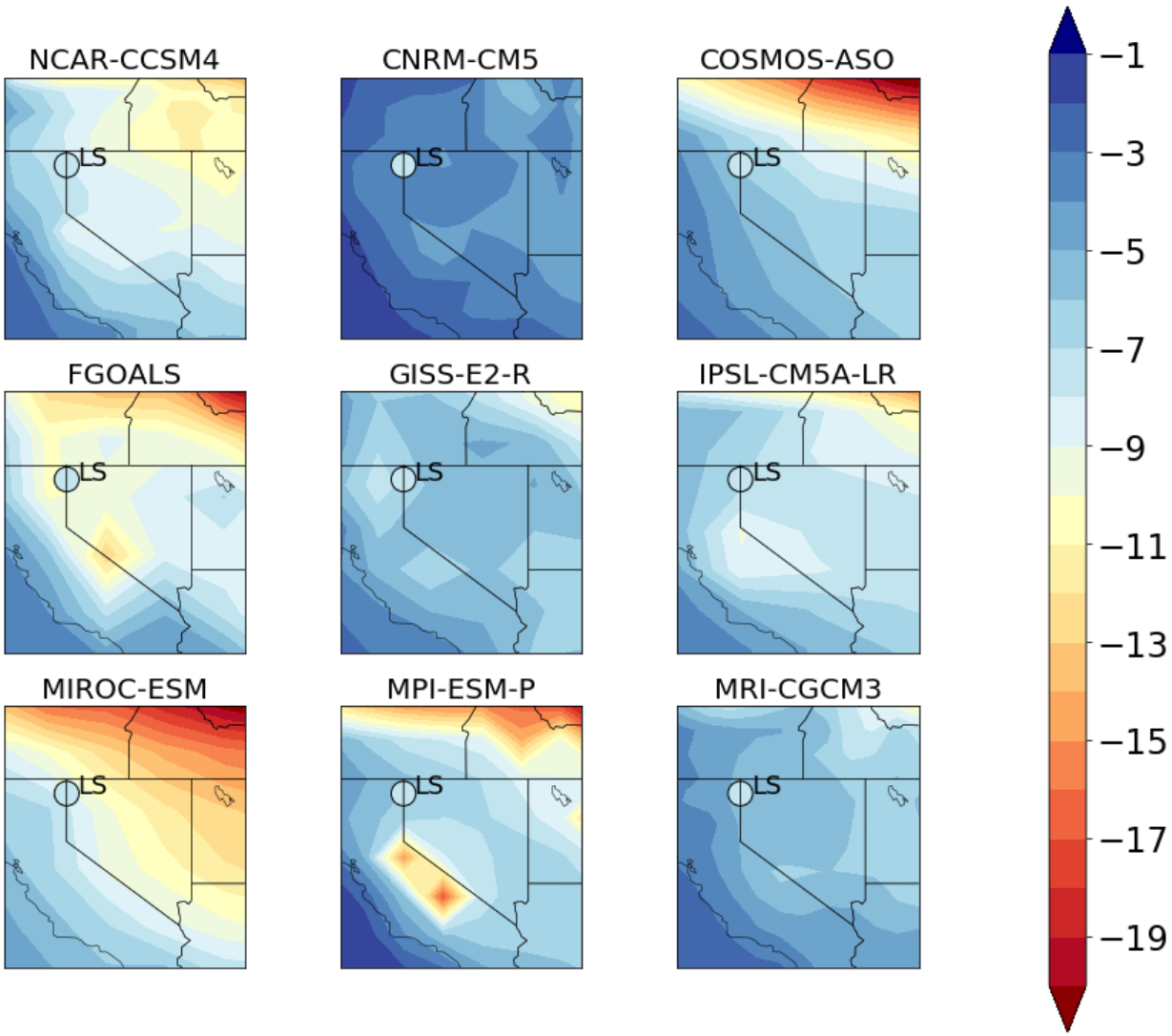

Figure 2.3: Mean annual surface air temperature anomaly between LGM and modern, as simulated by the 9 PMIP3 ensemble members, reported in ℃. The temperature anomaly is defined as LGM minus preindustrial temperatures for PMIP3, and LGM minus modern air temperatures for Lake Surprise. The point at the location of Lake Surprise corresponds to the average MAAT anomaly (-8.9 ± 1.4 ℃) calculated from Δ_{47} for all Lake Surprise LGM age samples (0.30± 1 ℃) and modern air temperature (9.2± 1 ℃).

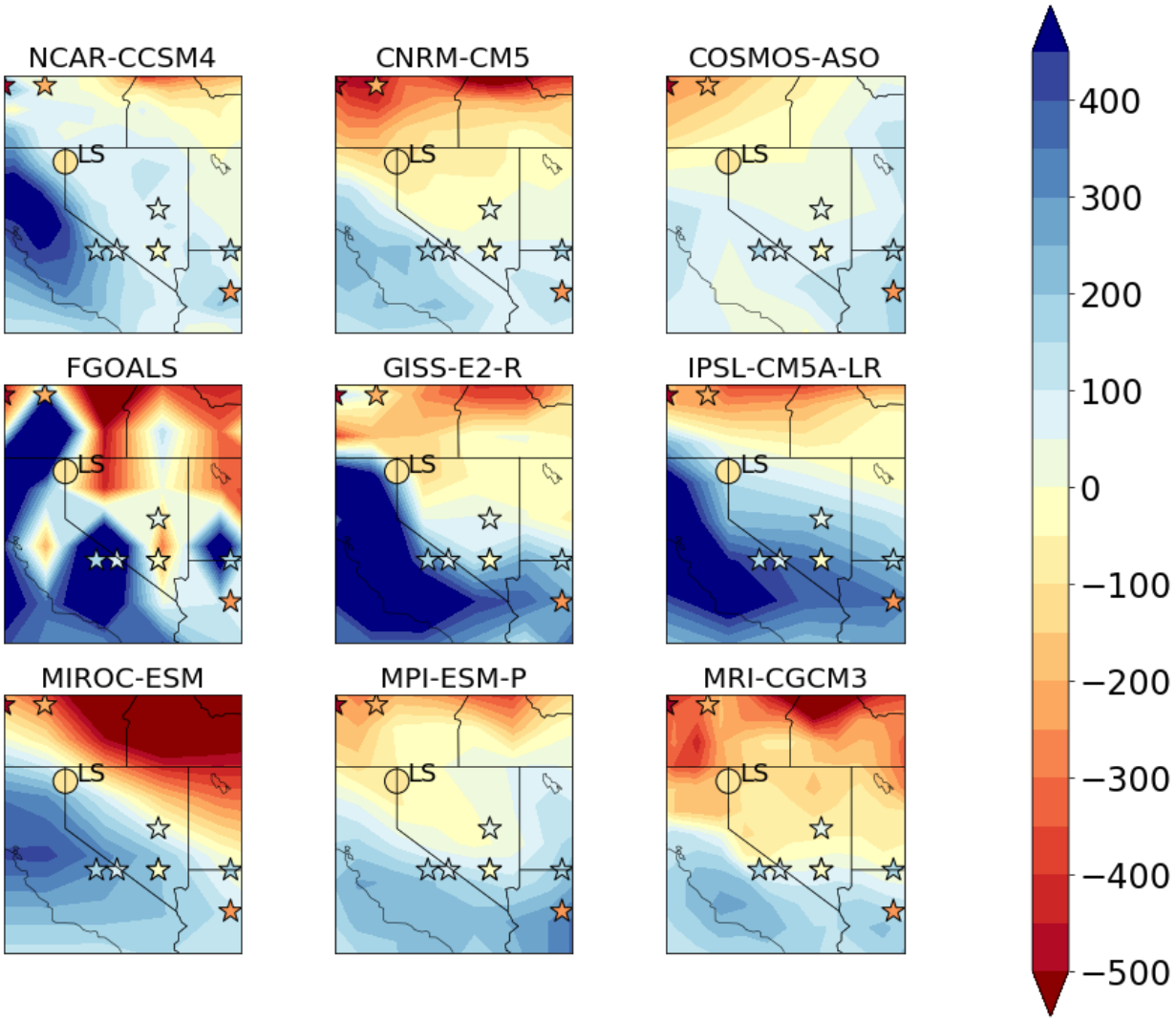

Figure 2.4: Mean annual precipitation anomaly between LGM and modern, as simulated by the 9 PMIP3 ensemble members, reported in mm/yr. The point at the location of Lake Surprise corresponds to the average precipitation anomaly (-76 ± 185 mm/yr) calculated from Equation S7 (490 ± 85 mm/yr) and modern precipitation rates (566 ± 165 mm/yr) for all Lake Surprise LGM age samples. The smaller stars are precipitation anomalies, reconstructed using pollen data in Bartlein et al. (2011).

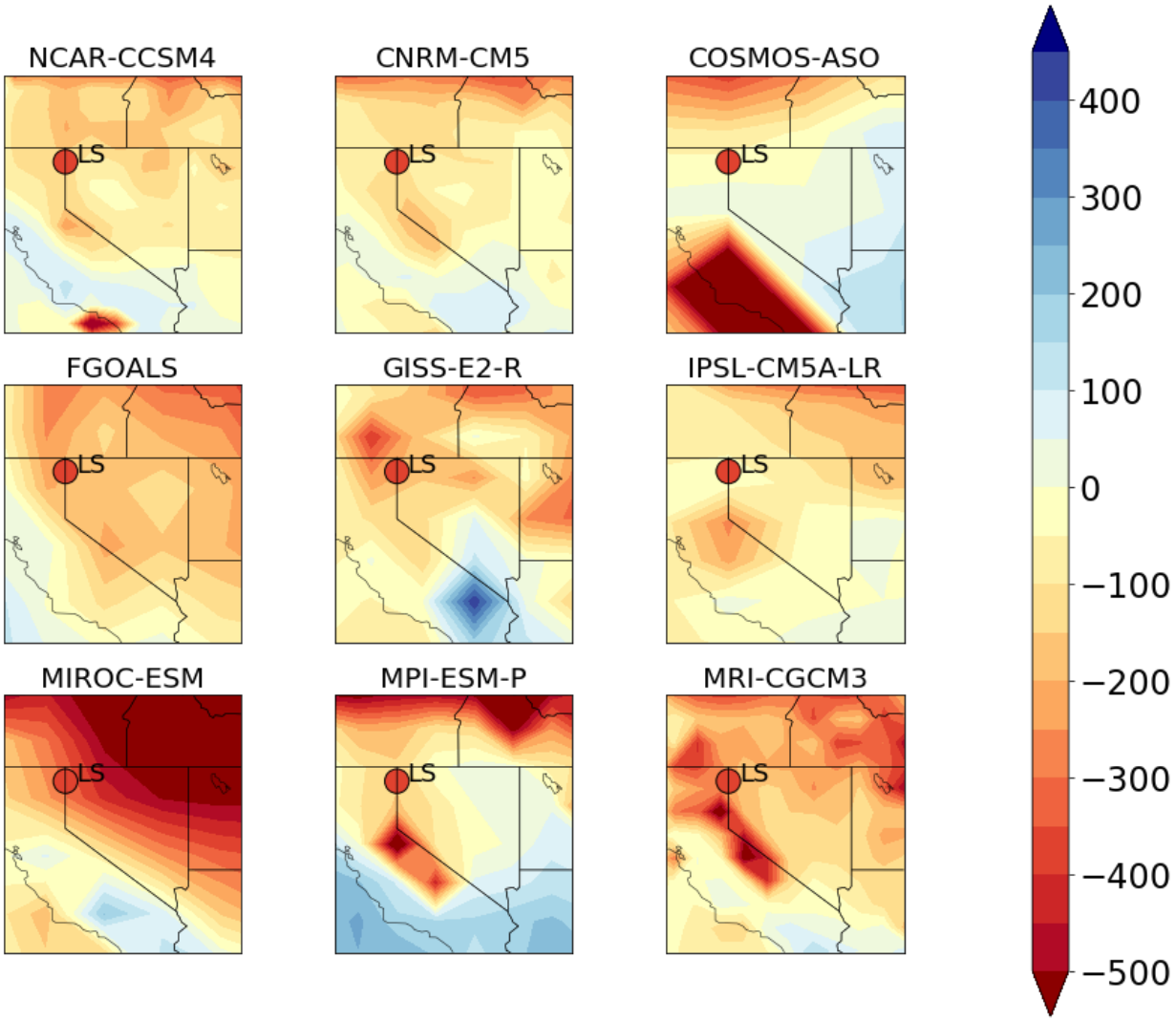

Figure 2.5: Mean annual evaporation anomaly between LGM and modern, as simulated by PMIP3 ensemble members, reported in mm/yr. The point at the location of Lake Surprise corresponds to the average weighted evaporation anomaly (-368 ± 100 mm/yr) derived from LGM samples (537 ± 65 mm/yr) and modern pan evaporation rate (905 ± 80 mm/yr).

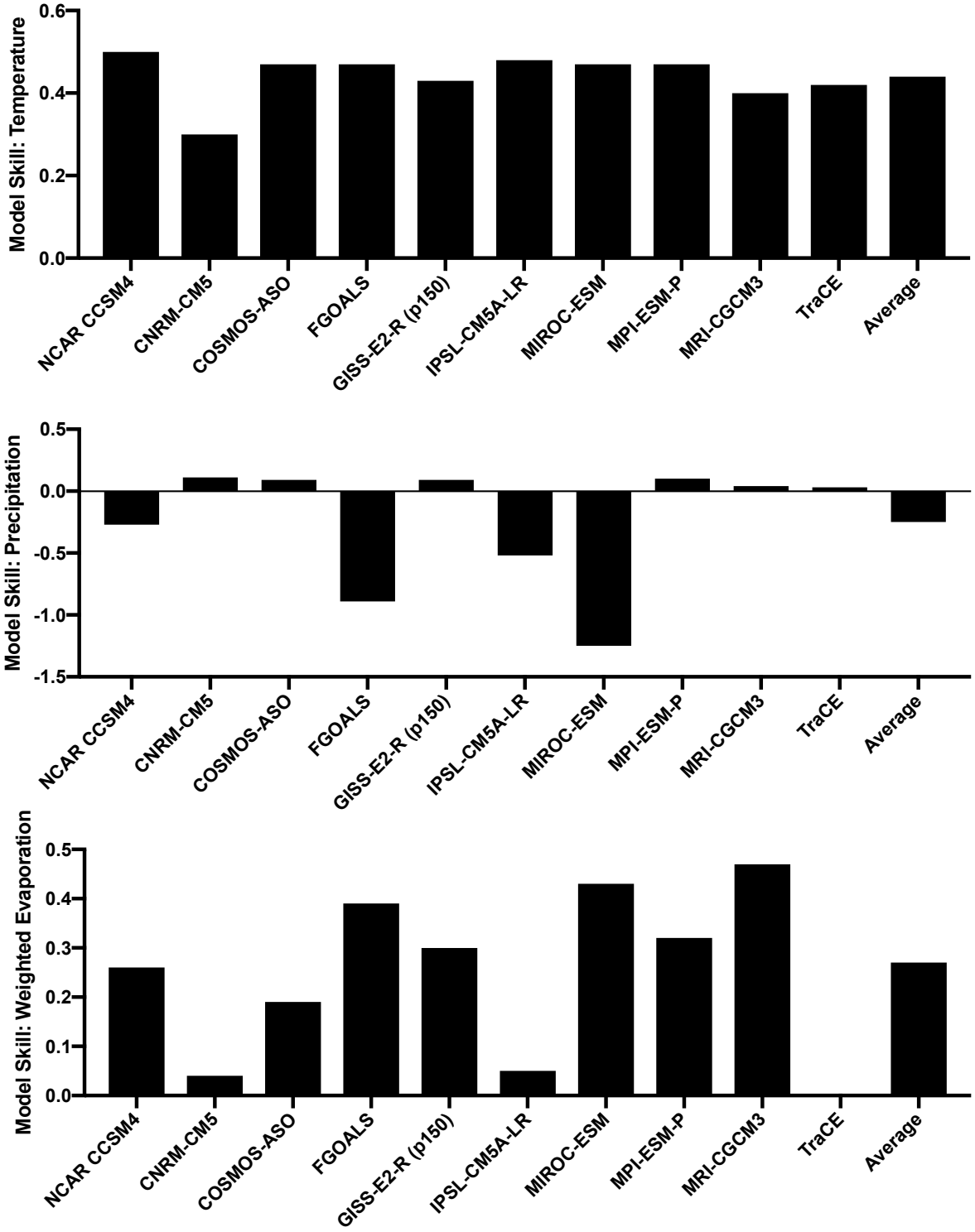

Figure 2.6: Model skill evaluation with respect to temperature, precipitation, and evaporation anomalies.

SUPPLEMENT

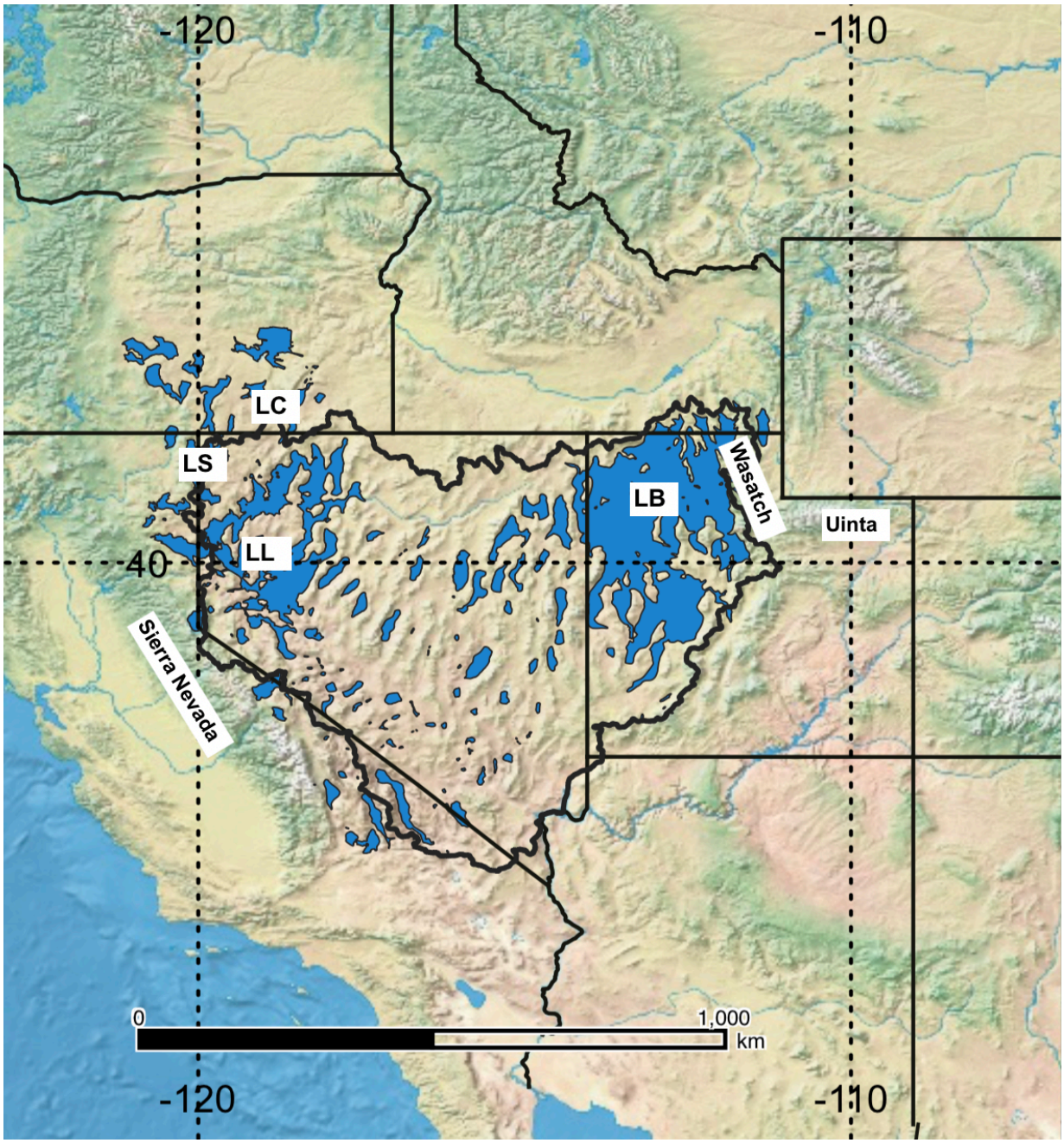

Figure S1: Map of sampling localities, with the estimated extent of pluvial lakes from the LGM and deglacial period shown in blue (pluvial lakes, digitized from Mifflin & Wheat, 1979 estimates). The perimeter of the Great Basin is outlined in black. The locations of Lake Surprise ("LS") and other major pluvial lakes—Lake Bonneville ("LB"), Lake Lahontan ("LL"), Lake Chewaucan ("LC")—are indicated on the map, as are major mountain ranges: the Sierra Nevada, the Wasatch, and the Uinta Mountains.

Table 2.S1: Clumped and Stable Isotope Data for Lake Surprise Samples

Sample Name	Δ47	Δ47 SE	$\delta^{18}O$	$\delta^{18}O$ SE	$\delta^{13}C$	$\delta^{13}C$ SE	^{14}C Age	^{14}C Age SD	IntCal13 Age (ka)	2σ min	2σ max	Elevation (m)
SVCW 17-PT1[1]	0.741	0.009	-3.8	0.03	3.7	0.02	13.52	0.34	16.30	15.29	17.29	1475
SVCW 17-PT2[1]	0.730	0.003	-3.8	0.07	3.7	0.04	13.39	0.16	16.11	15.64	16.61	1475
SVCW 17-PT3[1]	0.726	0.004	-3.9	0.22	3.7	0.09	13.79	0.19	16.68	16.13	17.26	1477
SVCW 17-PT4	0.726	0.004	-3.8	0.06	3.8	0.10	8.09	0.11	9.01	8.63	9.31	1475
SVDI 11-T14-1A	0.727	0.005	-2.6	0.10	3.6	0.18	10.79	0.05	12.70	12.64	12.76	1478
SVDI 11-T14-1B	0.739	0.001	-2.9	0.01	4.0	0.05	10.79	0.05	12.70	12.64	12.76	1478
SVDI 11-T14-1C	0.720	0.006	-2.8	0.09	3.6	0.06	10.79	0.05	12.70	12.64	12.76	1478
SVDI 11-T14-E[2]	0.708	—	-2.8	—	3.6	—	10.79	0.05	12.70	12.64	12.76	1478
SVDI 11-T2-1	0.736	0.005	-3.1	0.21	3.9	0.10	15.93	0.07	19.21	18.99	19.46	1454
SVDI 11-T3-2	0.731	0.005	-3.4	0.17	3.0	0.04	17.58	0.07	21.25	20.98	21.51	1438
SVDI 11-T4-1b	0.742	0.004	-2.9	0.04	3.6	0.04	17.28	0.06	20.84	20.63	21.05	1431
SVDI 12-T1	0.704	0.006	-3.5	0.06	3.7	0.18	17.56	0.60	21.22	20.97	21.46	1420
SVDI 12-T10-A	0.715	0.006	-3.6	0.14	3.6	0.08	12.60	0.07	14.96	14.94	15.18	1517
SVDI 12-T10-B	0.726	0.004	-3.3	0.06	3.5	0.13	12.60	0.05	14.96	14.94	15.18	1517
SVDI 12-T13	0.732	0.011	-3.2	0.08	3.7	0.02	17.49	0.09	21.13	20.84	21.43	1437
SVDI 12-T14	0.747	0.009	-3.6	0.10	3.7	0.06	12.75	0.05	15.19	15.01	15.36	1531
SVDI 12-T14-1C	0.717	0.002	-2.5	0.12	3.6	0.01	10.79	0.05	12.71	12.64	12.76	1531
SVDI 12-T15-B	0.712	0.015	-2.9	0.01	3.8	0.01	16.15	0.07	19.49	19.25	19.70	1433
SVDI 12-T3-A[1]	0.714	0.007	-3.3	0.01	3.6	0.06	18.03	0.28	21.82	21.08	22.44	1428
SVDI 12-T3-B[1]	0.724	0.005	-3.4	0.17	3.6	0.09	16.59	0.29	20.02	19.28	20.71	1428
SVDI 12-T4-A[1]	0.735	0.004	-3.3	0.12	3.6	0.02	18.78	0.27	22.70	22.04	23.35	1439
SVDI 12-T4-B[1]	0.741	0.005	-3.3	0.05	3.6	0.04	18.35	0.27	22.18	21.53	22.81	1439
SVDI 12-T5b	0.721	0.001	-3.7	0.02	3.4	0.01	9.47	0.04	10.71	10.58	10.79	1444
SVDI 12-T7[1]	0.738	0.003	-3.9	0.29	3.7	0.09	14.46	0.17	17.61	17.14	18.01	1473
SVDI 12-T9	0.731	0.004	-3.4	0.11	3.6	0.11	12.42	0.05	14.52	14.18	14.88	1509
SVDI 15-AE01	0.705	0.006	-3.3	0.10	3.8	0.04	15.55	0.06	18.81	18.66	18.94	1462
SVDI 15-AE02	0.699	0.009	-3.5	0.20	3.6	0.07	14.86	0.05	18.07	17.89	18.26	1470
SVDI 15-AE03	0.720	0.008	-3.0	0.18	3.5	0.09	12.09	0.05	13.96	13.79	14.10	1491
SVDI 15-AE05	0.713	0.009	-3.8	0.10	3.2	0.05	17.70	0.06	21.43	21.17	21.69	1443
SVDI 15-AE06	0.689	0.006	-3.4	0.10	3.5	0.04	18.20	0.10	22.07	21.82	22.34	1437
SVDI 15-BM03	0.720	0.008	-3.6	0.04	4.9	0.02	14.13	0.06	17.20	16.98	17.44	1440
SVDI 15-BM04	0.735	0.006	-4.0	0.16	3.6	0.11	16.20	0.06	19.56	19.34	19.78	1459
SVDI 15-BM08	0.692	0.006	-3.6	0.17	3.4	0.11	17.73	0.07	21.46	21.19	21.73	1441
SVDI 15-BM09	0.688	0.009	-3.4	0.18	3.1	0.10	16.43	0.06	19.82	19.61	20.03	1456
Modern Playa[2]	0.698	—	-2.7	—	3.6	—	—	—	—	—	—	1355

[1]Indicates Samples submitted for Desert Symposium, previously unpublished

[2]Indicates samples with too few runs to constrain standard error of the mean

Table 2.S2: Reconstructed Precipitation (P) and Evaporation (E) Rates from Two Models: Matsubara & Howard (M & H), or Linacre, (1993) and Ibarra et al. (2014). Units reported are mm/yr.

Sample Name	E: M&H	SE	E: Linacre (1993)	SE	P: M&H	SE	P: Ibarra et al. (2014)	SE
SV15BM04	1154	254	658	46	-243	423	411	57
SVCW 17-PT1	1460	170	695	53	173	298	427	64
SVCW 17-PT2	1595	200	698	53	361	340	431	65
SVCW 17-PT3	1596	216	747	62	361	361	462	71
SVCW 17-PT4	1565	245	747	63	319	402	455	70
SVDI 11-T14-1A	1476	321	743	62	194	506	369	69
SVDI 11-T14-1B	1116	66	640	41	-306	152	339	58
SVDI 11-T14-1C	1836	276	878	85	694	444	444	83
SVDI 11-T14-E	2286	51	1230	91	1318	132	614	108
SVDI 11-T2-1	1196	206	657	47	-181	361	351	57
SVDI 11-T3-2	1385	230	682	52	90	402	374	59
SVDI 11-T4-1b	992	182	623	41	-451	340	317	52
SVDI 12-T1	1452	193	689	55	194	361	370	59
SVDI 12-T10-A	2046	307	1022	99	964	465	619	105
SVDI 12-T10-B	1626	202	764	62	381	319	440	73
SVDI 12-T13	1370	425	744	69	69	673	397	69
SVDI 12-T14	852	417	691	47	-701	610	455	65
SVDI 12-T14-1C	1977	132	972	82	860	215	482	93
SVDI 12-T15-B	2148	603	1181	160	1152	923	585	126
SVDI 12-T3-A	2056	301	1030	106	1027	506	528	96
SVDI 12-T3-B	1651	226	763	69	465	402	402	71
SVDI 12-T4-A	1251	171	648	46	-98	319	349	55
SVDI 12-T4-B	1011	231	635	43	-431	402	352	53
SVDI 12-T5b	1763	83	798	70	610	194	452	74
SVDI 12-T7	1144	169	648	44	-264	298	415	59
SVDI 12-T9	1414	229	711	53	90	361	422	68
SVDI 15-AE01	2430	285	1370	118	1526	465	735	126
SVDI 15-AE02	2688	423	1028	135	1880	652	592	118
SVDI 15-AE03	1856	356	912	95	714	548	487	94
SVDI 15-AE05	2092	367	1071	118	1068	590	619	110
SVDI 15-AE06	3050	305	1241	158	2401	506	666	133
SVDI 15-BM03	1821	366	893	97	694	590	503	88
SVDI 15-BM04	1259	254	676	50	-98	423	425	60
SVDI 15-BM08	2931	291	1814	130	2234	485	982	156
SVDI 15-BM09	3132	417	1302	173	2505	652	723	145
SVDI 12-T2	1138	28	625	45	-243	132	253	50
SVDI 12-T4	535	36	609	38	-1091	132	312	50

Methods supplement

Clumped Isotope Analysis

Tufa was rinsed by hand in deionized water (DI) to remove loosely-held secondary material. In some cases, samples were sonicated in room-temperature DI for up to 30 minutes to remove loosely held contaminants and particles on the sample surface. For tufa samples, carbonate was extracted using a microdrill. To prevent potential bond reordering due to frictional heating, the drill speed during this process was limited in duration and in speed. Carbonate powder was subsequently homogenized using a mortar and pestle and treated using dilute (3%) H_2O_2 for 1-4 hours, following a published protocol for extracting and treating carbonates containing trace organics (e.g. Tripati et al., 2010). Following peroxide treatment, samples were dried in an oven at low heat (<50℃), and stored in a desiccator prior to analysis.

Carbonate clumped isotope measurements were carried out using at UCLA using a Thermo 253 isotope ratio mass spectrometer (IRMS). At least four replicates were measured of each sample. Carbonate samples were weighed into silver boats and digested under vacuum using a McCrea-style common acid bath maintained at 90°C (89.0 to 90.5°C) before analysis. Sample CO_2 is purified using an automated vacuum line and cryogenic freezing system, which isolates H_2O and minor contaminant species (e.g. N_2, O_2, other trace gases) from analyte CO_2, based on differential freezing points. The liberated gas passes through two separate gas traps to ensure removal of water and other compounds: the first containing ethanol, is kept at -76°C by dry ice, and the second is kept at -126°C by liquid nitrogen. The sample gas is then passed through a silver wool, which removes sulfur compounds. Remaining trace contaminants (e.g. halocarbons and hydrocarbons) are separated by passing the resultant gas through a Thermo

Trace GC Ultra gas chromatograph column, which is filled with a divinyl benzene polymer trap, Porapak Q, and maintained at -20℃.

After purification in the GC, the sample is transferred to the mass spectrometer. Samples are measured with a mass 44 ion beam at 16 V, with an Oztech working gas. Each sample is measured for a total of nine acquisitions, with each acquisition consisting of a peak centering, background adjustment, and alternate cycling between sample and reference gas ionization (e.g. Spencer & Kim, 2015). Total measurement time is 2.3 hours per sample. For an in-depth discussion of this process, the reader is directed to Spencer & Kim (2015) and Huntington et al. (2009).

After reaction in the mass spectrometer, isotope ratios are calculated using the Brand parameter set, which provides a correction for ^{17}O interference by specifying the ratio of ^{16}O to ^{17}O (Brand et al., 2010). An acid digestion correction of 0.082‰ is applied to data to account for digestion at 90 °C (Defliese et al., 2015). Error on Δ_{47} is reported as standard error of the mean, as this error is minimized by increasing the number of sample replicates (Huntington et al., 2009; Fernandez et al., 2017). Water $\delta^{18}O$ is calculated by applying the appropriate temperature-dependent water to calcite fractionation to measured carbonate samples (Kim & O'Neil, 1997).

Hydroclimate modelling:

Lake Evaporation Rate

Linacre (1993) creates a robust equation for lake-based evaporation that relies on inputs of latitude (Lat), temperature (T), dew-point temperature (T_d), wind speed (u), and elevation (z), and has been used for previous paleoclimate reconstructions (Jones et al., 2007; Ibarra et al., 2014, Mering, 2015). For our primary calculations, we assume u and z have remained constant

through time, and that T_d is offset a constant amount from temperature, which is reasonable, assuming small changes in RH (Linacre, 1993; Jones et al., 2007; Ibarra et al., 2014). We assume that T is equal to MAAT, but this assumption may bias our calculated evaporation rates to high values, were the lake frozen over (thus inhibiting evaporation) for a significant amount of each year. In our sensitivity analysis, we explore the effects of allowing u and RH to be altered within a reasonable range.

$$E_{MM/YR} = [0.015 + 4 * 10^{-4}T + 10^{-6}Z] \times [\frac{480(T+0.006z)}{84-Lat} - 40 + 2.3u(T - T_d)] \quad \text{Equation S1}$$

Weighted Evaporation Rate

To allow for more direct comparison between our clumped isotope derived lake evaporation rates and PMIP3 ET rates, we create a weighted evaporation that scales lake evaporation and ET from our models by the size of lake area and tributary area, respectively. ET is estimated as precipitation minus K_{run}, both of which are calculated in our model (see below).

$$Weighted\ Evaporation = \frac{(P - K_{run} \times A_t) + E_l \times A_l}{A_w - A_l} \quad \text{Equation S2}$$

Estimating Lake Area and Basin Hypsometry

The pluvial hydrologic index, $\frac{A_l}{A_w - A_l}$, or "HI" is a physical basin parameter that describes the ratio of lake surface area (A_L) to tributary area (A_W), and is a primary input in our precipitation rate calculation. Historically, it has been used as a means to determine the partitioning of rainfall into runoff and evaporation and otherwise approximate past hydroclimate, assuming minimal change in drainage area and a basin's hypsometric curvature (e.g., Mifflin & Wheat, 1979; Reheis, 1999; Ibarra et al., 2014; Ibarra et al., 2018). We calculate the HI

corresponding to each shoreline as a function of sample elevation (z) using a hypsometric curve from the HydroSHEDS/HydroBASINS datasets (e.g. Lehner et al., 2008; Lehner & Grill, 2013).

Lake Precipitation Rate

Beginning with the time-varying (t) water balance and $\delta^{18}O$ isotope mass balance equations for an inward draining lake and applying the product rule, we derive a function for calculating precipitation rate (modified from equations and derivations in: Jones et al., 2007; Steinman et al., 2013; Ibarra et al., 2014). The change in lake volume (V_L) is:

$$\frac{dV_L}{dt} = Q_w - Q_e \qquad \text{Equation S3}$$

where Q is the input (w) and evaporative (e) fluxes. Input fluxes are assumed to be both runoff and precipitation at this point, but are partitioned in subsequent equations using a runoff coefficient. Similarly, the isotope mass balance equation is given by:

$$\frac{d(\delta^{18}O_L \times V_L)}{dt} = (\delta^{18}O_w \times Q_w) - (\delta^{18}O_e \times Q_e) \qquad \text{Equation S4}$$

Applying the product rule to Equation S4, substituting the mass balance equation into the isotope balance equation and rearranging yields an expression for time-varying changes in lake water:

$$V_L \frac{d(\delta^{18}O_L)}{dt} + \delta^{18}O_L \frac{d(V_L)}{dt} = (\delta^{18}O_w \times Q_w) - (\delta^{18}O_e \times Q_e) \qquad \text{Equation S5}$$

$$V_L \frac{d(\delta^{18}O_L)}{dt} = (\delta^{18}O_w - \delta^{18}O_L) \times Q_w - (\delta^{18}O_e - \delta^{18}O_L) \times Q_e \qquad \text{Equation S6}$$

Assuming steady state and solving for precipitation rate (P), and assuming that $Q_e = A_L E_L$ and $Q_w = (P_L \times A_L) + (k_{run} \times P_L \times (A_w - A_L))$, where A is area of the lake (L) and watershed (w), E_L is the evaporation rate, and k_{run} is the runoff coefficient, we obtain an expression for the basin average precipitation rate:

$$P = \frac{E_L}{1+\frac{k_{run}}{\left(\frac{A_L}{A_w - A_L}\right)}} \times \frac{(\delta^{18}O_e - \delta^{18}O_L)}{(\delta^{18}O_w - \delta^{18}O_L)} \qquad \text{Equation S7}$$

This equation includes the commonly used "pluvial hydrologic index", modified by the isotope mass balance differences between lake water, input water, and evaporating water vapor. In previous work (Ibarra et al., 2014) a runoff coefficient (k_{run}) was assumed; however, as discussed by Broecker (2010), modern hydrologic observations suggest a non-linear response of runoff to changes in precipitation (e.g. Greve et al., 2015). We use the single parameter formulation for the Budyko curve calibrated by Greve et al. (2015) for the coterminous United States:

$$1 - k_{run} = \frac{ET}{P} = 1 + \frac{E_p}{P} - \left(1 + \left(\frac{E_p}{P}\right)^{\omega}\right)^{1/\omega} \qquad \text{Equation S8}$$

where ET is evapotranspiration, E_p is potential evapotranspiration (which we approximate by constraints on E_L from the clumped isotope results, described above), and ω is the adjustable calibrated Budyko landscape parameter. The use of this Budyko framework in terminal basin hydrologic modeling has been demonstrated in spatially explicit hydrologic modeling by Matsubara & Howard (2009) and Barth et al. (2016), and in similar regional modeling by Ibarra

et al. (2018) for Plio-Pleistocene watersheds of the Great Basin, justifying the incorporation of ω into this simplified isotope mass balance framework.

Given knowledge of evaporation rates and basin hypsometry, calculation or measurement of $\delta^{18}O$ values and assumptions of ω, Equations S7 and S8 can be solved simultaneously for P and k_{run}, given a calculated E_L and lake water $\delta^{18}O$ from Δ_{47}. Because of the non-linear nature of both equations we use a root-finding procedure to solve for the unknowns. This is carried out using the *multiroot* function in the R package 'rootSolve' (Soetaert, 2016), which uses a numerical Newton-Raphson method to find the roots of the two equations. Errors are propagated through random draws in the Monte Carlo routine by bootstrapping RH, T_d, and u, and assuming normal distributions for all input variable values (mean and standard deviation) except for ω, which has a skewed gamma distribution as calibrated by Greves et al. (2015) for the continental United States.

Inputs to Equation S8

Prior to implementing the simultaneous solution to Equations S7 and S8, several model variables need to be determined to populate the equations. We estimate lake evaporation rate (E_L) using Equation S1. We also implement a transfer function from Hren & Sheldon (2012) to calculate MAAT from seasonal (AMJJASO) water temperatures, T_w:

$$\text{MAAT (°C)} = -0.0146*T_w^2 + 1.753*T_w - 16.079 \qquad \text{Equation S9}$$

Basin hypsometric curves provide constraints on lake area (A_L) and basin area (A_w). Lake water isotopic composition ($\delta^{18}O_L$) is calculated from Δ_{47} derived temperature and the

temperature dependent equilibrium fractionation factor of Kim & O'Neil (1997). Meteoric water inputs ($\delta^{18}O_w$) into the lake are constrained from the modern average (-14.57 ± 0.6‰, 1σ), where we assume that source water effects and temperature effects roughly cancel (see discussion in Jones et al., 2007; Ibarra et al., 2014). Finally, to implement the isotope evaporation equation of Craig & Gordon (1965), the following assumptions are made to derive $\delta^{18}O_e$:

1. The kinetic fractionation factor is derived from Gonfiantini (1986), where the fractionation factor ε is a simple function of relative humidity: $1000 \ln(\alpha_{kin}) \approx \varepsilon = 14.2 \times (1 - RH/100)$, where RH is relative humidity.
2. The atmospheric vapor above the basin is in equilibrium with the incoming rainwater, which is calculated using the temperature dependent equilibrium fractionation factor equation from Majoube (1971). This parameter is needed for the Craig & Gordon (1965) evaporation equation to derive $\delta^{18}O_e$ in Equation S7.

This approach differs from that of Ibarra et al. (2014) and Jones et al. (2007), who assume a kinetic fractionation of $\alpha_{kin} = 0.994$ for $u \leq 6.8$ m/s. In similar work for closed-basin lake modeling (Ibarra et al., 2014; Ibarra & Chamberlain, 2015) the kinetic fractionation factor using the above equation from Gonfiantini (1986) was found to better approximate the range of possible values (given likely variations in RH), and has been used elsewhere.

Alternate Equations for Precipitation and Evaporation Rates

Rather than relying on isotopic constraints, Matsubara & Howard (2009) model lake precipitation as a function of temperature. This equation was calibrated in the Great Basin under late Pleistocene to modern conditions. Matsubara & Howard (2009) report two variations of this model: one assumes an aerially uniform and absolute amount of precipitation change (Equation S10), while the other calculates a fractional change in precipitation compared to the modern value (not shown). The former model was found to be more accurate for the far northern and

southern Great Basin, while the latter model was more appropriate for the interior of the Great Basin. In this supplement, we calculate precipitation using Equation S10, as this is likely more appropriate for the northerly Lake Surprise.

$$P - P_m = 0.36 + 0.057\times (T - T_m) \quad \text{Equation S10}$$

P = LGM Precipitation

P_m= Modern Precipitation = 566 mm/yr

T = LGM air temperature

T_m = Modern Mean Annual Air Temperature = 9.2℃

Matsubara & Howard (2009) also present a simplified model for evaporation, specific to the Great Basin, that relies only on inputs of latitude and elevation:

$$E_{[mm/yr]} = (0.15\times T + 0.0004\times Z - 0.54) \times 1000 \quad \text{Equation S11}$$

We report precipitation and evaporation rates from Equations S10 and S11, respectively, in Table 2.S2, along with our precipitation and lake evaporation estimates used in the main text.

Quantifying Model Skill

As in Hargreaves et al. (2013), we quantify model skill using an equation that weighs the ability of climate models to reproduce the magnitude and distribution of temperature and precipitation estimates from clumped isotopes:

$$\text{Model Skill} = 1 - \sqrt{\frac{(m_i - o_i)^2}{(n_i - o_i)^2}} \quad \text{Equation S12}$$

where m_i are the forecast results (from PMIP3), n_i is the reference state (in our case, taken to be zero, or no change between the LGM and present), and o_i are the observations (from clumped isotope analysis). As discussed in Lora (2018), results should be interpreted as a model's skill in depicting past climatic changes with respect to the null hypothesis, of no change between the LGM and modern. A perfect simulation would have a score of 1, a score of 0 would indicate that the model and reference state (no change) perform equally well, and a negative score would indicate that model error is greater than in the case of the null hypothesis.

Sensitivity Analysis

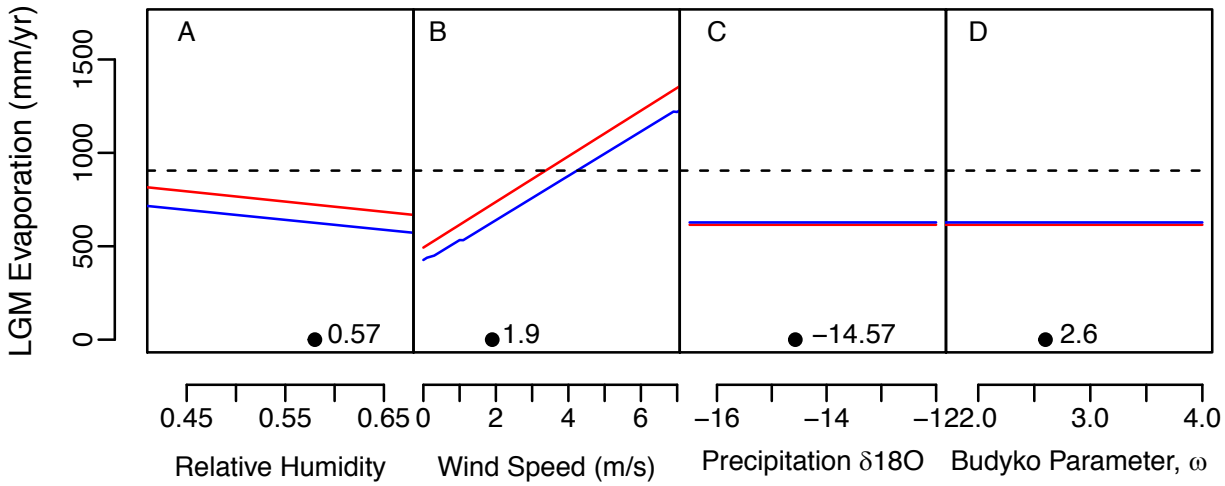

Figure 2.S2: Sensitivity of reconstructed evaporation rates for "average" sample (red line) and median sensitivity of all samples (blue line). Modern annual pan evaporation rate is from Ibarra et al., 2014 (black line). The mean x-axis value assumed outside this sensitivity analysis is based on modern climate data, and is indicated by the black point. Calculated evaporation is insensitive to changes in input precipitation $\delta^{18}O$ and ω.

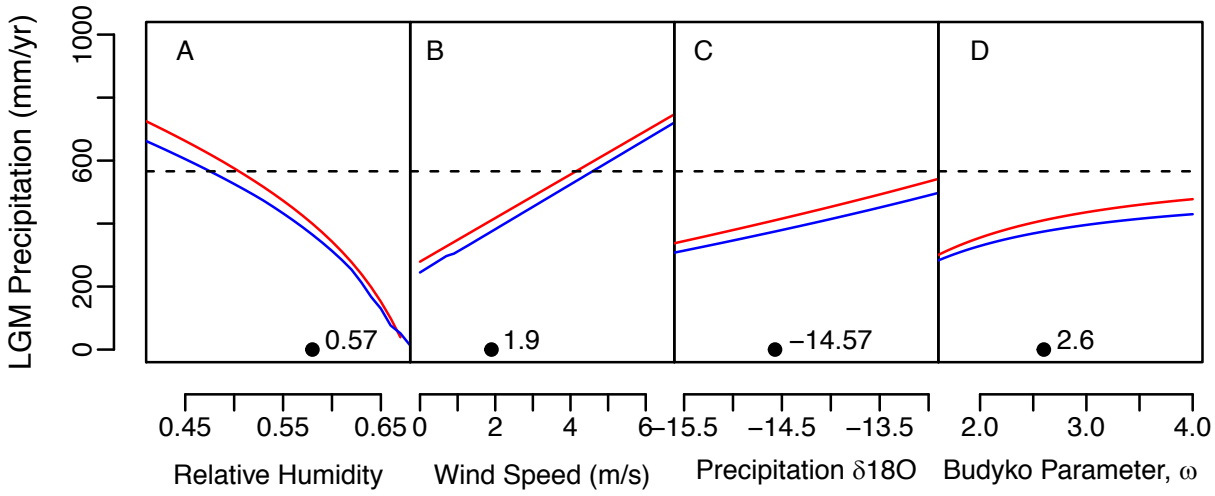

Figure 2.S3: Sensitivity of reconstructed precipitation rates for "average" sample (red line) and median sensitivity of all samples (blue line). Modern annual precipitation rate is from Ibarra et al., 2014 (black line). The mean x-axis value assumed outside this sensitivity analysis is based on modern climate data, and is indicated by the black point.

REFERENCES

Bartlein, P. J., Harrison, S. P., Brewer, S., Connor, S., Davis, B. A. S., Gajewski, K., Guiot J, Harrison-Prentice TI, Henderson A, Peyron O, & Prentice, I. C. (2011). Pollen-based continental climate reconstructions at 6 and 21 ka: a global synthesis. *Climate Dynamics*, *37*(3-4), 775-802.

Benson, L. V., Smoot, J. P., Lund, S. P., Mensing, S. A., Foit Jr, F. F., & Rye, R. O. (2013). Insights from a synthesis of old and new climate-proxy data from the Pyramid and Winnemucca lake basins for the period 48 to 11.5 cal ka. *Quaternary International*, *310*, 62-82.

Bernasconi, S. M., Müller, I. A., Bergmann, K. D., Breitenbach, S. F., Fernandez, A., Hodell, D. A., Jaggi, M., Meckler, A.N., Millan, I & Ziegler, M. (2018). Reducing Uncertainties in Carbonate Clumped Isotope Analysis Through Consistent Carbonate-Based Standardization. *Geochemistry, Geophysics, Geosystems*, *19*(9), 2895-2914.

Broecker, W. (2010). Long-term water prospects in the western United States. *Journal of Climate*, *23*(24), 6669-6683.

Craig, H., & Gordon, L. I. (1965). Deuterium and oxygen 18 variations in the ocean and the marine atmosphere.

Defliese, W. F., Hren, M. T., & Lohmann, K. C. (2015). Compositional and temperature effects of phosphoric acid fractionation on Δ47 analysis and implications for discrepant calibrations. *Chemical Geology*, *396*, 51-60.

Dansgaard, W. (1964). Stable isotopes in precipitation. *Tellus*, *16*(4), 436-468.

Dennis, K. J., Affek, H. P., Passey, B. H., Schrag, D. P., & Eiler, J. M. (2011). Defining an absolute reference frame for 'clumped' isotope studies of CO2. *Geochimica et Cosmochimica Acta*, *75*(22), 7117-7131.

Edwards, T. W. D., & McAndrews, J. H. (1989). Paleohydrology of a Canadian Shield lake inferred from 18O in sediment cellulose. *Canadian Journal of Earth Sciences*, *26*(9), 1850-1859.

Egger A.E., Ibarra, D.E., Widden, R, Langridge R.M., Marion, M, & Hall, J. (2018). Influence of Pluvial Lake Cycles on Earthquake Recurrence on the Northwestern Basin and Range, USA. *Geological Society of America* Special Paper 536, 1-28.

Eiler, J. M., & Schauble, E. (2004). 18O13C16O in Earth's atmosphere. *Geochimica et Cosmochimica Acta*, *68*(23), 4767-4777.

Eiler, J. M. (2007). “Clumped-isotope” geochemistry—The study of naturally-occurring, multiply-substituted isotopologues. *Earth and planetary science letters*, *262*(3-4), 309-327.

Fernandez, A., Müller, I. A., Rodríguez-Sanz, L., van Dijk, J., Looser, N., & Bernasconi, S. M. (2017). A reassessment of the precision of carbonate clumped isotope measurements: Implications for calibrations and paleoclimate reconstructions. *Geochemistry, Geophysics, Geosystems*, *18*(12), 4375-4386.

Galloway, R. W. (1970). The full-glacial climate in the southwestern United States. *Annals of the Association of American Geographers*, *60*(2), 245-256.

Gat, J. R. (1996). Oxygen and hydrogen isotopes in the hydrologic cycle. *Annual Review of Earth and Planetary Sciences*, *24*(1), 225-262.

Ghosh, P., Adkins, J., Affek, H., Balta, B., Guo, W., Schauble, E. A., Schrag, D. & Eiler, J. M. (2006). 13C–18O bonds in carbonate minerals: a new kind of paleothermometer. *Geochimica et Cosmochimica Acta*, *70*(6), 1439-1456.

Gonfiantini, R. (1986). Environmental isotopes in lake studies. *Handbook of environmental isotope geochemistry, the terrestrial environment*, *2*, 113-168.

Greve, P., Gudmundsson, L., Orlowsky, B., & Seneviratne, S. I. (2015). Introducing a probabilistic Budyko framework. *Geophysical Research Letters*, *42*(7), 2261-2269.

Guirguis, K. J., & Avissar, R. (2008). A precipitation climatology and dataset intercomparison for the western United States. *Journal of Hydrometeorology*, *9*(5), 825-841.

Hargreaves, J. C., Annan, J. D., Ohgaito, R., Paul, A., & Abe-Ouchi, A. (2013). Skill and reliability of climate model ensembles at the Last Glacial Maximum and mid-Holocene. *Climate of the Past*, *9*(2), 811-823.

Hudson, A. M., Quade, J., Ali, G., Boyle, D., Bassett, S., Huntington, K. W., A Cohen, K Lin, & Wang, X. (2017). Stable C, O and clumped isotope systematics and 14C geochronology of carbonates from the Quaternary Chewaucan closed-basin lake system, Great Basin, USA: Implications for paleoenvironmental reconstructions using carbonates. *Geochimica et Cosmochimica Acta*, *212*, 274-302.

Huntington, K. W., Eiler, J. M., Affek, H. P., Guo, W., Bonifacie, M., Yeung, L. Y., Thiagarajan N, Passey B, Tripati A, Daëron M, & Came, R. (2009). Methods and limitations of ‘clumped’ CO2 isotope (Δ47) analysis by gas-source isotope ratio mass spectrometry. *Journal of Mass Spectrometry*, *44*(9), 1318-1329.

Horton, T. W., Defliese, W. F., Tripati, A. K., & Oze, C. (2016). Evaporation induced 18O and 13C enrichment in lake systems: A global perspective on hydrologic balance effects. *Quaternary Science Reviews*, *131*, 365-379.

Hostetler, S., & Benson, L. V. (1990). Paleoclimatic implications of the high stand of Lake Lahontan derived from models of evaporation and lake level. *Climate dynamics*, *4*(3), 207-217.

Hostetler, S. W., Giorgi, F., Bates, G. T., & Bartlein, P. J. (1994). Lake-atmosphere feedbacks associated with paleolakes Bonneville and Lahontan. *Science*, *263*(5147), 665-668.

Hren, M. T., & Sheldon, N. D. (2012). Temporal variations in lake water temperature: Paleoenvironmental implications of lake carbonate δ18O and temperature records. *Earth and Planetary Science Letters*, *337*, 77-84.

Ibarra, D. E., & Chamberlain, C. P. (2015). Quantifying closed-basin lake temperature and hydrology by inversion of oxygen isotope and trace element paleoclimate records. *American Journal of Science*, *315*(9), 781-808.

Ibarra, D. E., Egger, A. E., Weaver, K. L., Harris, C. R., & Maher, K. (2014). Rise and fall of late Pleistocene pluvial lakes in response to reduced evaporation and precipitation: Evidence from Lake Surprise, California. *Geological Society of America Bulletin*, *126*(11-12), 1387-1415.

Ibarra, D. E., Oster, J. L., Winnick, M.J., Rugenstein, J. K. C., Byrne, M. P., & Chamberlain, C. P. (2018). Lake Area Constraints on Past Hydroclimate in the Western United States: Application to Pleistocene Lake Bonneville. *Lake Bonneville Geology Conference Proceedings*, 1-8.

Izumi, K., & Bartlein, P. J. (2016). North American paleoclimate reconstructions for the Last Glacial Maximum using an inverse modeling through iterative forward modeling approach applied to pollen data. *Geophysical Research Letters*, *43*(20), 10-965.

Jones, M. D., Roberts, C. N., & Leng, M. J. (2007). Quantifying climatic change through the last glacial–interglacial transition based on lake isotope palaeohydrology from central Turkey. *Quaternary Research*, *67*(3), 463-473.

Kaufman, D. S. (2003). Amino acid paleothermometry of Quaternary ostracodes from the Bonneville Basin, Utah. *Quaternary Science Reviews*, *22*(8-9), 899-914.

Kelson, J. R., Huntington, K. W., Schauer, A. J., Saenger, C., & Lechler, A. R. (2017). Toward a universal carbonate clumped isotope calibration: Diverse synthesis and preparatory methods suggest a single temperature relationship. *Geochimica et Cosmochimica Acta*, *197*, 104-131.

Kim, S. T., O'Neil, J. R., Hillaire-Marcel, C., & Mucci, A. (2007). Oxygen isotope fractionation between synthetic aragonite and water: influence of temperature and Mg2+ concentration. *Geochimica et Cosmochimica Acta*, *71*(19), 4704-4715.

Kirby, M. E., Feakins, S. J., Bonuso, N., Fantozzi, J. M., & Hiner, C. A. (2013). Latest Pleistocene to Holocene hydroclimates from Lake Elsinore, California. *Quaternary Science Reviews*, *76*, 1-15.

Laskar, J., Robutel, P., Joutel, F., Gastineau, M., Correia, A. C. M., & Levrard, B. (2004). A long-term numerical solution for the insolation quantities of the Earth. *Astronomy & Astrophysics*, 428(1), 261-285.

Lechler, A. R., Niemi, N. A., Hren, M. T., & Lohmann, K. C. (2013). Paleoelevation estimates for the northern and central proto–Basin and Range from carbonate clumped isotope thermometry. *Tectonics*, *32*(3), 295-316.

Lehner, B., & Grill, G. (2013). Global river hydrography and network routing: baseline data and new approaches to study the world's large river systems. *Hydrological Processes*, *27*(15), 2171-2186.

Lehner, B., Verdin, K., and Jarvis, A. (2008). New Global Hydrography Derived From Spaceborne Elevation Data. *Eos, Transactions American Geophysical Union*, 89(10), 93–94.

Lemons, D. R., Milligan, M. R., & Chan, M. A. (1996). Paleoclimatic implications of late Pleistocene sediment yield rates for the Bonneville Basin, northern Utah. *Palaeogeography, Palaeoclimatology, Palaeoecology*, *123*(1-4), 147-159.

Linacre, E. T. (1993). Data-sparse estimation of lake evaporation, using a simplified Penman equation. *Agricultural and Forest Meteorology*, *64*(3-4), 237-256.

Liu, S., Jiang, D., & Lang, X. (2018). A multi-model analysis of moisture changes during the last glacial maximum. *Quaternary Science Reviews*, *191*, 363-377.

Lora, J. M., Mitchell, J. L., & Tripati, A. E. (2016). Abrupt reorganization of North Pacific and western North American climate during the last deglaciation. *Geophysical Research Letters*, *43*(22), 11-796.

Lora, J. M., Mitchell, J. L., Risi, C., & Tripati, A. E. (2017). North Pacific atmospheric rivers and their influence on western North America at the Last Glacial Maximum. *Geophysical Research Letters*, *44*(2), 1051-1059.

Lora, J. M. (2018). Components and mechanisms of hydrologic cycle changes over North America at the Last Glacial Maximum. *Journal of Climate*, *31*(17), 7035-7051.

Lowenstein, T. K., Li, J., Brown, C., Roberts, S. M., Ku, T. L., Luo, S., & Yang, W. (1999). 200 ky paleoclimate record from Death Valley salt core. *Geology*, *27*(1), 3-6.

Lyle, M., Heusser, L., Ravelo, C., Yamamoto, M., Barron, J., Diffenbaugh, N. S., Herbert, T., & Andreasen, D. (2012). Out of the tropics: the Pacific, Great Basin Lakes, and Late Pleistocene water cycle in the western United States. *Science*, *337*(6102), 1629-1633.

Madsen, D. B., Rhode, D., Grayson, D. K., Broughton, J. M., Livingston, S. D., Hunt, J., Quade, J, D Schmidtt, & Shaver III, M. W. (2001). Late Quaternary environmental change in the Bonneville basin, western USA. *Palaeogeography, Palaeoclimatology, Palaeoecology*, *167*(3-4), 243-271.

Maher, K., Ibarra, D. E., Oster, J. L., Miller, D. M., Redwine, J. L., Reheis, M. C., & Harden, J. W. (2014). Uranium isotopes in soils as a proxy for past infiltration and precipitation across the western United States. *American Journal of Science*, *314*(4), 821-857.

Majoube, M. (1971). Oxygen-18 and deuterium fractionation between water and steam (in French). *Journal de Chimie Physique et de Physico-Chimie Biologique*, *68*, 1423-1436.

Maloney, E. D., Camargo, S. J., Chang, E., Colle, B., Fu, R., Geil, K. L., Hu Q, Jiang X, Johnson N, Karnauskas KB, & Kinter, J. (2014). North American climate in CMIP5 experiments: Part III: Assessment of twenty-first-century projections. *Journal of Climate*, *27*(6), 2230-2270.

Matsubara, Y., & Howard, A. D. (2009). A spatially explicit model of runoff, evaporation, and lake extent: Application to modern and late Pleistocene lakes in the Great Basin region, western United States. *Water Resources Research*, *45*(6).

McGee, D., Moreno-Chamarro, E., Marshall, J., & Galbraith, E. D. (2018). Western US lake expansions during Heinrich stadials linked to Pacific Hadley circulation. *Science advances*, *4*(11), 1-10.

Mering, J. A. (2015). New constraints on water temperature at Lake Bonneville from carbonate clumped isotopes. *Doctoral dissertation, UCLA*. 1-178.

Meyers, J. S. (1962). *Evaporation from the 17 western states*. US Government Printing Office.

Mifflin, M. D., & Wheat, M. M. (1979). Pluvial lakes and estimated pluvial climates of Nevada.

Morrill, C., Lowry, D. P., & Hoell, A. (2018). Thermodynamic and Dynamic Causes of Pluvial Conditions During the Last Glacial Maximum in Western North America. *Geophysical Research Letters*, *45*(1), 335-345.

Munroe, J. S., & Laabs, B. J. (2013). Latest Pleistocene history of pluvial Lake Franklin, northeastern Nevada, USA. *GSA Bulletin*, *125*(3-4), 322-342.

Oster, J. L., Ibarra, D. E., Winnick, M. J., & Maher, K. (2015). Steering of westerly storms over western North America at the Last Glacial Maximum. *Nature Geoscience*, *8*(3), 201.

Personius, S. F., Crone, A. J., Machette, M. N., Mahan, S. A., & Lidke, D. J. (2009). Moderate rates of late Quaternary slip along the northwestern margin of the Basin and Range Province, Surprise Valley fault, northeastern California. *Journal of Geophysical Research: Solid Earth*, *114*(B9).

Petryshyn, V. A., Lim, D., Laval, B. L., Brady, A., Slater, G., & Tripati, A. K. (2015). Reconstruction of limnology and microbialite formation conditions from carbonate clumped isotope thermometry. *Geobiology*, *13*(1), 53-67.

Reheis, M. (1999). Highest pluvial-lake shorelines and Pleistocene climate of the western Great Basin. *Quaternary Research*, *52*(2), 196-205.

Russell, R. J. (1927). *The Land Forms of Surprise Valley, Northwestern Great Basin*. University of California Press.

Rutz, J. J., Steenburgh, W. J., & Ralph, F. M. (2014). Climatological characteristics of atmospheric rivers and their inland penetration over the western United States. *Monthly Weather Review*, *142*(2), 905-921.

Santi, L., Arnold, A., Ibarra, D., Whicker, C., Mering, J., Oviatt, C. G., & Tripati, A. (2019). Lake level fluctuations in the Northern Great Basin for the last 25,000 years. *EarthArXiv*. 30 May, 2019. doi: 10.31223/osf.io/6as7t.

Smith, G. I., and F. A. Street-Perrott (1983). Pluvial lakes of the western United States, in The Late Pleistocene, edited by S. C. Porter, pp. 190– 212, Univ. of Minnesota Press, Minneapolis.

Soetaert, K., Cash, J., Mazzia, F., & Soetaert, M. K. (2016). Package 'bvpSolve'.

Spencer, C., & Kim, S. T. (2015). Carbonate clumped isotope paleothermometry: a review of recent advances in CO 2 gas evolution, purification, measurement and standardization techniques. *Geosciences Journal*, *19*(2), 357-374.

Steinman, B. A., & Abbott, M. B. (2013). Isotopic and hydrologic responses of small, closed lakes to climate variability: Hydroclimate reconstructions from lake sediment oxygen isotope records and mass balance models. *Geochimica et Cosmochimica Acta*, *105*, 342-359.

Talbot, M. R. (1990). A review of the palaeohydrological interpretation of carbon and oxygen isotopic ratios in primary lacustrine carbonates. *Chemical Geology: Isotope Geoscience Section*, *80*(4), 261-279.

Thompson, R. S., Anderson, K. H., & Bartlein, P. J. (1999). *Quantitative paleoclimatic reconstructions from late Pleistocene plant macrofossils of the Yucca Mountain region* (p. 39). US Department of the Interior, US Geological Survey.

Tripati, A. K., Eagle, R. A., Thiagarajan, N., Gagnon, A. C., Bauch, H., Halloran, P. R., & Eiler, J. M. (2010). 13C–18O isotope signatures and 'clumped isotope' thermometry in foraminifera and coccoliths. *Geochimica et cosmochimica acta*, *74*(20), 5697-5717.

Welker, J. M. (2012). ENSO effects on δ18O, δ2H and d-excess values in precipitation across the US using a high-density, long-term network (USNIP). *Rapid Communications in Mass Spectrometry*, *26*(17), 1893-1898.

Wolfe, B. B., Falcone, M. D., Clogg-Wright, K. P., Mongeon, C. L., Yi, Y., Brock, B. E., Amour, N.A.S., Mark, W.A. & Edwards, T. W. (2007). Progress in isotope paleohydrology using lake sediment cellulose. *Journal of Paleolimnology*, *37*(2), 221-231.

Wong, C. I., Potter, G. L., Montañez, I. P., Otto-Bliesner, B. L., Behling, P., & Oster, J. L. (2016). Evolution of moisture transport to the western US during the last deglaciation. *Geophysical Research Letters*, *43*(7), 3468-3477.

Clumped Isotope Thermometry and Hydroclimate Reconstructions of Late Pleistocene Pluvial Lakes in the Great Basin, Western North America

Lauren Santi[1], Alexandrea Arnold[1], Daniel E. Ibarra[2], Rico Lomarda[1],

Aradhna Tripati[1]

[1] Department of Earth, Planetary, and Space Sciences, Department of Atmospheric and Oceanic Sciences, Institute of the Environment and Sustainability, Center for Diverse Leadership in Science, University of California, Los Angeles, California, USA

[2]Department of Earth System Science, Stanford University, Stanford, California, USA

ABSTRACT

The Great Basin is a hydrographic and topographic province in North America, known for its overall arid climate and being the largest continuous area of endorheic watersheds. Remarkably, in stark contrast to the present, the province was characterized by numerous large-scale lake systems during the Last Glacial Maximum (LGM; ~23,000-19,000 years ago) and subsequent deglaciation (~19,000-11,000 years ago). The contrast between these hydrological states indicates significant changes in the water cycle led to modern aridification, with hypotheses proposed including changes in moisture sources, rainfall intensity, and lake evaporation rates. In this study, we use a thermodynamically-based tracer, carbonate clumped isotope thermometry, to constrain four variables in the hydrologic budget (temperature, precipitation rates, lake evaporation rates, and water $\delta^{18}O$) at a subset of LGM pluvial lakes: Lake Chewaucan, Lake Franklin, Mud Lake, and Lake Surprise. Our results indicate that different mechanisms sustained the spatially and temporally asynchronous growth of these post-LGM lakes. We infer that Lakes Chewaucan, Franklin, and Mud had elevated precipitation rates compared to modern at the time of maximum lake extent (~2.5, 5, and ~15 times modern values, respectively), while Lake Surprise instead had precipitation rates ~80% of modern. Furthermore,

our estimates of lake evaporation indicate that evaporation depression contributed to increased effective moisture at Lake Surprise and Mud Lake, but not at Lake Chewaucan or Lake Franklin. This variability in causal mechanisms for lake growth is interpreted with respect to proposed atmospheric forcings, and sheds light on local atmospheric variability in the western US, which is especially valuable in consideration of future climate change.

INTRODUCTION

The modern Great Basin encompasses a wide range of biomes and ecologies, but is largely characterized as an extensive desert region. It has consistently low levels of precipitation, with many regions receiving under 250 mm of rain a year, especially in the southern Great Basin and in the rain shadow of the Sierras (Comstock & Ehleringer, 1992). Sediments and proxy data paint a picture of a region that has experienced dramatic aridification due to changes in the water balance and major shifts in terrestrial ecosystems (Matsubara & Howard, 2009; Huntington et al., 2010; Hudson et al., 2017; McGee et al., 2018); furthermore, this region is poised to become drier in the future, of major concern given its current water-stressed state (e.g. Seager & Vecchi 2010; Cook et al., 2014; Maloney et al., 2014).

Here we explore the use of climate proxy data for the Last Glacial Maximum (LGM; 23,000-19,000 years ago) and deglacial period (~19,000-11,000 years ago) to understand mechanisms of aridification in the Great Basin. During the LGM and deglacial, large lakes and enhanced precipitation relative to evaporation characterized this region (e.g. Mifflin & Wheat,1979; Reheis, 1999; Lyle et al., 2012; Ibarra et al., 2018; Santi et al., 2019). Lake highstands and the timing of lake disappearance was asynchronous, including along zonal bands, implying that a complex interplay of factors with significant spatial variability is likely important

in the region (Hostetler & Benson, 1990; Negrini, 2002; Munroe & Laabs, 2012; Kirby et al., 2013). Lora (2018) suggests there may be a symmetric response of hydroclimate in the Great Basin to global warming and cooling, and that the LGM may thus represent a key time period for the study of future hydroclimate dynamics.

However, parsing out the specific contributions of different thermodynamic and dynamic processes that impact water transport to climate forcing in the Great Basin is unclear. Models and data provide ambiguous constraints on the magnitude of changes in temperature, precipitation, and evaporation rates. Proposed mechanisms for past lake shrinkage include changes in the strength and position of the polar jet stream (e.g. Hostetler & Benson, 1990; Negrini, 2002; Munroe & Laabs, 2012; Kirby et al., 2013), reduced transport by atmospheric rivers (e.g. Rutz & Steenburgh, 2014; Lora et al, 2015; Lora et al., 2017; Lora, 2018), increased evaporation rates (Smith & Street-Perrot,1983; Mering, 2015; Lora, 2018), changes in the strength and position of the wintertime Aleutian low and North Pacific high (COHMAP Members, 1988; Bromwich et al., 2004; Kim et al., 2008; Unterman et al., 2011), and/or changes in the strength of the summer monsoon (Lyle et al., 2012).

This study examines how hydrologic variables in different lakes in the Great Basin have evolved since the LGM using an interdisciplinary approach that draws on concepts from sedimentary geology, geochemistry, paleoclimate, and hydrology. We estimate temperature, precipitation rates, evaporation rates, and water $\delta^{18}O$ using a thermodynamic tracer – clumped isotope analyses of lake sediments. As described below, field sampling of lakes and geochemical analysis allows us to estimate temperature and water $\delta^{18}O$, while sampling of closed basin lakes allows us to neglect runoff. Therefore, only precipitation and evaporation would dictate lake elevation. Thus, precipitation can be derived using mass-balance approaches that incorporate

basin hypsometry, while evaporation can be modeled as a function of temperature. This approach lets us determine the quantitative contributions of changing precipitation and evaporation rates as mechanisms modulating lake levels in the Great Basin through time. Sample localities cover an extensive spatial range that allow for insights into how climate evolved through both time and space, including a greater understanding of atmospheric processes that have affected the growth and retreat of pluvial lakes. We use this information to evaluate the regional predictions of global climate models, and examine how climate change can alter ecosystem water balance in the West.

BACKGROUND

Previous Great Basin Field Studies

Lake hydrographs constructed from dated lake sediments track temporal changes in minimum lake level and can be interpreted as changes in effective moisture (precipitation relative to evaporation, or P-E) through time. In the Great Basin, existing lake hydrographs show evidence for an increase in lake levels beginning in the late LGM, with lake highstands occurring during the deglacial period (e.g. Licciardi, 2001; Adams et al., 2008; Kurth et al., 2011; Benson et al., 2013; Ibarra et al., 2014; Munroe & Laabs, 2014; Mering, 2015; Egger et al., 2018; Santi et al., 2019). It is notable that, although over 50 pluvial lakes have been documented in the Great Basin during the LGM and deglacial in the literature, most existing studies focus on a small subset, which typically include Lake Bonneville and Lake Lahontan and their subbasins (e.g. Hostetler & Benson, 1990; Benson et al., 1995; Godsey et al., 2005; Adams et al., 2008; Godsey et al., 2011; Benson et al., 2013; Miller et al., 2013; Mering, 2015; Oviatt, 2015; Petryshyn et al., 2016), in part because of their dramatic size at their maximum extent.

A range of different types of proxy evidence (including packrat middens, halite inclusions, tree lines, and pollen) indicate cold and wet conditions, with reduced evaporation rates compared to modern values (cf. Matsubara & Howard, 2009, their Table 1). However, there is significant uncertainty associated with existing reconstructions. Reconstructed precipitation rates range from 80 – 260% of modern, evaporation rates between 12-90% of modern, and temperature depressions of 3 -15°C (e.g. Matsubara & Howard, 2009; Ibarra et al., 2014). Hence, proxy data is only in rough agreement on the sign of evaporation and temperature changes relative to their modern values, while precipitation changes differ in their sign. Furthermore, the magnitude of these inferred changes varies appreciably between proxy systems. Finally, there are few studies that have examined how specific hydrologic variables (i.e., precipitation rate, or evaporation rate) vary spatially throughout the Great Basin; the most robust study that exists is based on pollen (Bartlein et al., 2011).

Evaluation of Climate Model Simulations of Hydroclimate Change

The International Panel for Climate Change (IPCC) is tasked with synthesizing, analyzing, and reporting the status of climate change at regular intervals (e.g. Pachaurie & Reisinger, 2007; Smith et al., 2009). Their work is largely based on climate models, which forecast or hindcast meteorological variables at set points in the future or the past. Paleoclimate studies can provide observational "benchmarks" and also enhance process-based understanding, both of which can contribute to improved process depiction in models that will play a critical role in policy and environmental planning in the decades to come.

The Paleoclimate Modeling Intercomparison Project 3 (PMIP3) represents the latest cooperative modeling process involving paleoclimate data, with two relevant steady-state

experiments: the Last Glacial Maximum (21 ka BP) and pre-industrial era (1850). Each of these set points in time is denoted as a model experiment and is run under prescribed boundary conditions, including greenhouse gas concentrations, continental configuration, and ice sheet extent. Transient models (e.g. Transient Climate Evolution, 'TraCE', which uses the Community Climate System Model Version 3) are simulations run with model output available at a much finer temporal resolution. However, there are no model intercomparison projects akin to PMIP3 for transient model performance.

Proxy data are invaluable, as they provide independent constraints on the response of the Earth system to climatic forcings (e.g. changes in incoming insolation) and, when compared to climate model hindcasts, can be used to evaluate model skill on a regional level (e.g COHMAP Members 1988; Bartlein et al., 2011; Braconnot et al., 2012; Hargreaves et al., 2013; Otto-Bliesner et al., 2014; Loomis et al., 2017; Lora et al., 2017; Lora, 2018). Lora et al. (2017) and Lora (2018) assessed model skill in reconstructing past precipitation rates in the Western US using a compilation of reference proxy data (e.g. sediment yields, pollen and halite inclusions), and compare process depiction between top-performing and under-performing climate models.

In the western United States, simulations from PMIP3 models generally exhibit poor agreement in regard to past changes in hydroclimates. Several climate models disagree not only over the magnitude of changes, but some over the sign of their predictions; while some PMIP3 models simulate less rainfall in the Great Basin during the LGM, others simulate more (Fig. 3.5). Furthermore, model output from an established transient climate model 'TraCE' is run at a relatively low resolution (3.75° by 3.75°), which is limiting, given the relative proximity of our four lake basins.

To provide well-constrained assessments of model skill in the Great Basin, our study adds thermodynamically-based temperature, precipitation, and evaporation constraints derived from a set of novel approaches that utilize a stable isotope proxy, clumped isotopes. These constraints provide observational benchmarks for comparison to PMIP3 and TraCE model output.

LOCALITY INFORMATION AND METHODS

Locality Information

Samples are derived from the shorelines of a series of closed basin paleolakes within the Great Basin of the western United States (Supplemental Fig. 3.S1). For this study, we collected carbonate sediments from paleoshorelines of Lakes Franklin, Mud, and Surprise. We chose these lake basins because they span a significant zonal and meridional range, and remained closed-basin lakes even at their highest extents (e.g. Mifflin & Wheat, 1978; Reheis, 1999). We also include novel analysis on samples that were previously reported in published studies from Lake Chewaucan (Hudson et al., 2017; Egger et al., 2018), Lake Surprise (Ibarra et al., 2014; Santi et al., 2019), and Mud Lake (Dickerson, 2006; Dickerson, 2009).

Lake shorelines were identified through a combination of literature review and Google Earth observations. At each sample locality, we recorded GPS coordinates, and the elevation of each sample was later determined using the USGS Elevation Point Query Service, which reports ⅓ arc-second elevation data across the continental United States with an elevation resolution of ~3 meters.

Geologic Settings of Lake Basins

Lake Chewaucan

Lake Chewaucan (42.7°N, 120.5°W) was located in southern Oregon, and was comprised of four subbasins: Summer Lake, Upper Chewaucan Marsh, Lower Chewaucan Marsh, and Albert Lake. Today, Albert Lake and Summer Lake are modern lakes that become desiccated during the mid to late summer each year, at times completely drying up. Conversely, in the past, these four subbasins have had variable connectivity, depending on the lake levels. Past lake shorelines are found between 1305-1383 m, with tufa comprising our sample set. Using modern weather station data from Lakeview, OR, modern day mean annual air temperature (MAAT) near Lake Chewaucan is 7.6 ±1°C, while mean annual precipitation and pan evaporation rates are 240 ± 50 mm/yr and 1075 ± 80 mm/yr, respectively.

Lake Franklin

Lake Franklin (40°N, 115°W) was located in northeast Nevada, just east of Ruby Valley. This pluvial lake has been previously studied in Licciardi (2001) and Munroe & Laabs (2013), and has an estimated highstand between 16,800 ± 130 and 15,070 ± 100 yr B.P (Munroe & Laabs, 2013). Lake shorelines are found between 1819-1850 m, with gastropod shells and tufa comprising the sample set. Modern day MAAT is 7.8 ±1°C, while the modern precipitation and pan evaporation rates in Ruby Valley are 191 ± 80 mm/yr and 1177 ± 90 mm/yr, respectively (Shevenell, 1996). Lake elevation data is compiled from Licciardi (2001), Munroe & Laabs (2013), and Santi et al. (2019), while all stable and clumped isotope data is from this study.

Mud Lake

Mud Lake (37.8°N, 118°W), was a small lake located in southern Nevada, just south of Tonopah. Geological and sedimentological evidence of this region (including the nearby Stonewall Flat) indicates that the region once held several small lakes, one of which was Mud Lake (e.g. Dickerson, 2006; Dickerson, 2009). Evidence of past lake shorelines can be found between 1591-1609 m, with some offset around the perimeter due to Holocene age faulting (Dickerson, 2006). Modern MAAT at Mud Lake (Silver Peak, NV) is 11.8± 0.5°C, while modern precipitation and pan evaporation rates are 171 ± 80 mm/yr and 2672 ± 80 mm/yr, respectively.

Previous paleoclimate analyses in the Mud Lake area are synthesized in other publications (e.g. Dickerson, 2006; Dickerson, 2009; Dickerson, 2014; Dickerson & Foreman, 2014). Many regional paleoclimate analyses use desert varnish and packrat middens as proxies for past climate, indicating that precipitation rates were elevated to ~260% of their current value during the late deglacial period (Dickerson & Foreman, 2014). In this work, we report clumped and stable isotope values for previously published stromatolites, collected from the paleoshorelines of Mud Lake (Dickerson, 2006; Dickerson, 2009).

Lake Surprise

Lake Surprise (41.5°N, 120°W) was located in northeast California, and occupied the modern-day Surprise Valley. Importantly, this location lies in a climatic transition zone between the Great Basin and the Pacific Northwest, which are typically modeled as being wetter than modern (Great Basin) and drier than modern (Pacific Northwest) during the LGM (Kim et al., 2008; Laîné et al., 2009; Braconnot et al., 2012). Modern MAAT at Lake Surprise is 9.2± 1°C,

while modern precipitation and pan evaporation rates are 566 ± 165 mm/yr and 905 ± 80 mm/yr, respectively (Ibarra et al., 2014). Reconstructed lake hydrographs imply a rapid moisture forcing at ~16 ka, culminating in a post-LGM highstand at 15.19 ka, at a maximum lake elevation 176 meters above the modern playa (Ibarra et al., 2014; Santi et al., 2019).

Carbonate Materials

Photosynthetic requirements for carbonate formation imply that carbonate presence can be used to provide reasonably precise constraints on minimum lake elevation at the time of carbonate precipitation (e.g., Felton et al., 2006; Hren & Sheldon, 2012; Zimmerman et al., 2012; Ibarra et al., 2014; Petryshyn et al., 2015; Horton et al., 2016). As such, carbonate is a common material for clumped isotope analysis, given its ability to constrain past lake levels and its ubiquity in many relevant paleoclimate sites (e.g. Hren & Sheldon, 2012; Huntington et al., 2010, 2015; Petryshyn et al., 2015; Horton et al., 2016; Egger et al., 2018). In this study, our carbonate samples are comprised of tufa, stromatolites, and gastropod shells, all collected from the perimeters of closed basin lakes (Table 3.1).

Radiocarbon Dating

Lake Surprise samples from Santi et al. (2019) were radiocarbon dated via Accelerator Mass Spectrometry (AMS) at UC Irvine. Ibarra et al. (2014) and Egger et al. (2018) dated samples by AMS at Beta Analytic, Inc. and DirectAMS, respectively. A subset of samples from Ibarra et al. (2014) were dated using uranium-series methods. All Lake Franklin and Mud Lake samples were dated using radiocarbon methods.

For all radiocarbon results we use *IntCal13* to convert conventional ^{14}C ages to calibrated ^{14}C ages, expressed as thousands of years before present, "ka". We plot the median calibrated probability and the 2σ uncertainty. All sample ages are included in Table 3.1.

Clumped Isotope Measurements

Mass spectrometry was completed at UCLA on a trio of mass spectrometers (See Supplement), with at least four replicates of each sample. Error on Δ_{47} is reported as standard error of the mean, as this error is minimized by increasing the number of sample replicates (Fernandez et al., 2017). All clumped and stable isotope data is included in Table 3.2.

Clumped Isotope Constraints on Past Hydroclimates

Modern microbialites, tufas, and other types of lacustrine carbonates indicate clumped isotope values can be robustly used to reconstruct carbonate formation temperature, with water temperatures typically indicating formation in the summer or spring through fall (Kele et al., 2015; Petryshyn et al., 2015; Horton et al., 2016; Bernasconi et al., 2018). We use Δ_{47} to calculate water temperature by applying the temperature calibration equation of Bernasconi et al. (2018) because it uses the same carbonate standard-based reference frame as our data. Air temperature is derived from water temperature using a water to air transfer function from Hren & Sheldon (2012), which assumes preferential carbonate formation between April and October. Water $\delta^{18}O$ is calculated by applying the material-specific fractionation factor of Kim & O'Neil (1997) to measured carbonate $\delta^{18}O$.

We estimate past evaporation rates using a modified version of the Penman equation, derived specifically for lake evaporation, as applied in Mering (2015) and Ibarra et al. (2014).

This equation uses input of wind speed (u), temperature (T), dew point temperature (T_d), elevation (z), and latitude (Lat) to estimate lake evaporation (See Chapter 2 Supplement). We assume past values of u, z, and Lat are identical to modern values, which themselves are multi-year weather station averages. Temperature is derived from Δ_{47}, and T_d is assumed to be a constant offset from air temperature. We convert this estimate of lake-based evaporation to a basin-scale evaporation rate by assigning a weight to lake evaporation based on the relative area of the lake during each time period, and scaling evapotranspiration (a result of our precipitation model; see below and Chapter 2 Supplement) on land by the relative area of the tributary. Weighted evaporation rates are used for comparison to climate model evapotranspiration. Finally, we estimate past precipitation rates using a clumped isotope-constrained P and E modeling approach used by Mering (2015) on Lake Bonneville, combined with the isotope mass balance model of Ibarra et al. (2014), first used for Surprise Valley, which itself was modified from Jones et al. (2007). Descriptions and derivations of the above equations are included in the Chapter 2 Supplement.

RESULTS

Lake Level Histories as Reconstructed from ^{14}C and U-Th Ages

On Fig. 3.1 we compile lake hydrographs for each basin, which are interpreted as minimum lake levels. Hydrographs include both new data and data compiled from existing literature (e.g. Lillquist 1994; Munroe & Laabs, 2012; Dickerson, 2006; Dickerson, 2009; Ibarra et al., 2014; Hudson et al., 2017; Egger et al., 2018; Santi et al., 2019). From top to bottom, basins are plotted from geographic northeast to southwest, respectively.

Geochemical Evidence of Closed Basin Behavior from $\delta^{13}C$ and $\delta^{18}O$

Calculation of precipitation rates from clumped and bulk isotope values using a steady-state model is dependent on the assumption that samples are taken from a closed basin; that is, the only input of water is from precipitation and the only output is from evaporation. One diagnostic tool to show closed basin character is to plot $\delta^{13}C$ against $\delta^{18}O$, where strong positive covariance between $\delta^{13}C$ and $\delta^{18}O$ has been historically associated with closed basin behavior and evaporative enrichment (e.g. Talbot, 1990; Horton et al., 2016). A plot of $\delta^{13}C$ against $\delta^{18}O$ for each lake basin is presented in Supplemental Fig. 3.S2, with the Pearson Correlation Coefficient (PCC) for each data set included in each subplot.

To a first order, all lake basins show positive covariation in $\delta^{13}C$ and $\delta^{18}O$. Lake Surprise has the strongest covariation between $\delta^{13}C$ and $\delta^{18}O$ (PCC = 0.91). Mud Lake (PCC = 0.80) and Lake Franklin (PCC = 0.55) also show positive correlation. Lake Chewaucan demonstrates strong positive covariation for one sample set (PCC = 0.83), while the other instead shows a slight negative correlation (PCC = -0.20). We note that the latter sample set is taken from Summer Lake, a subbasin that supports a shallow modern lake. Overall, these data support closed basin conditions (with the possible exception of a few samples from Lake Chewaucan), thus justifying the use of a steady-state mass balance equation for precipitation.

Clumped Isotope Constraints on Past Hydroclimates

For each basin, we plot the temporal evolution of water temperature (Fig. 3.2a), air temperature (Fig. 3.2b), water $\delta^{18}O$ (Fig. 3.3a), precipitation rate (Fig. 3.3b), and weighted evaporation rate (Fig 3.3c).

To a first order, average MAATs during the LGM and deglacial period at Lake Chewaucan, Lake Franklin, and Lake Surprise are lower than their modern values. At Lake Franklin, Mud Lake, and Lake Surprise, calculated MAAT decreases throughout the deglacial period, while it increases during the late deglacial period at Lake Chewaucan.

Water $\delta^{18}O$ shows both temporal and spatial variability. Samples from Lake Surprise have the highest temporal resolution, and indicate a maximum variability of ~4‰ in water $\delta^{18}O$. Mud Lake shows much less variability in water $\delta^{18}O$, although large gaps of time separate data points. Data from Lake Chewaucan and Lake Franklin indicate large positive excursions in water $\delta^{18}O$ during relatively short (~2 ka) periods of time. While some basins indicate significant $\delta^{18}O$ excursions (~10‰ in 2 ka for some lake basins), this magnitude of variability is observed in other lake $\delta^{18}O$ reconstructions on similar timescales (e.g. Edwards & McAndrews, 1989; Wolfe et al., 2007).

Reconstructed precipitation and evaporation rates decrease through time at Lake Franklin, Mud Lake, and Lake Surprise, but increase during the late deglacial period at Lake Chewaucan. Weighted evaporation rates demonstrate similar trends to precipitation rates.

We estimate the thermodynamic versus dynamic contribution to changing lake levels (See Table 3.3 and description in Supplement), as in Ibarra et al. (2018). Results are reported for each lake basin, for both the LGM and deglacial period.

Evaluation of Climate Model Simulations of Hydroclimate Change

We compare our temperature and precipitation estimates to nine PMIP3 models, as well as one transient climate model: 'TraCE' (Figs. 3.4-3.8). For each plot, we show anomalies of the climatological variable, defined as the difference between the LGM and the modern value. For

comparison with PMIP3 (Figs. 3.4-3.6), we use an average of all samples dated between 19-23 ka along with modern weather station data. We note that there are no LGM-aged samples for Lake Franklin. For comparison with TraCE output (Figs. 3.7-3.8), we plot an average of all samples dated within the corresponding period of time. On each model-data comparison figure (Figs. 3.4-3.8), we include the average analytical uncertainty for all samples included in the given time frame. While not explicitly included in this error analysis, we attach a table with descriptions of additional sources of uncertainty in the supplement (Table 3.S1).

Following Hargreaves et al. (2013), we calculate model skill in reproducing the magnitude of temperature, precipitation, and weighted evaporation estimates, derived using clumped isotope analysis (Fig. 3.9). For Lake Chewaucan and Lake Surprise, we calculate model skill with respect to our LGM aged samples; however, for Lake Franklin, we calculate model skill with respect to deglacial values, as there are no LGM samples from Lake Franklin. We do not include a model skill analysis for Mud Lake, due to the limited number of observations. Our model skill for temperature ranges from a minimum of -0.62 to a maximum of 0.68, with generally positive model skills for Lake Chewaucan and Lake Surprise and negative model skill for Lake Franklin. Our model skill for precipitation ranges from a minimum of -7.76, to a maximum of 0.21, with overall negative skill for all three lake basins. Our model skill for weighted evaporation ranges from a minimum of -0.66 to a maximum of 0.64, with an overall positive skill for Lake Surprise and Lake Chewaucan. Overall, climate models have the highest skill scores for Lake Surprise, and the lowest skill scores for Lake Franklin.

DISCUSSION

Lake Level Histories as Reconstructed from ^{14}C and U-Th Ages

Santi et al. (2019) describes lake hydrographs for Lakes Chewaucan, Franklin, Mud, and Surprise (Fig. 3.1), which we briefly summarize here. Overall, we observe non-synchronous timing in lake highstands between basins, progressing from the southeast to the northwest during the deglacial period. In many cases, lake transgressions to highstand levels (from moderate stillstand levels) happened in a relatively short period of time between 17 and 14 ka, while regressions typically occurred over a much longer period.

Lake Chewaucan

Lake Chewaucan was the last of the four lakes to reach highstand levels during the deglacial, between 13-14 ka. This timing is consistent with a previously proposed northwest-trending change in moisture delivery during the deglacial period (Lyle et al., 2012; McGee et al., 2018; Morrill et al., 2018; Oster et al., 2015). Despite reasonable scatter in data prior to the LGM, lake level trajectories indicate a decrease in lake elevation between 25-20 ka. Following an initial LGM lake level rise, there is a short desiccation at ~16 ka, prior to the highstand at 1356 m, between 13-14 ka. Lake Chewaucan began to steadily recede ~13 ka, continuing into the early Holocene.

Lake Franklin

Between 22.5-20 ka, Lake Franklin stood at an elevation of ~1823 m, before rapidly transgressing to ~1830 m in the late LGM. Several anomalously high elevation samples taken during the early deglacial period are hypothesized to have come from a higher-elevation marsh

environment, rather than the lake shoreline itself (Munroe & Laabs, 2013). Lake Franklin reached its highstand elevation of 1850 m between 16.8-17.3 ka. The lake regression continued at a much slower rate than its transgression, progressing slowly over the rest of the deglacial period.

Mud Lake

The lake hydrograph for Mud Lake is the least constrained of the four lakes studied here. We note stable lake levels during the LGM and deglacial period, indicating consistently higher than modern levels of effective precipitation. With this given sample set, we are not able to discern definitive evidence of lake transgression or regression during the deglacial period.

Lake Surprise

At Lake Surprise, we see evidence of a rapid increase in lake levels at ~15.8 ka, prior to an ultimate highstand at ~16 ka. This rapid precipitation forcing is also observed at Lake Franklin and Lake Lahontan (e.g. Benson et al., 2013; Munroe & Laabs, 2013; Santi et al., 2019). Following its highstand, the hydrograph shows that Lake Surprise regressed over a much longer period of time, throughout the remainder of the deglacial period. We suggest that this gradual decrease in lake levels could be due to lake basin geometry: Lake Surprise was deep (~180 m, versus ~90 m for Lake Chewaucan; Egger et al., 2018) and had a high hydrologic index compared to more southerly lakes Franklin, Lahontan, and Bonneville (Santi et al., 2019). Furthermore, Surprise Valley has a relative lack of western-boundary orographic barriers compared to other lake basins, thus decreasing the potential for a rain shadow effect on precipitation (e.g. the southern Cascades to the west of Lake Chewaucan) (Egger et al., 2018).

Clumped Isotope Constraints on Past Hydroclimates

Across all lake basins, water temperatures for LGM and deglacial samples fall within the range of 7-20℃ (Fig. 3.2a). Water temperatures are the highest at Mud Lake, which is the lowest latitude lake and also the lowest in elevation. Water temperatures are the lowest at the more northerly and higher elevation lakes Chewaucan, Franklin, and Surprise. We translate our water temperatures to MAATs using a transfer function from Hren & Sheldon (2012), which assumes most carbonate growth occurs during the warm season, April to October (e.g., Purton & Brasier, 1997; Dettman et al., 1999; Goodwin et al., 2003; Versteegh et al., 2010) (Fig. 3.2b). We calculate water δ^{18}O using our measured carbonate δ^{18}O and the mineral specific fractionation from Kim & O'Neil (1997) (Fig. 3.3a). We calculate past precipitation rates using an isotope mass balance equation from Ibarra et al. (2014) and Jones et al. (2007) and lake-based evaporation using an equation based on a simplification of the Penman equation (Figs. 3.3b-3.3c). We derive the equation for precipitation rate and report the equations used for lake evaporation and weighted evaporation in the Chapter 2 Supplement. Finally, we estimate and discuss the thermodynamic versus dynamic contribution to changing lake levels in each location (See Supplement).

Lake Chewaucan

This is the northernmost site, and water temperatures during the LGM (19-23 ka) were 5.5± 2.5℃, corresponding to MAATs of -1.0± 2.5°C (Hren & Sheldon, 2012; Hudson et al., 2017). This indicates an average air temperature depression of 8.6±2.7℃ during the LGM, as implied by clumped isotope data and modern weather station temperature. Similarly, Hudson et al. (2017) report water temperatures derived from modern and LGM tufas, that correspond to a

10.0± 2.8℃ decrease in LGM MAAT, using the same published transfer function. Our estimates compare favorably with other Great Basin temperature depressions implied by pollen (10-11℃; Galloway, 1970), hydrologic mass balance modeling (10℃; Smith & Street-Perrot, 1983), and packrat midden plant assemblages (8℃; Thompson et al., 1999).

Water $\delta^{18}O$ shows a significant degree of variability, but ultimately increases to a maximum of 0.1‰ by ~13 ka. This increase in water $\delta^{18}O$ could be consistent both with changes in the dominant lake moisture source (e.g. decreasing contribution from the isotopically depleted North Pacific storm track versus the comparatively enriched atmospheric rivers) or with changes in the seasonality of precipitation, whereby summer precipitation is isotopically enriched relative to winter precipitation in the southwestern US (Welker et al., 2012). Alternatively, these changes in water $\delta^{18}O$ could be explained by changing temperature, with a change of 0.24‰ to 0.48‰ per ℃ expected for water warming from a starting temperature of 20℃ (Dansgaard, 1964). As this increase in water $\delta^{18}O$ coincides with increasing air temperatures, this hypothesis is consistent with the data. Furthermore, we calculate a large thermodynamic control on effective moisture during both the LGM (63%) and the deglacial period (68%; Table 3.3) at Lake Chewaucan (See Table 3.3 and Supplement).

Reconstructed precipitation rates show a sharp increase during the late deglacial period, coincident with the timing of lake highstand, to ~250% of modern. Similarly, weighted evaporation rates show constant values throughout the early deglacial, with a sharp increase around the time of the lake highstand. Overall, our results indicate that Lake Chewaucan was sustained by increased precipitation rates, despite increasing evaporation rates due elevated late-deglacial water temperatures.

Lake Surprise

From the Δ_{47} of a modern carbonate analyzed at Lake Surprise, we calculate a water temperature of 17.6±2℃, corresponding to a MAAT of 10.3 ±2℃. This estimate agrees well with modern MAAT recorded at nearby Cedarville, CA (9.2±1℃). For our LGM samples, we calculate an average water temperature of 10.2±1℃, corresponding to a MAAT of 0.3±1℃. Overall, modern weather station data and LGM-averaged temperatures indicate that the LGM was 8.9±1.4℃ colder than modern MAAT at Cedarville, NV, also in line with estimates of Great Basin LGM temperature depression based on pollen (10-11℃; Galloway, 1970), hydrologic mass balance modeling (10℃; Smith & Street-Perrot, 1983), and packrat midden plant assemblages (8℃; Thompson et al., 1999).

Water δ^{18}O demonstrates quasi-periodic behavior, with a maximum range of ~4‰ over the course of the LGM and deglacial periods. Lake Surprise water δ^{18}O demonstrates the least intra-basin variability of the four basins studied here. As Lake Surprise demonstrates the strongest closed-basin behavior of all basins (Fig. 3.S2), this is not an unexpected result.

LGM precipitation rates at Lake Surprise were lower than their modern average of 566 mm/yr, declining during the deglacial, and plateauing at ~80% of modern. Weighted evaporation rates show a similar trend, decreasing during the LGM and reaching a plateau during the deglacial period, at a value below the modern pan evaporation rate of 905 mm/yr (Ibarra et al., 2014). While weighted evaporation rates are not directly comparable to pan evaporation rates; this decreasing trend in evaporation, coupled with decreasing precipitation rates in the same period of time, indicate that evaporation depression likely played a much more important role than increased precipitation flux at Lake Surprise. This finding is consistent with the work of Oster et al. (2015) and Lora et al. (2017), who posit that Great Basin precipitation exhibited a

pronounced dipole during the LGM, and that northern Great Basin pluvial lakes (e.g. Lake Surprise) were driven more by temperature depression and subsequent reductions in evaporation rate, rather than by increased precipitation rates, as in the southern Great Basin.

We estimate a balance of thermodynamic (52%) and dynamic (48%) control on water balance during both the LGM and deglacial period (Table 3.3), suggesting that a complex interplay of factors was important in driving water balance at Lake Surprise.

Lake Franklin

During the mid-deglacial period, average water temperature at lake Franklin was 13.8±1.5°C, corresponding to a MAAT of -5.3±1.5°C. Modern MAAT at Lake Franklin is 7.8±1°C, indicating 13.1±1.8°C of air warming between the LGM and the present day. Our results indicate a greater degree of LGM cooling than is implied by packrat middens during the mid-deglacial period (5.5°C; Thompson et al., 1999); however, our results indicate similar cooling as indicated by trees lines and pollen (10-11°C; Galloway, 1970), and hydrologic mass balance models (10°C; Smith & Street-Perrott, 1983) during the LGM. Similar to Lake Chewaucan, water $\delta^{18}O$ also increases by ~4‰ at Lake Franklin between ~14-16 ka, but in this case, it is not coincident with a notable increase in air temperature. In this case, we infer that changing water $\delta^{18}O$ is likely due to variations in precipitation source rather than temperature. Thus, as expected, we estimate a lower deglacial thermodynamic contribution to water balance at Lake Franklin (35.5%, Table 3.3).

Precipitation rates at Lake Franklin reached their peak at 16 ka, coincident with the lake highstand, and decreased throughout the remainder of the deglacial period. This trend is coincident with a gradual regression of lake levels following a ~16 ka highstand (Fig. 3.1c).

Overall, precipitation rates are elevated ~500% relative to their modern value of 191 mm/yr, throughout both the LGM and deglacial periods. Lake evaporation rates at Lake Franklin show a fair degree of variability, but also decrease following the lake highstand. Similarly, weighted evaporation rates decrease, starting ~16 ka. These data suggest that increased precipitation, rather than reduced evaporation rates, were important in the growth of post-LGM Lake Franklin, as both precipitation and evaporation rates were at local maxima during the lake highstand.

Mud Lake

Average LGM lake temperature at Mud Lake was 17.4±2.5℃, corresponding to a MAAT of 10.0±2.5℃. Modern MAAT at Mud Lake is 11.8±1℃, implying 1.8±2.7℃ of air cooling since the LGM. Our data suggest that the coolest period occurred during the late deglacial (12 ka), with water temperatures of 8.3±1.7℃, corresponding to a MAAT of -2.5±1.7℃, and indicating a maximum temperature depression of 14.3±2℃.

Water $\delta^{18}O$ at Mud Lake is consistent throughout the deglacial period, although this may be due to the low sampling resolution of our data. We note that water $\delta^{18}O$ from Mud Lake is in line with, albeit slightly enriched, compared to values from other lake basins. As Mud Lake is significantly farther south than Lake Chewaucan, Lake Franklin, and Lake Surprise, this likely reflects differences in the dominant moisture source or seasonality of precipitation. Proportionally, southeast Nevada receives a larger amount of its precipitation in the summer compared to the more northern lake basins (Higgins et al., 1996; Xie & Arkin, 1996), and summer precipitation is known to be isotopically enriched relative to winter precipitation in the southwest United States (e.g. Yapp, 1985).

Mud Lake is representative of the southern side of the precipitation dipole of Oster et al. (2015) and Lora et al. (2017). As expected in the southern Great Basin, we find a significant increase in precipitation rates at Mud Lake between the early LGM and mid deglacial period (~15x modern values), coupled with a relatively small temperature depression during the LGM. With regard to lake evaporation rate, we find a small increase between the early and mid-deglacial periods and a significant decrease between the mid to late deglacial periods. Finally, we calculate a much smaller thermodynamic control on both LGM (40%) and deglacial period (39%) water balance, implying that dynamic transport of water vapor likely played a much greater role in driving lake growth (Table 3.3). Taken together, we conclude that Mud Lake, similar to Lake Chewaucan and Lake Franklin, was sustained by enhanced precipitation rather than decreasing levels of lake evaporation driven by temperature depression, and unlike Lake Chewaucan, was driven largely by dynamic transport of water vapor.

Evaluation of Climate Model Simulations of Hydroclimate Change

PMIP3 - LGM data comparison

We compare each climatic variable (temperature, precipitation, evaporation) derived from clumped isotope analysis to PMIP3 simulations. For each lake basin, we calculate an anomaly by subtracting the modern climatological value from the average value derived from LGM samples. We also calculate an estimate of the analytical error carried through from mass spectrometry, with additional sources of uncertainty described in Table 3.S1. In this PMIP3 analysis, we include samples only from Lake Chewaucan, Mud Lake, and Lake Surprise, as these three lake basins have samples that formed during the LGM.

In Fig. 3.4, we overlay MAAT anomalies derived from clumped isotope analysis over output from PMIP3 simulations. In the northwest Great Basin, Lake Surprise and Lake Chewaucan have intermediate temperature anomalies (8.9±1.4℃ & 8.6±2.7℃, respectively), Mud Lake has a smaller (1.8±1.8℃) LGM temperature anomaly. Our anomalies for Lakes Chewaucan and Surprise are consistent with all PMIP3 anomalies, within our analytical error of ~2-3℃. However, our anomaly for Mud Lake is much smaller than most PMIP3 simulations at that location, with the closest PMIP3 anomaly, -4℃, produced by CNRM-CM5.

In Fig. 3.5, we compare our clumped isotope derived precipitation anomalies from Equation S7 to PMIP3 anomalies. At Lake Surprise, we calculate a negative precipitation anomaly (-76 ± 185 mm/yr), implying drier than modern conditions during the LGM. This result is consistent with most models, save NCAR CCSM4 and IPSL-CM5A-LR. At Lake Chewaucan, we calculate a positive anomaly (60±90 mm/yr), implying wetter than modern conditions. This result is consistent with NCAR CCSM4, FGOALS, and IPSL-CM5A-LR. At Mud Lake we calculate a large positive precipitation anomaly (1545±230 mm/yr), indicating LGM conditions that were much wetter than modern. While this amount of rainfall is much greater than modern precipitation rates at Mud Lake (171 mm/yr), it is similar to modern precipitation rates at similar latitudes, just east of the Sierra Nevada (Smith & Reimann, 2008). Hence, while this amount of LGM precipitation is far greater than what is recorded today, it is within the realm of possibility, given a significantly altered climatic state. This large positive anomaly at Mud Lake is most consistent with FGOALS, GISS-E2-R, IPSL-CM5A-LR, and MPI-ESM-P.

In Fig. 3.6, we overlay our basin-scale weighted evaporation rates from clumped isotope analysis on PMIP3 evapotranspiration anomalies. For Lake Surprise, we calculate an LGM evaporation anomaly of -368 ± 100 mm/yr, implying decreased evaporation rates during the

LGM. This result is consistent with MIROC-ESM and MRI-CGCM3. For Lake Chewaucan, we calculate a larger LGM evaporation anomaly of -708±100 mm/yr. While this anomaly is most consistent with MIROC-ESM and MRI-CGCM3, we note that the magnitude of our inferred anomaly is larger than all climate model simulations. Finally, for Mud Lake, we calculate an evaporation anomaly of -1064 ± 130 mm/yr. This anomaly is of greater magnitude than any PMIP3 simulation, and implies an LGM evaporation rate on par with modern-day Florida and the tropics (Smith & Reimann, 2008). Our elevated LGM evaporation rates at Mud Lake are an average of MAAT calculated from just two LGM carbonates; additional analysis from future LGM-aged samples at Mud Lake will indicate if this implied anomaly is accurate. While MRI-CGCM3 does simulate a large negative anomaly at the location of Mud Lake, the magnitude of this anomaly is smaller than our simulated proxy anomaly.

PMIP3 - LGM and deglacial data comparison

We perform similar calculations of data anomalies, using only deglacial age (19,000-10,000 ka BP) samples. Unlike above, we do not directly compare our results to PMIP3 output, as PMIP3 does not produce deglacial simulations.

Compared to the LGM, Lake Surprise and Lake Chewaucan have intermediate negative deglacial temperature anomalies (8.1±1.1 & 6.2±1.8℃, respectively). In contrast, Lake Franklin has a larger negative deglacial temperature anomaly (13.1±1.8℃), while Mud Lake has a positive anomaly (5.6±1.8℃).

With regard to precipitation, we calculate a negative anomaly for Lake Surprise (-127 ± 210 mm/yr), implying drier than modern conditions during the deglacial period. For all other lake basins, we calculate positive anomalies. Lake Chewaucan has a small positive anomaly (251

± 90 mm/yr), while Lake Franklin and Mud Lake have much higher precipitation anomalies (2100 ±260 mm/yr & 2370 ±420 mm/yr, respectively).

With respect to weighted evaporation rates, we calculate negative deglacial anomalies for all lake basins: -438 ±110 mm/yr (Lake Chewaucan), -55 ±140 mm/yr (Lake Franklin), -1075 ±130 mm/yr (Mud Lake), and -159 ±110 mm/yr (Lake Surprise). All results indicate evaporation depression from deglacial cooling; however, the magnitude of this depression is the greatest at Mud Lake.

TraCE

Based on our qualitative model evaluation, there is no steady state model that is able to adequately recreate both the magnitude and trends of precipitation, evaporation, and temperature anomalies implied by clumped isotope data. We next compare our proxy-derived temperature and precipitation rates to model output from a transient climate model 'TraCE', averaged over four discrete time periods during the LGM and deglacial period (Figs. 3.7-3.8). For more direct comparison to PMIP3 plots, we use the same scale as in Figs. 3.4-3.6.

On Fig. 3.7, we overlay temperature anomalies from proxy data over TraCE surface temperature anomalies. We note an overall mismatch between Δ_{47} derived temperatures and TraCE model output, compared to PMIP3 simulations. We observe the best spatial model-data agreement during the LGM period, but worse agreement during the subsequent deglacial time slices. We also note that Δ_{47} for Mud Lake predicts climates that are both warmer than TraCE and colder than TraCE, depending on the time period.

On Fig. 3.8, we overlay proxy estimates of precipitation anomalies during each time period on TraCE precipitation anomalies. We note that the pattern of LGM drying versus

moisture increase is reversed compared to PMIP3 simulations, with TraCE predicting dryer than modern conditions in the south, rather than the northern Great Basin. We note that TraCE is most in line with our predictions for Lake Surprise, indicating a moderate LGM and deglacial precipitation decrease for most time periods.

Model Skill Evaluation

In addition to the previous qualitative approach towards model evaluation, we perform a formal evaluation of climate model output of surface air temperature, precipitation rate, and evapotranspiration (Fig. 3.9). In this analysis, model skill is taken to represent the ability of climate models to reproduce the magnitude of temperature, precipitation, and weighted evaporation estimates from clumped isotopes (See Chapter 2 Supplement and Hargreaves et al., 2013).

For most models, precipitation skill scores are close to zero or slightly negative. Our poorest performing models, showing zero or large negative skill scores for all lake basins, are FGOALS, GISS-E2-R (p 150), and MIROC-ESM. Our 10-member ensemble average demonstrates a slight negative model skill for all three ancient lakes. We note that our lowest performing models overlap significantly with those found in an existing model-proxy comparison in the Great Basin (Lora, 2018). This work similarly found MIROC-ESM and GISS-E2-R (p 150) were amongst the worst performers.

With regard to temperature, we find much more consistent skill scores, with most in the 0.2-0.5 range for Lake Surprise and Lake Chewaucan, and all skill scores greater than zero. In contrast, for Lake Franklin, three models (NCAR CCSM4, FGOALS, and MIROC-ESM) demonstrate negative model skill. These low-scoring models simulate

significantly colder LGM temperatures than the ensemble average. We note that our Lake Franklin samples are deglacial (rather than LGM) age, and thus are not as well-suited to this evaluation of PMIP3 model skill for the LGM.

Finally, we calculate model skill scores for each basin using clumped isotope derived weighted evaporation rates. Similar to climate model skill scores for temperature, our values indicate fair model skill, with most between 0.3-0.6. The exceptions are GISS-E2-R (p150), MIROC-ESM, and MRI-CGCM3, which have large negative skill scores for Lake Franklin, and predict smaller evapotranspiration anomalies than the PMIP3 ensemble average.

CONCLUSIONS

In this work, we compare the hydrological histories of four post-LGM pluvial lakes in the Great Basin: Lake Chewaucan, Lake Surprise, Mud Lake, and Lake Franklin. These lake basins comprise a wide range in modern hydroclimates and elevations, and also constitute a wide spread in latitude and longitude. Lake level histories for each basin indicate rapid effective precipitation forcings juxtaposed with slower lake regressions for both Lake Franklin and Lake Surprise, while the hydrograph for Lake Chewaucan suggests a slower effective moisture forcing. The hydrograph for Mud Lake needs further constraints on lake level to discern effective moisture trends in southern NV. Correlations between carbonate $\delta^{18}O$ and $\delta^{13}C$ suggest that all lakes demonstrate closed-basin behavior, with the exception of a few Lake Chewaucan samples. In the four basins analyzed here, we see evidence for a wide range in causal mechanisms driving lake growth.

Deglacial cooling and below-modern precipitation rates led up to the lake highstand at Lake Surprise, suggesting that temperature depressions drove reductions in lake evaporation that were an important driver of hydrologic budgets. This period was also associated with a slight decrease in water $\delta^{18}O$, leading up to the highstand at ~16 ka. Our findings are consistent with a previously proposed north/south precipitation dipole, with temperature depression and decreased lake evaporation rates as primary drivers of lake growth, rather than increased precipitation, in the northwest Great Basin.

When Lake Franklin achieved its highstand at 16 ka, water temperature, lake evaporation, and precipitation rates were all at maximums, before beginning their declines during the mid to late deglacial periods. This decrease in deglacial water temperature coincides with an increase in water $\delta^{18}O$, indicating that changes in water $\delta^{18}O$ are not due to temperature effects, but perhaps due to a change in moisture source. As such, we calculate a significant dynamic contribution to increased effective moisture at Lake Franklin.

MAAT at Mud Lake decreased significantly between the mid deglacial period and the late deglacial period, with a late deglacial temperature anomaly of -14.3 ± 1.8℃. This significant deglacial temperature anomaly is coupled with greatly enhanced precipitation rates throughout the LGM and early deglacial period, providing support for the proposed north/south dipole in precipitation and temperature anomalies. Despite a considerable decrease in water temperature during the late deglacial period, water $\delta^{18}O$ shows negligible change. To be consistent with the large observed temperature decrease, this constancy in water $\delta^{18}O$ likely reflects some variation in moisture source. We estimate a significant dynamic contribution to increased effective moisture at Mud Lake, as implied by temperature and water $\delta^{18}O$ changes.

Finally, Lake Chewaucan shows an increase in water and air temperatures in the period leading up to its highstand. Increasing deglacial temperatures are coupled with increasing precipitation and weighted evaporation rates, as well as increasing water $\delta^{18}O$. This increase in water $\delta^{18}O$ is consistent with increasing water temperature. We conclude that lake growth at Chewaucan was achieved due to increasing precipitation rates, in spite of increasing lake evaporation rates.

We qualitatively compare our results to both steady-state (PMIP3) and transient climate model simulations (TraCE). We take this analysis further by providing quantitative estimates of model skill with respect to simulated precipitation rate, surface air temperature, and evapotranspiration. Overall, the best skill scores are achieved for temperature and weighted evaporation, with most climate models achieving fair or moderate skill. Skill score for precipitation rate is more variable, with models showing the highest skill scores for Lake Surprise, and the lowest for Lake Franklin. Similar to Lora (2018), we find that GISS-E2-R (p 150) and MIROC-ESM were amongst the worst performers in the region.

Based on our reconstructions, we suggest that more than one environmental factor is required to explain the observed changes in hydrologic budgets. We find evidence for both evaporation depression and increased precipitation rates driving lake growth, with variation in causal mechanisms happening on a relatively small spatial scale. Results at Mud Lake and Lake Surprise are compatible with the north/south precipitation dipole proposed to explain variations in causal mechanisms for lake growth; however, lakes Franklin and Chewaucan have much higher weighted evaporation rates than this hypothesis would suggest. Ultimately, we suggest that our work could be extended to a larger number of lake basins, to provide a more comprehensive look at post-LGM hydroclimate in the Great Basin.

FIGURES

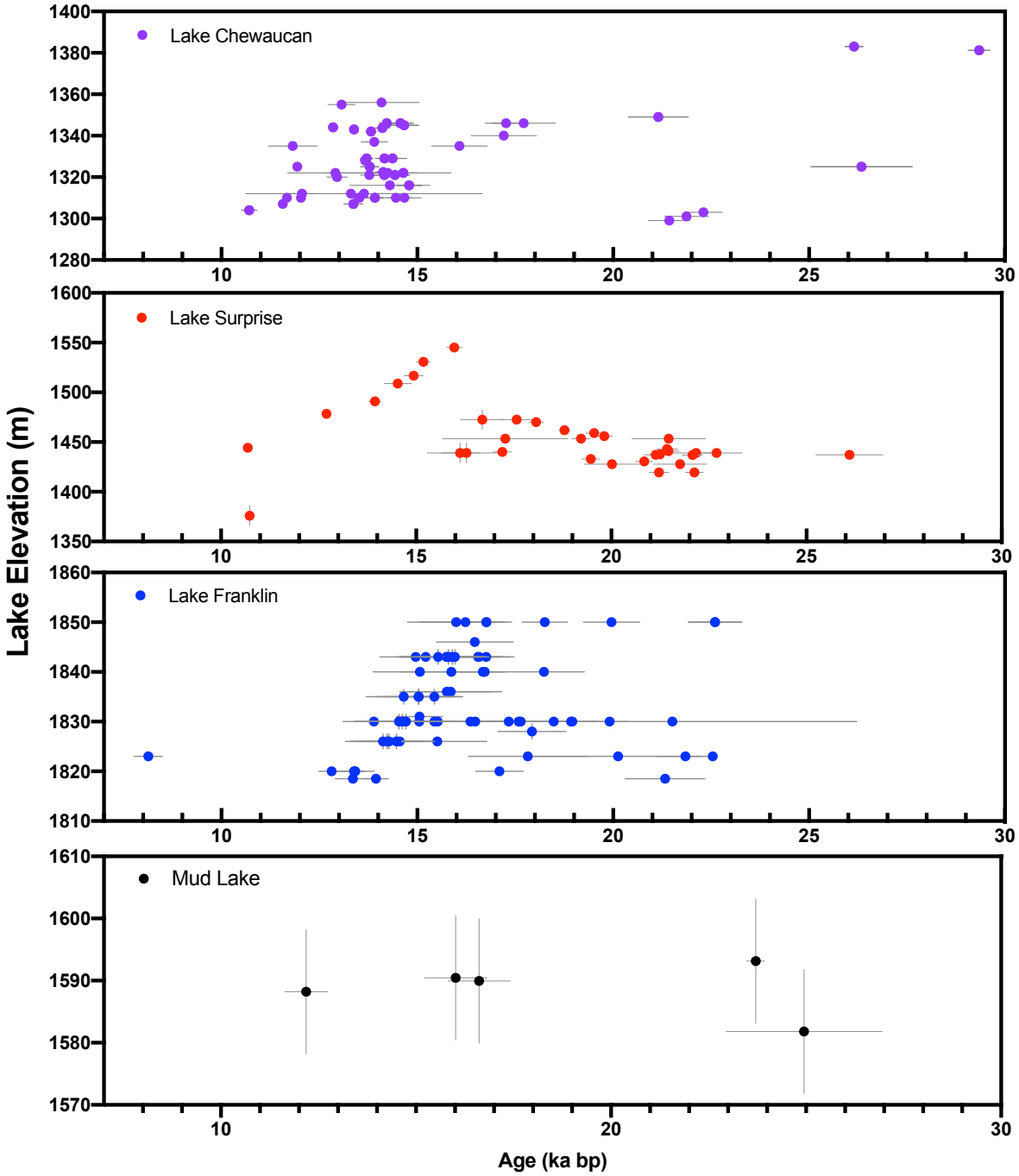

Figure 3.1: Radiocarbon and U-series based lake hydrographs for Great Basin lakes. From top to bottom, basins are plotted from geographic north(west) to south(east). Errors in ages represent 2σ uncertainties and elevation errors are the same as originally reported for previous data.

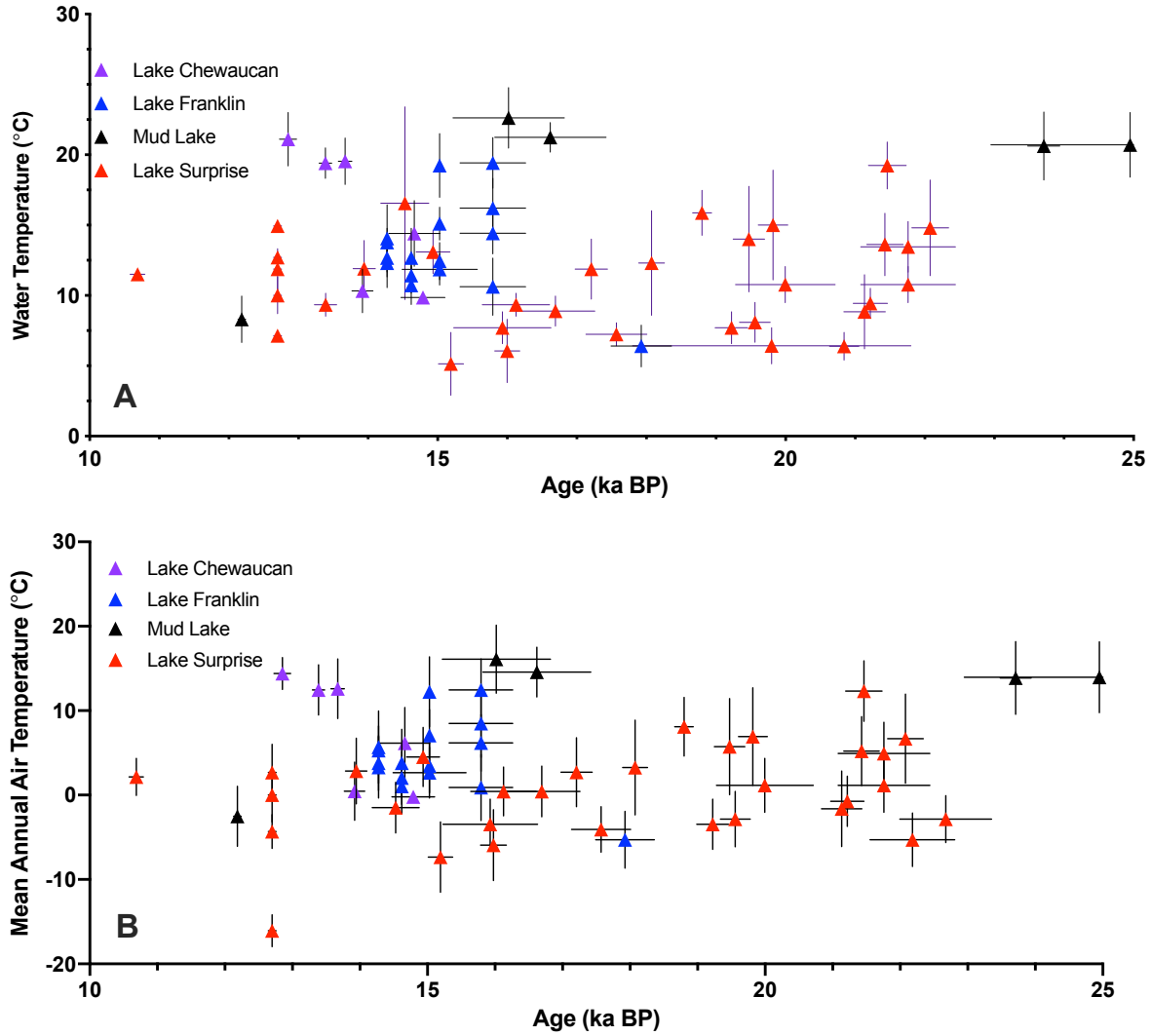

Figure 3.2: Reconstructed water temperature (A) Mean Annual Air Temperature (B) for LGM and deglacial samples. Mean Annual Air Temperature is derived using the April-October transfer function from Hren & Sheldon (2012). Moderns MAATS are 7.6±1°C (Lake Chewaucan), 7.8±1°C (Lake Franklin), 11.8±0.5°C (Mud Lake), and 9.2±1°C (Lake Surprise).

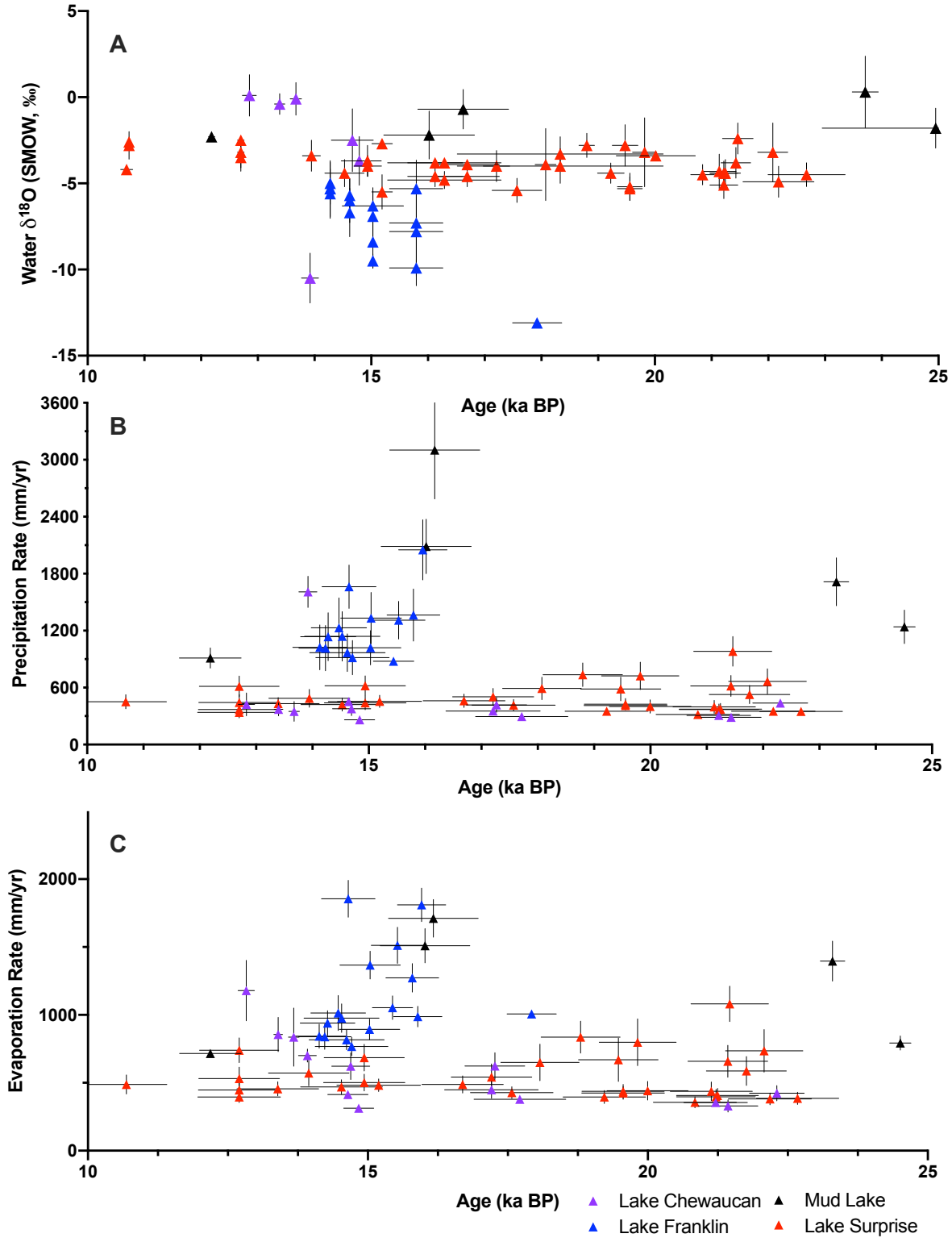

Figure 3.3: Reconstructed water $\delta^{18}O$ (A), precipitation rates (B), and evaporation rates (C) for LGM and deglacial samples. Modern precipitation rates are 242 mm/yr (Lake Chewaucan), 191 mm/yr (Lake Franklin), 171 mm/yr (Mud Lake), and 566 mm/yr (Lake Surprise). Modern pan evaporation rates are 2672 mm/yr (Lake Chewaucan), 1177 mm/yr (Lake Franklin), 2672 mm/yr (Mud Lake), and 905 mm/yr (Lake Surprise).

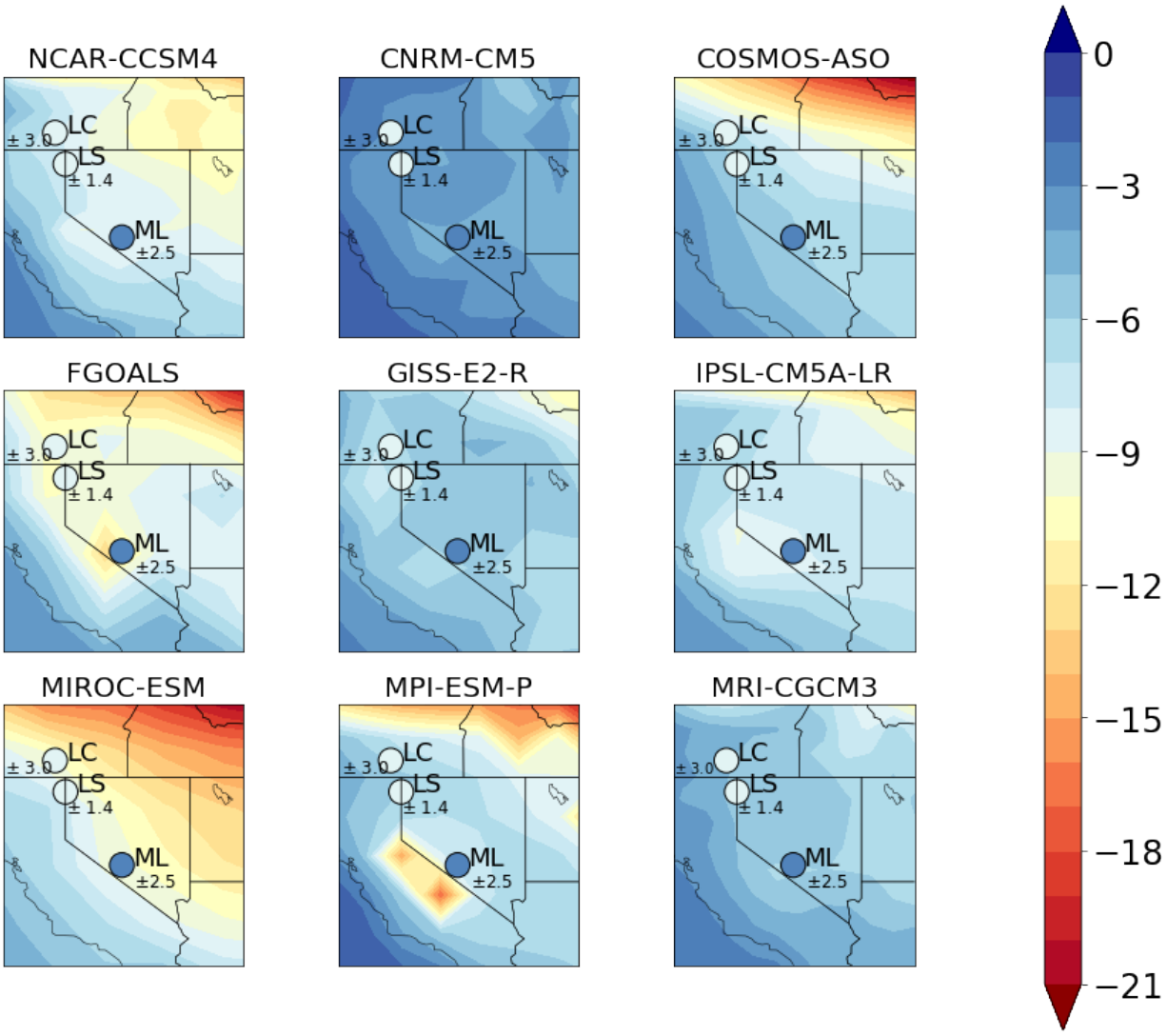

Figure 3.4: Mean annual surface air temperature anomalies (LGM minus preindustrial simulation), reported in °C. For each lake basin, we apply average LGM temperatures (from Δ_{47}) and modern air temperatures from nearby weather stations. We include the average analytical error associated with calculations of temperature anomalies beside each basin.

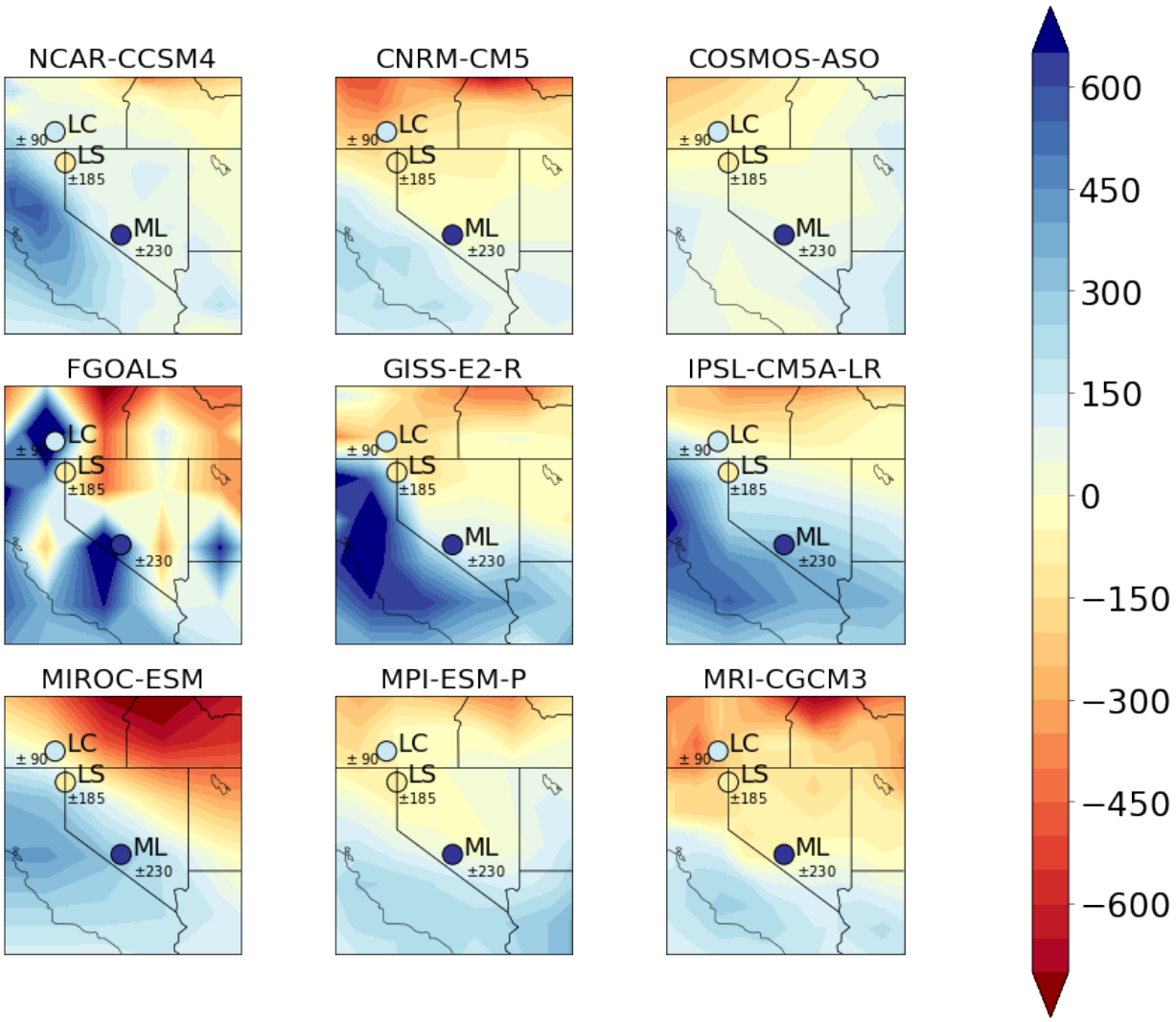

Figure 3.5: Mean annual precipitation anomalies (LGM minus preindustrial simulation), reported in mm/yr. For each lake basin, we apply average LGM (or early deglacial) precipitation rates (from Δ_{47}) and modern precipitation rates from nearby weather stations. We include the average analytical error associated with calculations of precipitation anomalies at each lake basin, as carried through from Δ_{47} error from mass spectrometry.

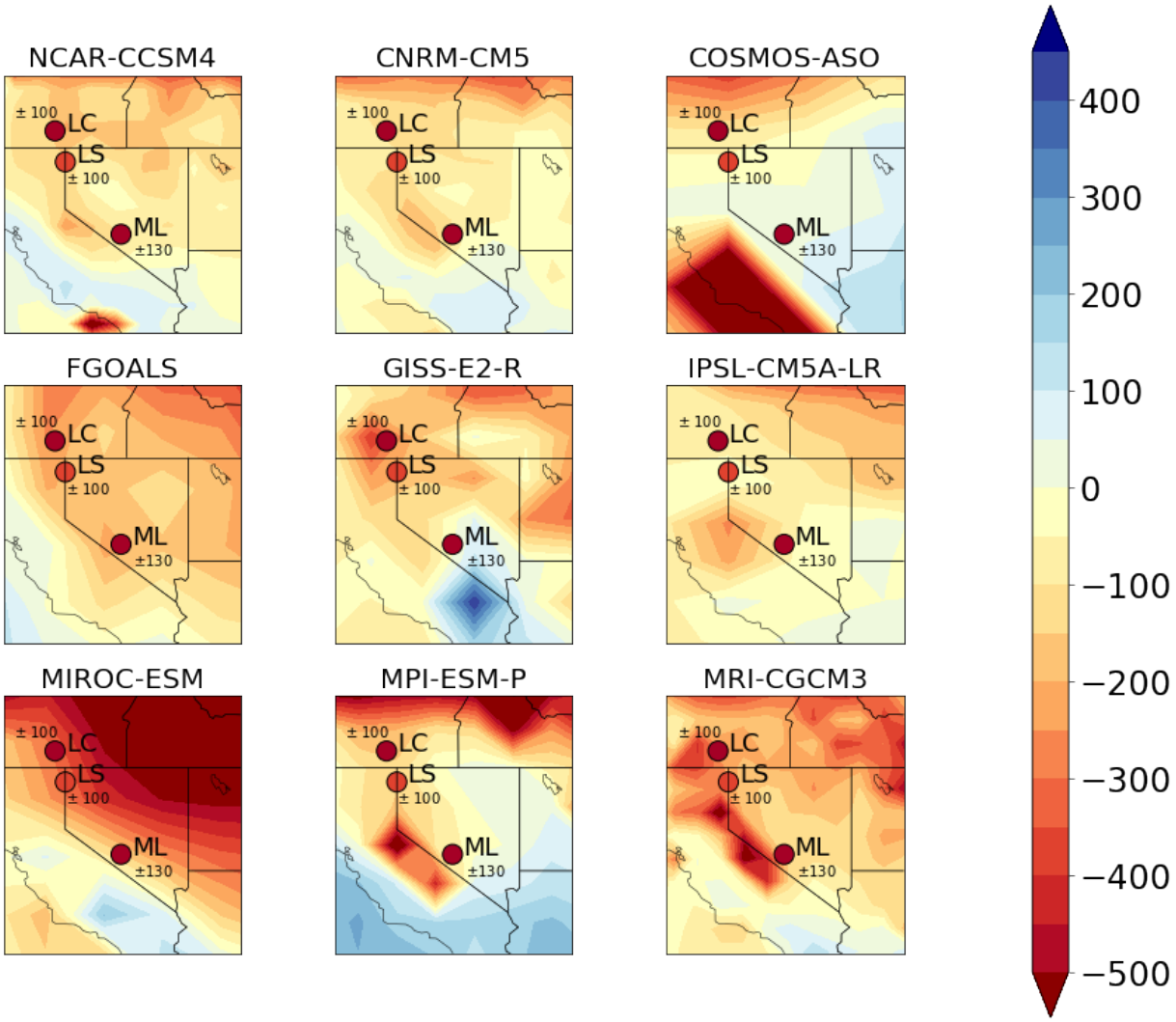

Figure 3.6: Mean annual evaporation anomalies (LGM minus preindustrial simulation), reported in mm/yr. For each lake basin, we apply average LGM (or early deglacial) weighted evaporation rates (derived from Δ_{47}) and modern pan evaporation rates from nearby weather stations. We include the average analytical error associated with calculations of evaporation anomalies, as carried through from Δ_{47} error from mass spectrometry.

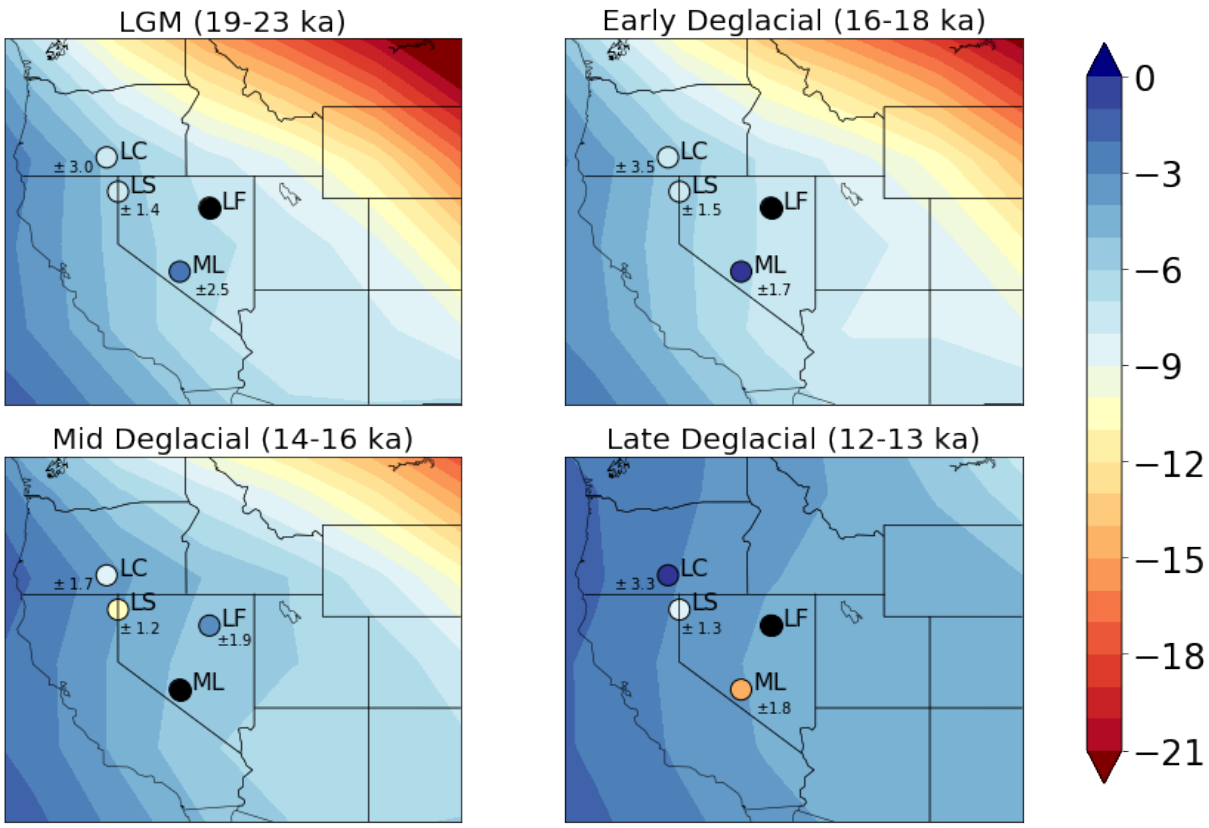

Figure 3.7: Comparison of proxy-derived and TraCE temperature anomalies (°C). Modern temperature for TraCE is an average of model output between 1960-1980. Black markers indicate an absence of data from the given time period. We include the average analytical error associated with calculations of the temperature anomaly at each basin, as carried through from Δ_{47} error from mass spectrometry.

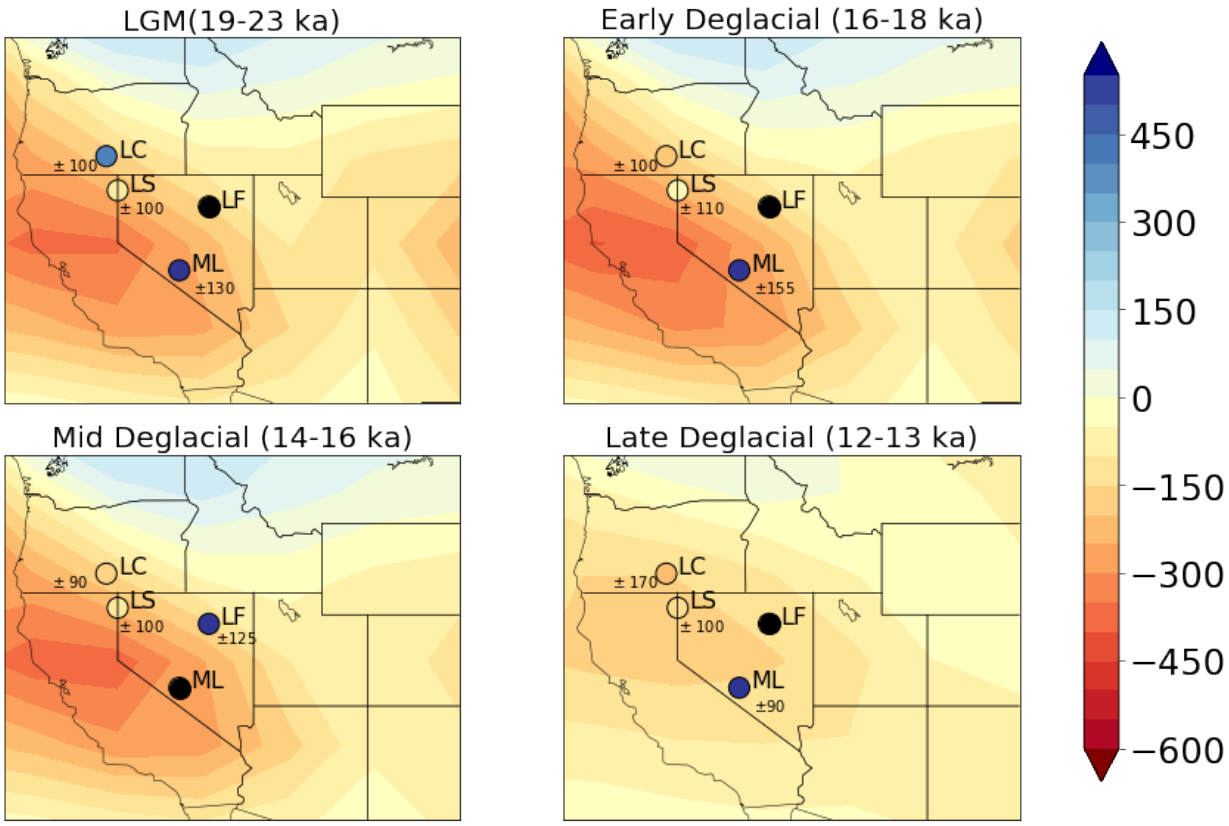

Figure 3.8: Comparison of proxy-derived and TraCE precipitation anomalies (mm/yr). Modern precipitation rate for TraCE is an average of model output between 1960-1980. Black markers indicate an absence of data from the given time period. We include the average analytical error associated with calculations of precipitation anomalies at each basin, as carried through from Δ_{47} error from mass spectrometry.

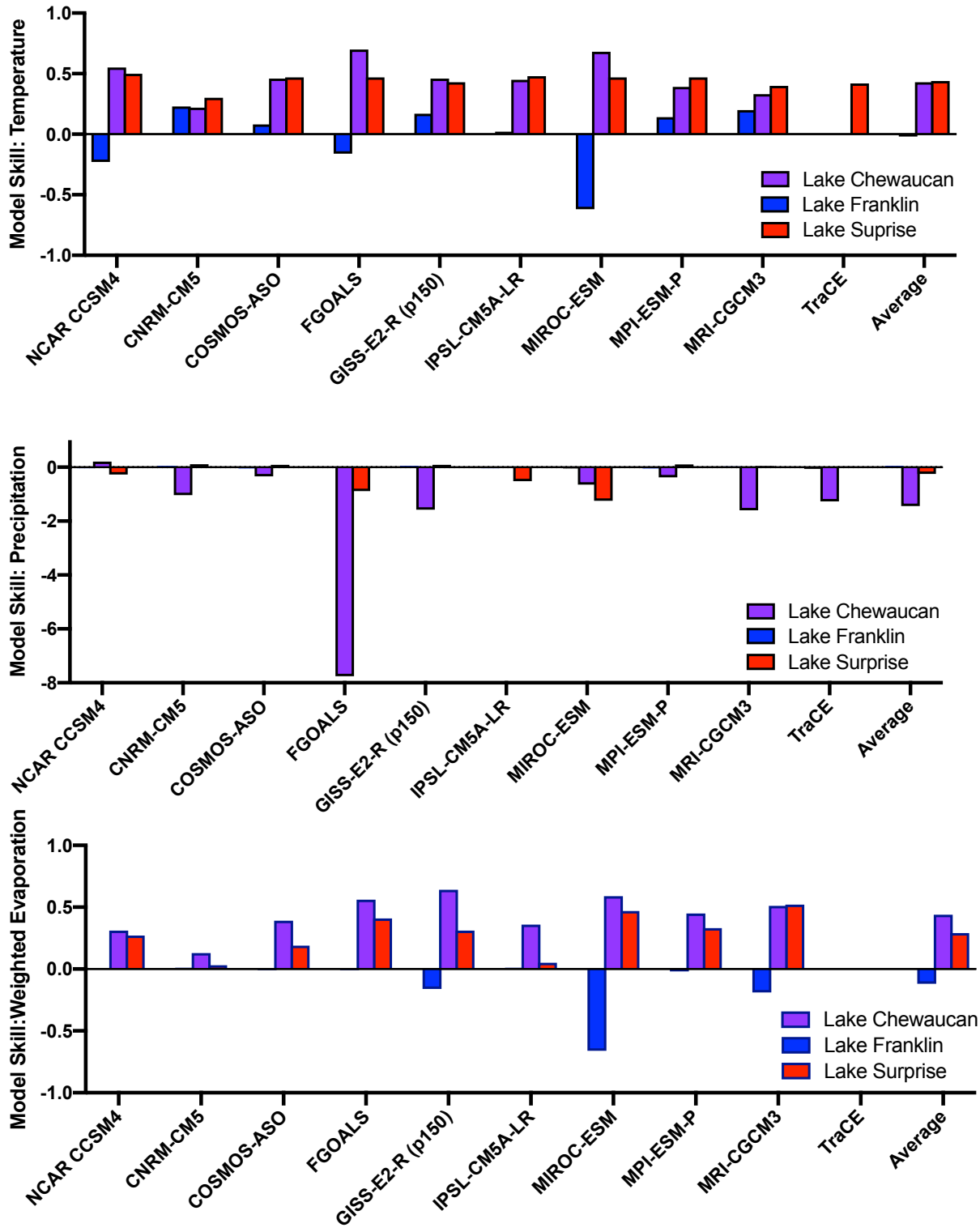

Figure 3.9: Model skill evaluation for temperature, precipitation, and (weighted) evaporation anomalies, as determined for PMIP3 and TraCE climate models.

TABLES

Table 3.1: New Great Basin Carbonate Samples

Lake Basin	Sample Name	Sample Type	^{14}C Age	^{14}C Age SD	IntCal13 Age (ka)	2σ min	2σ max	Elevation (m)	HI
Chewaucan	SL15AE02	Tufa	21.92	0.09	26.12	25.92	26.38	1383	0.62
Chewaucan	SL15AE06	Tufa	11.57	0.04	13.40	13.30	13.48	1343	0.51
Chewaucan	SL15JH05	Tufa	11.87	0.04	13.68	13.57	13.77	1328	0.46
Chewaucan	SL15JH06	Tufa	22.15	0.08	26.35	26.11	26.62	1325	0.44
Chewaucan	SL15JH07	Tufa	12.07	0.05	13.92	13.77	14.07	1405	0.69
Chewaucan	SL15AE08	Tufa	10.98	0.04	12.83	12.73	12.97	1344	0.51
Chewaucan	SL15AE05	Tufa	12.49	0.05	14.70	14.30	15.03	1345	0.51
Chewaucan	SLT3-1B	Tufa	12.53	0.04	14.84	14.77	15.11	1316	0.39
Franklin	FranklinRW1_60_1A	Gastropod	12.26	0.11	14.23	13.82	14.77	1826	0.21
Franklin	FranklinRW1_60_2A	Gastropod	12.37	0.12	14.47	14.04	15.02	1826	0.21
Franklin	FranklinRW1_60_2B	Gastropod	12.20	0.13	14.13	13.75	14.72	1826	0.21
Franklin	FranklinRW2_90_1A	Gastropod	12.52	0.19	14.71	14.04	15.34	1838	0.36
Franklin	FranklinRW2_90_1B	Gastropod	12.40	0.16	14.53	14.00	15.14	1838	0.36
Franklin	FranklinRW3_78_1A	Gastropod	12.48	0.12	14.65	14.16	15.12	1841	0.39
Franklin	FranklinRW3_78_1B	Gastropod	12.91	0.12	15.44	15.09	15.82	1841	0.39
Franklin	FranklinRW3_78_1C	Gastropod	12.67	0.12	15.03	14.38	15.45	1841	0.39
Franklin	FranklinFRB_170_1	Tufa	14.73	0.18	17.93	17.49	18.36	1848	0.48
Franklin	FranklinHS1_86_1A	Gastropod	13.23	0.14	15.89	15.41	16.28	1843	0.49
Franklin	FranklinHS186_1B	Gastropod	12.98	0.16	15.53	15.09	16.03	1843	0.49
Franklin	FranklinHS1_86_1C	Gastropod	13.28	0.14	15.96	15.49	16.36	1843	0.49
Mud	ML07-04	Tufa	23.71	0.23	27.82	27.45	28.29	1593	1.48
Mud	ML08-03	Tufa	16.02	0.08	19.34	19.08	19.57	1590	1.46
Mud	ML08-04	Tufa	16.62	0.08	20.05	19.80	20.31	1590	1.45
Mud	RD05-95	Tufa	24.75	0.20	28.79	28.35	29.29	1582	1.40
Mud	RD05-10	Stromatolite	23.56	0.17	27.69	27.43	27.96	1595	1.49
Mud	CMud17_2	Tufa	10.03	0.19	11.62	11.12	12.25	1588	1.40
Surprise	SVDI12-T4A	Tufa	18.78	0.27	22.70	22.04	23.35	1439	0.33
Surprise	SVDI12-T4B	Tufa	18.35	0.27	22.18	21.53	22.81	1439	0.33
Surprise	SVDI12-T7	Tufa	14.46	0.17	17.61	17.14	18.01	1473	0.42
Surprise	SVDI12-T3A	Tufa	18.03	0.28	21.82	21.08	22.44	1428	0.31
Surprise	SVDI12-T3B	Tufa	16.59	0.29	20.02	19.28	20.71	1428	0.31
Surprise	SVCW17-PT1	Tufa	13.52	0.34	16.30	15.29	17.29	1475	0.44
Surprise	SVCW17-PT2	Tufa	13.39	0.16	16.11	15.64	16.61	1475	0.44
Surprise	SVCW17-PT3	Tufa	13.79	0.19	16.68	16.13	17.26	1477	0.45

Table 3.2: New Clumped and Stable Isotope Results for Northern Great Basin Pluvial Lakes

Lake Basin	Sample Name	Δ_{47}	Δ_{47} SE	$\delta^{18}O$ (VPDB,‰)	$\delta^{18}O$ SE	$\delta^{13}C$ (VPDB,‰)	$\delta^{13}C$ SE
Chewaucan	SL15AE02[1]	0.706	0.006	-1.6	0.09	3.7	0.10
Chewaucan	SL15AE06[1]	0.692	0.004	-1.7	0.03	3.7	0.01
Chewaucan	SL15JH05[1]	0.691	0.006	-1.4	0.06	3.3	0.04
Chewaucan	SL15JH06[1]	0.707	0.004	-9.2	0.05	-3.9	0.06
Chewaucan	SL15JH07[1]	0.726	0.006	-9.8	0.19	-2.8	0.31
Chewaucan	SL15AE08[1]	0.673	0.015	-1.5	0.06	2.1	0.05
Chewaucan	SL15AE05[1]	0.710	0.009	-2.6	0.31	3.1	0.19
Chewaucan	SLT3-1B[1]	0.728	0.012	-2.9	0.11	1.7	0.14
Chewaucan	CHL13-5[2]	0.745	0.011	-3.0	0.05	3.3	0.02
Chewaucan	CHL14-29-1[2]	0.779	0.014	-3.4	0.02	3.6	0.01
Chewaucan	CHL13-2[2]	0.804	0.011	-3.1	0.06	3.4	0.01
Chewaucan	CHL13-22[2]	0.765	0.012	-3.6	0.04	3.7	0.08
Chewaucan	CHL14-30[2]	0.781	0.014	-5.1	0.03	1.9	0.02
Chewaucan	CHL14-32-1[2]	0.777	0.014	-3.5	0.01	3.8	0.03
Franklin	FranklinRW1_60_1A	0.718	0.007	-4.3	0.09	1.5	0.17
Franklin	FranklinRW1_60_2A	0.714	0.005	-4.3	0.15	2.0	0.32
Franklin	FranklinRW1_60_2B	0.711	0.009	-4.9	0.22	2.1	0.09
Franklin	FranklinRW2_90_1A	0.724	0.005	-4.4	0.12	3.3	0.45
Franklin	FranklinRW2_90_1B	0.717	0.008	-5.8	0.11	2.5	0.10
Franklin	FranklinRW3_78_1A	0.692	0.008	-8.8	0.24	-6.3	0.06
Franklin	FranklinRW3_78_1B	0.718	0.005	-8.5	0.13	-3.0	0.20
Franklin	FranklinRW3_78_1C	0.720	0.004	-5.2	0.08	3.1	0.35
Franklin	FranklinFRB_170_1	0.742	0.006	-11.5	0.06	-2.1	0.05
Franklin	FranklinHS1_86_1A	0.725	0.008	-8.5	0.11	-5.0	0.13
Franklin	FranklinHS186_1B	0.703	0.008	-7.1	0.17	-6.6	0.25
Franklin	FranklinHS1_86_1C	0.710	0.006	-5.8	0.04	-6.8	0.02
Mud	ML07-04[3]	0.726	0.013	-1.2	0.16	4.2	0.12
Mud	ML08-03[3]	0.615	0.028	-4.4	0.36	-0.5	0.19
Mud	ML08-04[3]	0.685	0.004	-2.3	0.17	2.6	0.39
Mud	RD05-95[3]	0.748	0.012	-3.1	0.39	1.0	0.23
Mud	RD05-10[3]	0.689	0.014	-3.3	0.14	1.3	0.06
Mud	CMud17_2	0.752	0.007	-1.1	0.14	2.0	0.07
Surprise	SVCW17-PT1	0.741	0.009	-3.8	0.03	3.7	0.02
Surprise	SVCW17-PT2	0.730	0.003	-3.8	0.07	3.7	0.04
Surprise	SVCW17-PT3	0.726	0.004	-3.9	0.22	3.7	0.09
Surprise	SVCW 17-PT4	0.726	0.004	-3.8	0.06	3.8	0.10
Surprise	SVDI 11-T14-1A	0.727	0.005	-2.6	0.10	3.8	0.17
Surprise	SVDI 11-T14-1B	0.739	0.001	-2.9	0.01	3.8	0.01
Surprise	SVDI 11-T14-1C	0.720	0.006	-2.8	0.09	3.7	0.06
Surprise	SVDI 11-T14-E[4]	0.708	—	-2.8	—	3.6	—
Surprise	SVDI 11-T2-1	0.736	0.004	-3.1	0.29	3.9	0.10
Surprise	SVDI 11-T3-2	0.731	0.005	-3.4	0.17	3.0	0.04
Surprise	SVDI 11-T4-1b	0.742	0.004	-2.9	0.01	3.6	0.04
Surprise	SVDI 12-T1	0.704	0.006	-3.5	0.06	3.7	0.18
Surprise	SVDI 12-T10-A	0.715	0.006	-3.6	0.14	3.6	0.08
Surprise	SVDI 12-T10-B	0.726	0.003	-3.3	0.05	3.5	0.13
Surprise	SVDI 12-T13	0.732	0.011	-3.2	0.08	3.7	0.02
Surprise	SVDI 12-T14	0.747	0.009	-3.6	0.10	3.7	0.06
Surprise	SVDI 12-T14-1C	0.717	0.002	-2.5	0.12	3.6	0.01
Surprise	SVDI 12-T15-B	0.712	0.015	-2.9	0.00	3.8	0.01
Surprise	SVDI 12-T3-A	0.714	0.007	-3.3	0.10	3.6	0.06
Surprise	SVDI 12-T3-B	0.724	0.005	-3.4	0.17	3.6	0.09
Surprise	SVDI 12-T4-A	0.735	0.004	-3.3	0.12	3.6	0.02
Surprise	SVDI 12-T4-B	0.741	0.005	-3.3	0.05	3.6	0.04
Surprise	SVDI 12-T5b	0.721	0.001	-3.7	0.02	3.4	0.01

Surprise	SVDI 12-T7	0.738	0.003	-3.9	0.29	3.7	0.09
Surprise	SVDI 12-T9	0.731	0.004	-3.4	0.11	3.6	0.11
Surprise	SVDI 15-AE01	0.705	0.006	-3.3	0.10	3.8	0.04
Surprise	SVDI 15-AE02	0.699	0.009	-3.5	0.20	3.6	0.07
Surprise	SVDI 15-AE03	0.720	0.008	-3.0	0.18	3.5	0.09
Surprise	SVDI 15-AE05	0.713	0.009	-3.8	0.10	3.2	0.05
Surprise	SVDI 15-AE06	0.689	0.006	-3.4	0.10	3.5	0.04
Surprise	SVDI 15-BM03	0.720	0.008	-3.6	0.04	4.9	0.02
Surprise	SVDI 15-BM04	0.735	0.006	-4.0	0.16	3.6	0.11
Surprise	SVDI 15-BM08	0.692	0.006	-3.6	0.17	3.4	0.11
Surprise	SVDI 15-BM09	0.688	0.009	-3.4	0.18	3.1	0.10

[1]Sample provided by Anne Egger
[2]Clumped and stable isotope results from Hudson et al. (2017)
[3]Sample provided by Robert Dickerson and Victoria Petryshyn
[4]Indicates samples with too few runs to constrain standard error of the mean

Table 3.3: Thermodynamic and Dynamic Controls on Lake Level

Basin	Thermodynamic (%, LGM)	Dynamic (%, LGM)	Thermodynamic (%, deglacial period)	Dynamic (%, deglacial period)
Lake Chewaucan	63.0	37.0	68.0	32.0
Lake Franklin	NA	NA	35.5	64.5
Mud Lake	39.5	60.5	39.0	61.0
Lake Surprise	52.0	48.0	49.0	51.0

SUPPLEMENT

Supplementary Figures

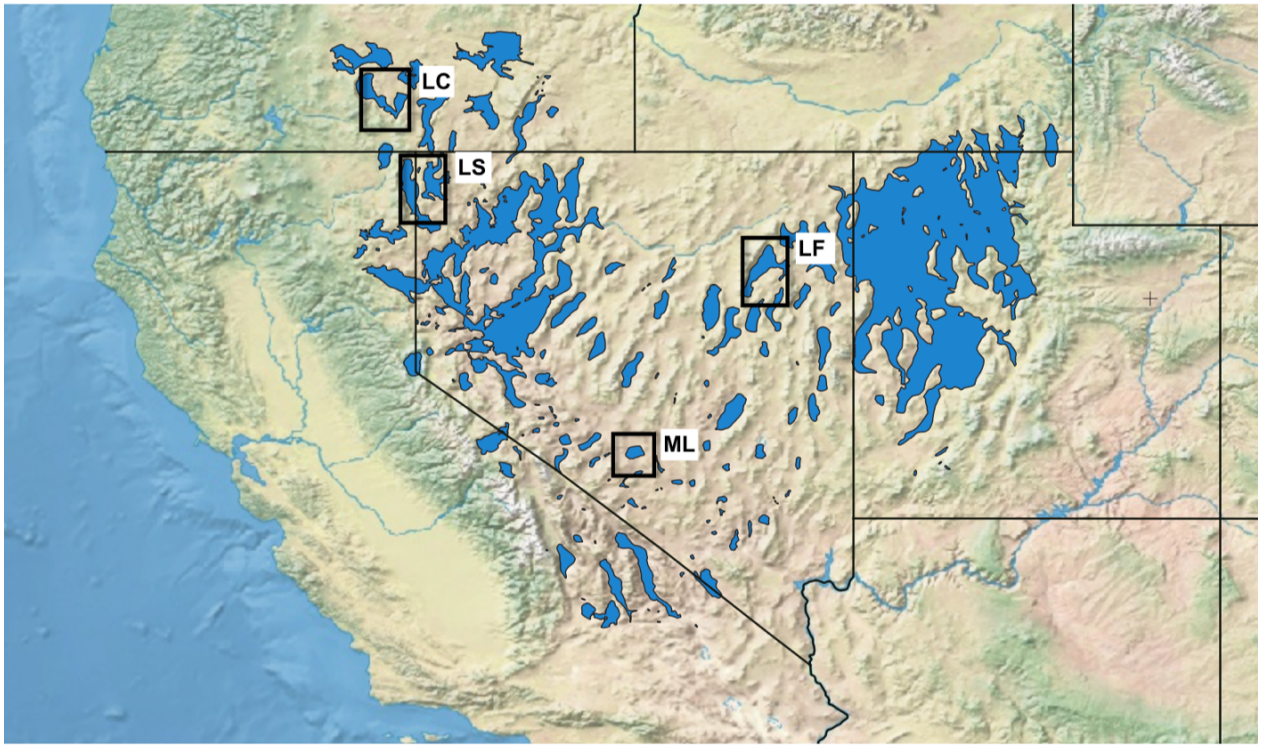

Figure 3.S1: Map of the western United States, with the estimated extent of pluvial lakes from the LGM and deglacial period shown in blue (digitized from Mifflin & Wheat, 1979 estimates). The location of Lake Chewaucan (LC), Lake Franklin (LF), Mud Lake (ML), and Lake Surprise (LS) are indicated by black boxes.

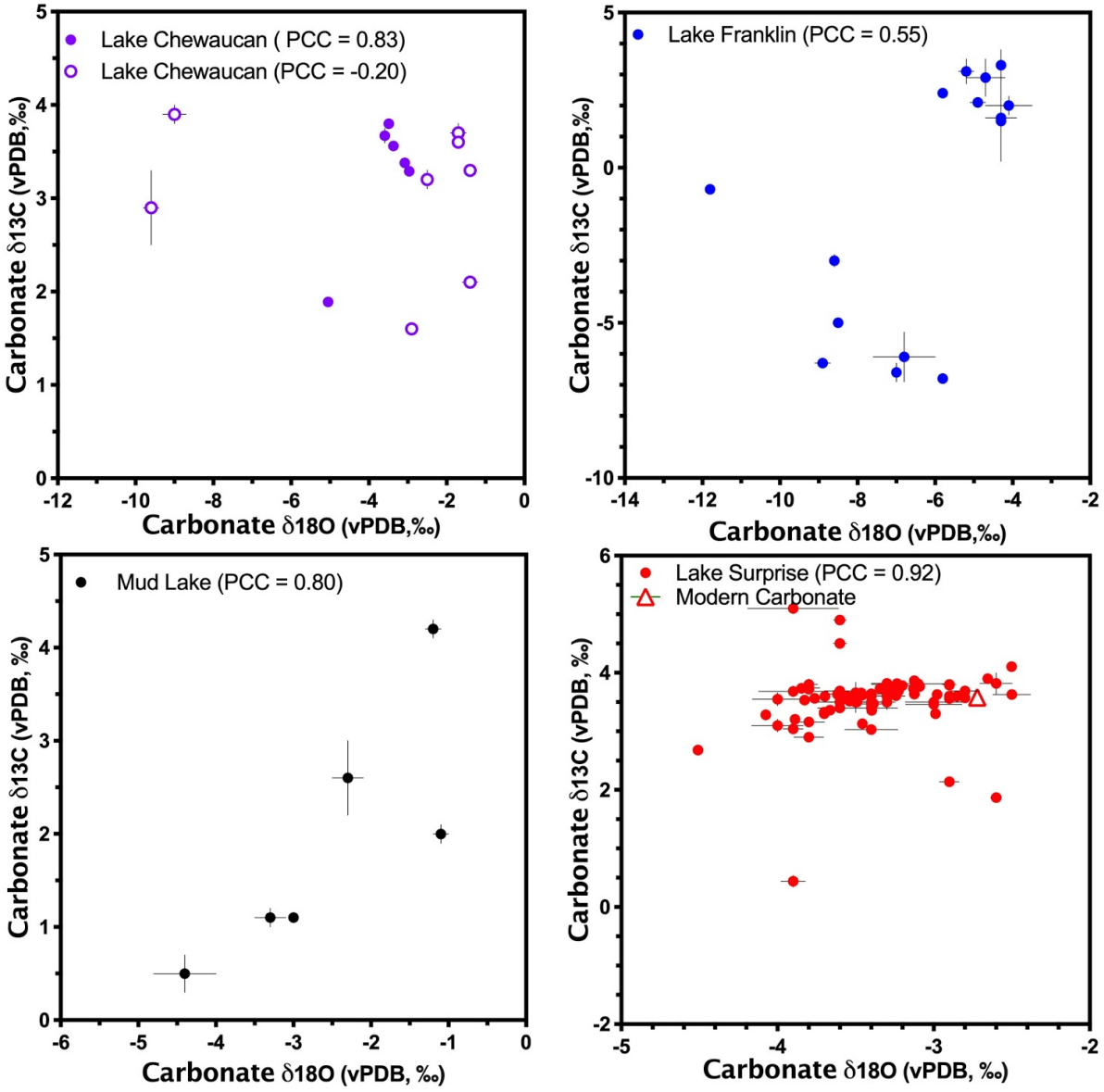

Figure 3.S2: $\delta^{13}C$ vs $\delta^{18}O$ plots. Positive correlation of carbon and oxygen isotopes provides evidence of closed lake basin behavior. Note that for some samples, error bars are smaller than the marker. Lake Chewaucan after Hudson et al. (2017) (closed circles) and Egger et al., 2018 (open circles).

Supplementary Tables

Table 3.S1: List of assumptions involved in reconstructions of past hydroclimate

Water and Air Temperature	**Precipitation Rate**	**Evaporation Rate**
No species-specific vital effects on Δ_{47}	Lake was not frozen over for significant amounts of time	Lake was not frozen over for significant amounts of time
Carbonate formation occurs preferentially from April-October	Relative humidity was near its modern value	Relative humidity was near its modern value
	Average wind speed was near its modern value	Average wind speed was near its modern value
	Water $\delta^{18}O$ was near its modern value (implies little change in water source)	Water $\delta^{18}O$ was near its modern value (implies little change in water source)
	ω was near its modern values (implies similar vegetation and basin characteristics)	ω was near its modern values (implies similar vegetation and basin characteristics)
	Little or no differential isostatic rebound	Little or no differential isostatic rebound
	Lakes were inward-draining	
	System was in isotopic steady state	
	Atmospheric vapor above basin is in equilibrium with incoming rainwater	
	Kinetic fractionation factor is a function of relative humidity, which itself is similar to the modern annual average	

Methods Supplement

Clumped Isotope Measurements

Mass spectrometry was completed at UCLA on a trio of mass spectrometers. On the first of the three machines, a Thermo 253 Dual Inlet Gas Source isotope ratio mass spectrometer (IRMS), carbonate samples are introduced after using a McCrea-style common acid bath for sample digestion. Acid temperature is held constant between 89.0℃ to 90.5℃. After dissolution of carbonate samples in the common acid bath, the resultant mixture of gas (primarily CO_2, but also N_2, O_2, and other trace gases) is purified in an automated vacuum line, which removes contaminant gases based on their differential freezing points. The liberated gas passes through two separate gas traps to ensure removal of water and other compounds: the first containing ethanol, is kept at -76°C by dry ice, and the second is kept at -126°C by liquid nitrogen. The sample gas is then passed through a silver wool "getter", which removes sulfur compounds. Remaining trace contaminants (e.g. halocarbons and hydrocarbons) are separated by moving the resultant gas through a Thermo Trace GC Ultra gas chromatograph column, which is filled with a divinyl benzene polymer trap, Porapak Q, at -20℃. After reaction in the GC, the sample is moved to a dual inlet IRMS. The ion source is maintained at 16,000 mV, and the amount of reference gas is automatically adjusted to produce a gas pressure that matches that of the standard. Each sample is measured for a total of nine acquisitions, with each acquisition consisting of a peak centering, background adjustment, and alternate cycling between sample and reference gas ionization (e.g. Spencer & Kim, 2015). Total measurement time is 2.3 hours per sample.

The other two mass spectrometers contain nuCarb sample preparation systems interfaced to a Nu Perpsective IRMS. These machines both utilize the acid drip method, whereby a small

amount (200 μL) of phosphoric acid is released into individual vials of carbonate powder, and the resultant CO_2 gas from each vial is sequentially analyzed on the mass spectrometer. After conversion to CO_2 gas, an initial sample beam is recorded for each sample. Depending on the magnitude of this beam, samples are either stored in the sample bellows or the sample coldfinger (a small volume chamber in front of the capillary), before transfer to the mass spectrometer. Each gas sample is measured in the Perspective IRMS for a total of three acquisitions. Throughout each measurement, the sample and reference beams are monitored and adjusted, such that a beam current of 50 nA (user-specified) is maintained. The total measurement time for the NuCarb coupled to the Perspective IRMS is ~1.5 hours per sample, and the internal precision is 0.01‰.

Quantifying Thermodynamic and Dynamical Controls on Lake Level

We estimate the thermodynamic contribution to changing lake levels using the following procedure:

1. We calculate the precipitation anomaly for each sample, using LGM and deglacial precipitation rates from Equation S7 (See Chapter 2 Supplement) and subtract modern precipitation rate from each sample.
2. We calculate a weighted evaporation anomaly, using LGM and deglacial weighted evaporation rates, as calculated using Equation S2 (See Chapter 2 Supplement). For modern weighted evaporation rates, we assume a steady state condition, whereby modern weighted evaporation is equal to modern precipitation.
3. We then calculate the thermodynamic contribution as the weighted evaporation anomaly divided by the total anomaly (Equation S1).

$$Thermodynamic\ Component\ (\%) = 100 \times \frac{(e_{weighted} - P_{modern})}{(e_{weighted} - P_{modern}) + (P - P_{modern})} \quad \text{Equation S1}$$

Note that this calculation assumes that all changes in evapotranspiration and lake evaporation are due to reduced temperatures and remaining moisture balance to build the lake is driven by

increased precipitation delivered by dynamic mechanisms. Thus, for samples with higher formation temperatures and thus higher lake evaporation rates Equation S1 is negative. For these samples we do not report an assessment of thermodynamic vs. dynamic contribution to the mass balance solutions. This framework used here is a first order attempt to link the thermodynamic and dynamic mechanisms for moisture convergence on a region used in studies of the terrestrial moisture budget (Seager et al., 2014; Lora, 2018), where the thermodynamic mechanism is changes in specific humidity independent of circulation and the dynamic mechanism represents changes in circulation (i.e. moisture delivery) independent of humidity changes.

REFERENCES

Adams, K. D., Goebel, T., Graf, K., Smith, G. M., Camp, A. J., Briggs, R. W., & Rhode, D. (2008). Late Pleistocene and early Holocene lake-level fluctuations in the Lahontan Basin, Nevada: Implications for the distribution of archaeological sites. *Geoarchaeology*, *23*(5), 608-643.

Benson, L.V., Kashgarian, M., & Rubin, M. (1995). Carbonate deposition, Pyramid Lake subbasin, Nevada: 2. Lake levels and polar jet stream positions reconstructed from radiocarbon ages and elevations of carbonates (tufas) deposited in the Lahontan basin. *Palaeogeography, Palaeoclimatology, Palaeoecology*, *117*(1-2), 1-30.

Benson, L. V., Smoot, J. P., Lund, S. P., Mensing, S. A., Foit Jr, F. F., & Rye, R. O. (2013). Insights from a synthesis of old and new climate-proxy data from the Pyramid and Winnemucca lake basins for the period 48 to 11.5 cal ka. *Quaternary International*, *310*, 62-82.

Bernasconi, S. M., Müller, I. A., Bergmann, K. D., Breitenbach, S. F., Fernandez, A., Hodell, D. A., Jaggi, M., Meckler, A.N., Millan, I & Ziegler, M. (2018). Reducing Uncertainties in Carbonate Clumped Isotope Analysis Through Consistent Carbonate-Based Standardization. *Geochemistry, Geophysics, Geosystems*, *19*(9), 2895-2914.

Braconnot, P., Harrison, S. P., Kageyama, M., Bartlein, P. J., Masson-Delmotte, V., Abe-Ouchi, A., Otto-Bliesner, B & Zhao, Y. (2012). Evaluation of climate models using palaeoclimatic data. *Nature Climate Change*, *2*(6), 417.

Bromwich, D. H. *et al.* Polar MM5 simulations of the winter climate of the Laurentide Ice Sheet at the LGM. *J. Clim.* **17,** 3415–3433 (2004). COHMAP Members, Climatic changes of the last 18,000 years—observations and model simulations. *Science,* 241, 1043–1052.

Comstock, J. P., & Ehleringer, J. R. (1992). Plant adaptation in the Great Basin and Colorado plateau. *The Great Basin Naturalist*, 195-215.

Cook, B. I., Smerdon, J. E., Seager, R., & Coats, S. (2014). Global warming and 21st century drying. *Climate Dynamics*, *43*(9-10), 2607-2627.

Dansgaard, W. (1964). Stable isotopes in precipitation. *Tellus*, *16*(4), 436-468.

Dee, S. G., Russell, J. M., Morrill, C., Chen, Z., & Neary, A. (2018). PRYSM v2. 0: A Proxy System Model for Lacustrine Archives. *Paleoceanography and Paleoclimatology*, *33*(11), 1250-1269.

Dettman, D. L., Reische, A. K., & Lohmann, K. C. (1999). Controls on the stable isotope composition of seasonal growth bands in aragonitic fresh-water bivalves (Unionidae). *Geochimica et Cosmochimica Acta*, *63*(7-8), 1049-1057.

Dickerson, Robert P. (2006). Old lakes and young playas: Nellis Air Force Base geological study and Quaternary history of four playas on the Nevada Test and Training Range; Morgan Printing, Austin, Texas, 176p.

Dickerson, Robert P. (2009). Lakes, wetlands, and meadows, paleoclimate and environments of the playas of the Nevada Test and Training Range; Morgan Printing, Austin, Texas, 154p

Dickerson, R.P. (2010). Paleo-Wetland Facies of Stonewall Flat, Nevada, During the Pleistocene/Holocene Climate Shift. *In 2010 GSA Annual Meeting*.

Dickerson, R., & Forman, (2014). Surface Geology, Paleoclimate, and Paleoenvironment of the Stonewall Mountain and Stonewall Flat Area, Nevada Test and Training Range.

Dickerson, R., & Malczyk, N. (2014). Quaternary geologic studies on playas of the Nevada Test and Training Range in support of the Nellis Air Force Base training mission. *Reviews in Engineering Geology*, *22*, 159-176.

Eagle, R. A., Schauble, E. A., Tripati, A. K., Tütken, T., Hulbert, R. C., & Eiler, J. M. (2010). Body temperatures of modern and extinct vertebrates from 13C-18O bond abundances in bioapatite. *Proceedings of the National Academy of Sciences*, *107*(23), 10377-10382.

Edwards, T. W. D., & McAndrews, J. H. (1989). Paleohydrology of a Canadian Shield lake inferred from 18O in sediment cellulose. *Canadian Journal of Earth Sciences*, *26*(9), 1850-1859.

Egger A.E., Ibarra, D.E., Widden, R, Langridge R.M., Marion, M, & Hall, J. (2018). Influence of Pluvial Lake Cycles on Earthquake Recurrence on the Northwestern Basin and Range, USA. *Geological Society of America* Special Paper 536, 1-28.

Felton, A., Jewell, P. W., Chan, M., & Currey, D. (2006). Controls of tufa development in pleistocene lake Bonneville, Utah. *The Journal of geology*, *114*(3), 377-389.

Fernandez, A., Müller, I. A., Rodríguez-Sanz, L., van Dijk, J., Looser, N., & Bernasconi, S. M. (2017). A reassessment of the precision of carbonate clumped isotope measurements: Implications for calibrations and paleoclimate reconstructions. *Geochemistry, Geophysics, Geosystems*, *18*(12), 4375-4386.

Galloway, R. W. (1970). The full-glacial climate in the southwestern United States. *Annals of the Association of American Geographers*, *60*(2), 245-256.

Ghosh, P., Eiler, J., Campana, S. E., & Feeney, R. F. (2007). Calibration of the carbonate 'clumped isotope' paleothermometer for otoliths. *Geochimica et Cosmochimica Acta*, *71*(11), 2736-2744.

Godsey, H. S., Currey, D. R., & Chan, M. A. (2005). New evidence for an extended occupation of the Provo shoreline and implications for regional climate change, Pleistocene Lake Bonneville, Utah, USA. *Quaternary Research*, *63*(2), 212-223.

Godsey, H. S., Oviatt, C. G., Miller, D. M., & Chan, M. A. (2011). Stratigraphy and chronology of offshore to nearshore deposits associated with the Provo shoreline, Pleistocene Lake Bonneville, Utah. *Palaeogeography, Palaeoclimatology, Palaeoecology*, 310(3-4), 442-450.

Goodwin, D. H., Schone, B. R., & Dettman, D. L. (2003). Resolution and fidelity of oxygen isotopes as paleotemperature proxies in bivalve mollusk shells: models and observations. *Palaios*, *18*(2), 110-125.

Guirguis, K. J., & Avissar, R. (2008). A precipitation climatology and dataset intercomparison for the western United States. *Journal of Hydrometeorology*, *9*(5), 825-841.

Hargreaves, J. C., Annan, J. D., Ohgaito, R., Paul, A., & Abe-Ouchi, A. (2013). Skill and reliability of climate model ensembles at the Last Glacial Maximum and mid-Holocene. *Climate of the Past*, *9*(2), 811-823.

Higgins, R. W., Janowiak, J. E., & Yao, Y. P. (1996). *A gridded hourly precipitation data base for the United States (1963-1993)*. US Department of Commerce, National Oceanic and Atmospheric Administration, National Weather Service.

Horton, T. W., Defliese, W. F., Tripati, A. K., & Oze, C. (2016). Evaporation induced 18O and 13C enrichment in lake systems: A global perspective on hydrologic balance effects. *Quaternary Science Reviews*, *131*, 365-379.

Hostetler, S., & Benson, L. V. (1990). Paleoclimatic implications of the high stand of Lake Lahontan derived from models of evaporation and lake level. *Climate dynamics*, *4*(3), 207-217.

Hren, M. T., & Sheldon, N. D. (2012). Temporal variations in lake water temperature: Paleoenvironmental implications of lake carbonate δ18O and temperature records. *Earth and Planetary Science Letters*, *337*, 77-84.

Hudson, A. M., Hatchett, B. J., Quade, J., Boyle, D. P., Bassett, S. D., Ali, G., & Marie, G. (2019). North-south dipole in winter hydroclimate in the western United States during the last deglaciation. *Scientific reports*, *9*(1), 4826.

Hudson, A. M., Quade, J., Ali, G., Boyle, D., Bassett, S., Huntington, K. W., A Cohen, K Lin, & Wang, X. (2017). Stable C, O and clumped isotope systematics and 14C geochronology of carbonates from the Quaternary Chewaucan closed-basin lake system, Great Basin, USA: Implications for paleoenvironmental reconstructions using carbonates. *Geochimica et Cosmochimica Acta*, *212*, 274-302.

Huntington, K. W., Wernicke, B. P., & Eiler, J. M. (2010). Influence of climate change and uplift on Colorado Plateau paleotemperatures from carbonate clumped isotope thermometry. *Tectonics*, *29*(3).

Ibarra, D. E., Egger, A. E., Weaver, K. L., Harris, C. R., & Maher, K. (2014). Rise and fall of late Pleistocene pluvial lakes in response to reduced evaporation and precipitation: Evidence from Lake Surprise, California. *Geological Society of America Bulletin*, *126*(11-12), 1387-1415.

Ibarra, D. E., Oster, J. L., Winnick, M.J., Rugenstein, J. K. C., Byrne, M. P., & Chamberlain, C. P. (2018). Lake Area Constraints on Past Hydroclimate in the Western United States: Application to Pleistocene Lake Bonneville. *Lake Bonneville Geology Conference Proceedings*, 1-8.

Jones, M. D., Roberts, C. N., & Leng, M. J. (2007). Quantifying climatic change through the last glacial–interglacial transition based on lake isotope palaeohydrology from central Turkey. *Quaternary Research*, *67*(3), 463-473.

Kim, S. J., Crowley, T. J., Erickson, D. J., Govindasamy, B., Duffy, P. B., & Lee, B. Y. (2008). High-resolution climate simulation of the last glacial maximum. *Climate Dynamics*, *31*(1), 1-16.

Kim, S. T., O'Neil, J. R., Hillaire-Marcel, C., & Mucci, A. (2007). Oxygen isotope fractionation between synthetic aragonite and water: influence of temperature and Mg2+ concentration. *Geochimica et Cosmochimica Acta*, *71*(19), 4704-4715.

Kirby, M. E., Feakins, S. J., Bonuso, N., Fantozzi, J. M., & Hiner, C. A. (2013). Latest Pleistocene to Holocene hydroclimates from Lake Elsinore, California. *Quaternary Science Reviews*, *76*, 1-15.

Kurth, G., Phillips, F. M., Reheis, M. C., Redwine, J. L., & Paces, J. B. (2011). Cosmogenic nuclide and uranium-series dating of old, high shorelines in the western Great Basin, USA. *Geological Society of America Bulletin*, *123*(3-4), 744-768.

Laîné, A., Kageyama, M., Salas-Mélia, D., Voldoire, A., Riviere, G., Ramstein, G., Planton, S., Tyteca, S. & Peterschmitt, J. Y. (2009). Northern hemisphere storm tracks during the last glacial maximum in the PMIP2 ocean-atmosphere coupled models: energetic study, seasonal cycle, precipitation. *Climate Dynamics*, *32*(5), 593-614.

Licciardi, J. M. (2001). Chronology of latest Pleistocene lake-level fluctuations in the pluvial Lake Chewaucan basin, Oregon, USA. *Journal of Quaternary Science: Published for the Quaternary Research Association*, *16*(6), 545-553.

Lillquist, K. D. (1994). Late Quaternary Lake Franklin: lacustrine chronology, coastal geomorphology, and hydrostatic deflection in Ruby Valley and northern Butte Valley, Nevada. *Doctoral dissertation, University of Utah, Salt Lake City, Utah*, 2618-2618.

Liu, Z., Otto-Bliesner, B. L., He, F., Brady, E. C., Tomas, R., Clark, P. U., Carlson, A. E., Lynch-Stieglitz, J., Curry, W, & Erickson, D. (2009). Transient simulation of last deglaciation with a new mechanism for Bølling-Allerød warming. *Science*, *325*(5938), 310-314.

Loomis, S. E., Russell, J. M., Verschuren, D., Morrill, C., De Cort, G., Damsté, J. S. S., Olago, D., Eggermont, H., Street-Perrott, F.A., & Kelly, M. A. (2017). The tropical lapse rate steepened during the Last Glacial Maximum. *Science advances*, *3*(1), e1600815.

Lora, J. M., Mitchell, J., Risi, C. M., & Tripati, A. K. (2015). Atmospheric rivers enhanced water delivery to southwestern North America at the Last Glacial Maximum. In *AGU Fall Meeting Abstracts*.

Lora, J. M., Mitchell, J. L., Risi, C., & Tripati, A. E. (2017). North Pacific atmospheric rivers and their influence on western North America at the Last Glacial Maximum. *Geophysical Research Letters*, *44*(2), 1051-1059.

Lora, J. M., Mitchell, J. L., & Tripati, A. E. (2016). Abrupt reorganization of North Pacific and western North American climate during the last deglaciation. *Geophysical Research Letters*, *43*(22), 11-796.

Lora, J. M. (2018). Components and mechanisms of hydrologic cycle changes over North America at the Last Glacial Maximum. *Journal of Climate*, *31*(17), 7035-7051.

Lyle, M., Heusser, L., Ravelo, C., Yamamoto, M., Barron, J., Diffenbaugh, N. S., Herbert, T., & Andreasen, D. (2012). Out of the tropics: the Pacific, Great Basin Lakes, and Late Pleistocene water cycle in the western United States. *Science*, *337*(6102), 1629-1633.

Maloney, E. D., Camargo, S. J., Chang, E., Colle, B., Fu, R., Geil, K. L., Hu Q, Jiang X, Johnson N, Karnauskas KB, & Kinter, J. (2014). North American climate in CMIP5 experiments: Part III: Assessment of twenty-first-century projections. *Journal of Climate*, *27*(6), 2230-2270.

Matsubara, Y., & Howard, A. D. (2009). A spatially explicit model of runoff, evaporation, and lake extent: Application to modern and late Pleistocene lakes in the Great Basin region, western United States. *Water Resources Research*, *45*(6).

McGee, D., Moreno-Chamarro, E., Marshall, J., & Galbraith, E. D. (2018). Western US lake expansions during Heinrich stadials linked to Pacific Hadley circulation. *Science advances*, *4*(11), 1-10.

Mering, J. A. (2015). New constraints on water temperature at Lake Bonneville from carbonate clumped isotopes. *Doctoral dissertation, UCLA*. 1-178.

Mifflin, M. D., & Wheat, M. M. (1979). Pluvial lakes and estimated pluvial climates of Nevada.

Miller, D. M., Oviatt, C. G., & Mcgeehin, J. P. (2013). Stratigraphy and chronology of Provo shoreline deposits and lake-level implications, Late Pleistocene Lake Bonneville, eastern Great Basin, USA. *Boreas*, 42(2), 342-361.

Morrill, C., Lowry, D. P., & Hoell, A. (2018). Thermodynamic and Dynamic Causes of Pluvial Conditions During the Last Glacial Maximum in Western North America. *Geophysical Research Letters*, *45*(1), 335-345.

Munroe, J. S., & Laabs, B. J. (2013). Latest Pleistocene history of pluvial Lake Franklin, northeastern Nevada, USA. *GSA Bulletin*, *125*(3-4), 322-342.

Negrini, R. M. (2002). Pluvial lake sizes in the northwestern Great Basin throughout the Quaternary Period. *Smithsonian Institution Press, Washington, DC,* 11-52.

Oster, J. L., Ibarra, D. E., Winnick, M. J., & Maher, K. (2015). Steering of westerly storms over western North America at the Last Glacial Maximum. *Nature Geoscience*, *8*(3), 201.

Otto-Bliesner, B. L., Russell, J. M., Clark, P. U., Liu, Z., Overpeck, J. T., Konecky, B., Nicholson, S., He, F., & Lu, Z. (2014). Coherent changes of southeastern equatorial and northern African rainfall during the last deglaciation. *Science*, *346*(6214), 1223-1227.

Oviatt, C. G. (2015). Chronology of Lake Bonneville, 30,000 to 10,000 yr BP. *Quaternary Science Reviews*, *110*, 166-171.

Pachauri, R. K., & Reisinger, A. (2007). IPCC fourth assessment report. *IPCC, Geneva*, *2007*.

Petryshyn, V. A., Rivera, M. J., Agić, H., Frantz, C. M., Corsetti, F. A., & Tripati, A. E. (2016). Stromatolites in Walker Lake (Nevada, Great Basin, USA) record climate and lake level changes~ 35,000 years ago. *Palaeogeography, palaeoclimatology, palaeoecology*, *451*, 140-151.

Purton, L., & Brasier, M. (1997). Gastropod carbonate δ18O and δ13C values record strong seasonal productivity and stratification shifts during the late Eocene in England. *Geology*, *25*(10), 871-874.

Reheis, M. (1999). Highest pluvial-lake shorelines and Pleistocene climate of the western Great Basin. *Quaternary Research*, *52*(2), 196-205.

Rutz, J. J., Steenburgh, W. J., & Ralph, F. M. (2014). Climatological characteristics of atmospheric rivers and their inland penetration over the western United States. *Monthly Weather Review*, *142*(2), 905-921.

Santi, L., Arnold, A., Ibarra, D., Whicker, C., Mering, J., Oviatt, C. G., & Tripati, A. (2019). Lake level fluctuations in the Northern Great Basin for the last 25,000 years. *EarthArXiv*. 30 May, 2019. doi: 10.31223/osf.io/6as7t.

Seager, R., & Vecchi, G. A. (2010). Greenhouse warming and the 21st century hydroclimate of southwestern North America. *Proceedings of the National Academy of Sciences*, *107*(50), 21277-21282.

Seager, R., Neelin, D., Simpson, I., Liu, H., Henderson, N., Shaw, T., Kushnir, Y., Ting, M. & Cook, B. (2014). Dynamical and thermodynamical causes of large-scale changes in the hydrological cycle over North America in response to global warming. *Journal of Climate*, *27*(20), 7921-7948.

Shevenell, L. A. (1996). *Statewide potential evapotranspiration maps for Nevada*. Nevada Bureau of Mines and Geology, University of Nevada.

Smith, D.B., & Reimann, C. (2008). Low-density geochemical mapping and the robustness of geochemical patterns. Geochemistry: Exploration, Environment, Analysis, 8(3-4), 219-227.

Smith, J. B., Schneider, S. H., Oppenheimer, M., Yohe, G. W., Hare, W., Mastrandrea, M. D., Patwardhan A, Burton I, Corfee-Morlot J, Magadza CH, & Füssel, H. M. (2009). Assessing dangerous climate change through an update of the Intergovernmental Panel on Climate Change (IPCC)"reasons for concern". *Proceedings of the national Academy of Sciences*, *106*(11), 4133-4137.

Smith, G. I., and F. A. Street-Perrott (1983). *Pluvial lakes of the western United States, in The Late Pleistocene,* edited by S. C. Porter. Minneapolis, MN: Univ. of Minnesota Press.

Soetaert, K., Cash, J., Mazzia, F., & Soetaert, M. K. (2016). Package 'bvpSolve'.

Spencer, C., & Kim, S. T. (2015). Carbonate clumped isotope paleothermometry: a review of recent advances in CO 2 gas evolution, purification, measurement and standardization techniques. *Geosciences Journal*, *19*(2), 357-374.

Suarez, M. B., & Passey, B. H. (2014). Assessment of the clumped isotope composition of fossil bone carbonate as a recorder of subsurface temperatures. *Geochimica et Cosmochimica Acta*, *140*, 142-159.

Talbot, M. R. (1990). A review of the palaeohydrological interpretation of carbon and oxygen isotopic ratios in primary lacustrine carbonates. *Chemical Geology: Isotope Geoscience Section*, *80*(4), 261-279.

Tripati, A. K., Eagle, R. A., Thiagarajan, N., Gagnon, A. C., Bauch, H., Halloran, P. R., & Eiler, J. M. (2010). 13C–18O isotope signatures and 'clumped isotope' thermometry in foraminifera and coccoliths. *Geochimica et cosmochimica acta*, *74*(20), 5697-5717.

Unterman, M. B., Crowley, T. J., Hodges, K. I., Kim, S. J., & Erickson, D. J. (2011). Paleometeorology: High resolution Northern Hemisphere wintertime mid-latitude dynamics during the Last Glacial Maximum. *Geophysical Research Letters*, *38*(23).

Versteegh, E. A., Vonhof, H. B., Troelstra, S. R., Kaandorp, R. J., & Kroon, D. (2010). Seasonally resolved growth of freshwater bivalves determined by oxygen and carbon isotope shell chemistry. *Geochemistry, Geophysics, Geosystems*, *11*(8).

Welker, J. M. (2012). ENSO effects on δ18O, δ2H and d-excess values in precipitation across the US using a high-density, long-term network (USNIP). *Rapid Communications in Mass Spectrometry*, *26*(17), 1893-1898.

Wolfe, B. B., Falcone, M. D., Clogg-Wright, K. P., Mongeon, C. L., Yi, Y., Brock, B. E., Amour, N.A.S., Mark, W.A. & Edwards, T. W. (2007). Progress in isotope paleohydrology using lake sediment cellulose. *Journal of Paleolimnology*, *37*(2), 221-231.

Xie, P., & Arkin, P. A. (1996). Analyses of global monthly precipitation using gauge observations, satellite estimates, and numerical model predictions. *Journal of climate*, *9*(4), 840-858.

Yapp, C. J. (1985). D/H variations of meteoric waters in Albuquerque, New Mexico, USA. *Journal of Hydrology*, *76*(1-2), 63-84.

Zimmerman, S. R., Steponaitis, E., Hemming, S. R., & Zermeño, P. (2012). Potential for accurate and precise radiocarbon ages in deglacial-age lacustrine carbonates. *Quaternary Geochronology*, *13*, 81-91.